Sulfate and Selenium (IV) Adsorption by Hydrothermal Activated Coal Fly Ash based Synthesized Zeolites

Anis Usmani

A Thesis Submitted in Partial Fulfillment of the Requirements for the Degree of Master in Chemical Engineering

Prince of Songkla University

2018

Sulfate and Selenium (IV) Adsorption by Hydrothermal Activated Coal Fly Ash based Synthesized Zeolites

Anis Usmani

A Thesis Submitted in Partial Fulfillment of the Requirements for the Degree of Master in Chemical Engineering
Prince of Songkla University
2018

Thesis Title	Sulfate and Selenium (IV) Adsorption by Hydrothermal Activated Coal Fly Ash based Synthesized Zeolites
Author	Miss Anis Usmani
Major Program	Chemical Engineering

Major Advisor

.....
(Assoc.Prof.Dr. Lupong Kaewsichan)

Examining Committee :

.....,.....Chairperson
(Asst.Prof.Dr. Arthit Neramittagapong)

.....Committee
(Assoc.Prof.Dr. Ram Yamsaengsung)

.....Committee
(Assoc.Prof.Dr. Lupong Kaewsichan)

.....Committee
(Asst.Prof.Dr. Suratsawadee Kungsanant)

The Graduate School, Prince of Songkla University, has approved this thesis as partial fulfillment of the requirements for the Master Degree of Chemical Engineering

.....
(Prof. Dr.Damrongsak Faroongsarng)
Dean of Graduate School

This is to certify that the work here submitted is the result of the candidate's own investigations. Due acknowledgement has been made of any assistance received.

..... Signature
(Assoc.Prof.Dr. Lupong Kaewsichan)
Major Advisor

..... Signature
(Anis Usmani)
Candidate

I hereby certify that this work has not been accepted in substance for any degree, and is not being currently submitted in candidature for any degree.

..... Signature
(Anis Usmani)
Candidate

ชื่อวิทยานิพนธ์ การดูดซับซัลเฟตและซีลีเนียม (IV) โดยใช้ซีโอไลต์สังเคราะห์จากเถ้าลอยถ่านหินกระตุ้นด้วยวิธีไฮโดรเทอร์มอล
ผู้เขียน นางสาว อนีส อุษมานี
สาขาวิชา วิศวกรรมเคมี
ปีการศึกษา 2560

บทคัดย่อ

ถ่านหินโดยทั่วไปประกอบด้วยสารอนินทรีย์และแร่ธาตุ การใช้ประโยชน์ในโรงไฟฟ้าถ่านหินปล่อย SO_x, NO_x, และโลหะหนักอื่นๆ ในกระบวนการเผาไหม้ที่ก่อเกิดปัญหารุนแรงต่อสิ่งแวดล้อม เถ้าลอยนับว่าเป็นของเสียที่มีมูลค่าเนื่องจากอุดมด้วยซิลิกา จึงมีความพยายามในการเพิ่มมูลค่าการใช้ประโยชน์เหล่านี้ การใช้งานเป็นตัวดูดซับได้รับความสนใจ อย่างไรก็ตามความท้าทายคือองค์ประกอบของแคลเซียมออกไซด์ที่สูงของเถ้าลอย ซึ่งมีผลต่อการเกิดผลึก การศึกษาครั้งนี้เพื่อพัฒนาวัสดุซีโอไลต์จากเถ้าลอยถ่านหินโดยกระตุ้นด้วยเบสโดยการบ่มแบบไฮโดรเทอร์มอล ซึ่งไม่ผ่านขั้นตอนการทำให้บริสุทธิ์ ด้วยซีโอไลต์มีขนาดเล็กและรูพรุนสูง จึงถูกใช้เพื่อการดูดซับมลภาวะอย่างซัลเฟต เนื่องจากซัลเฟตมีความเป็นพิษสูงเมื่อถูกสะสมในอวัยวะของสิ่งมีชีวิต ซัลเฟตมักถูกละลายในความเข้มข้นสูงบริเวณรอบโรงงานถ่านหิน การสังเคราะห์ซีโอไลต์ดำเนินการผ่านวิธีไฮโดรเทอร์มอล (105-180 องศาเซลเซียส เวลา 6-72 ชั่วโมง) ใช้เทคนิคการวิเคราะห์ต่างๆได้แก่ เครื่องเอ็กซ์เรย์ดิฟแฟรกชัน เอ็กซ์เรย์ฟลูออเรสเซน ฟลูเรียร์ทรานส์ฟอร์ม อินฟราเรดสเปคโทรมิเตอร์ และค่าประจุที่พื้นผิว จากผลวิเคราะห์แร่ธาตุจากเอ็กซ์เรย์ดิฟแฟรกชันพบว่ามีองค์ประกอบของ Na-P1 โซดาไลท์ และ แคนคริไนท์ ในซีโอลท์สังเคราะห์ปรากฏอยู่ ผลยืนยันกลุ่มของอลูมิโนซิลิเกตที่มีการเชื่อมต่อกันแบบเตตระฮีดรัลหรือเฮกซะกอนัลด้วยกลุ่มไฮเดรท นอกจากนี้ขนาดอนุภาคของซีโอไลต์สังเคราะห์มีขนาดเส้นผ่านศูนย์กลาง 0.3-0.15 ไมโครเมตร พื้นที่ผิวจำเพาะและปริมาตรรูพรุนมีค่า 65.38 ± 0.27 ตารางเมตรต่อกรัม และ 15.02 ลูกบาศก์เซนติเมตรต่อกรัมตามลำดับ ค่าจุดศูนย์ไร้ประจุบนพื้นผิวอยู่ระหว่างค่าพีเอช 6-8 ของสารละลาย ค่าพีเอชที่ลดลงจะทำให้ค่าประจุพื้นผิวเป็นบวกในขณะที่พีเอชของสารละลายที่เพิ่มขึ้นส่งผลให้ค่าประจุเป็นลบ ที่อุณหภูมิสูงขึ้นและระยะเวลาในการบ่มนานขึ้นระยะแคนแคริไนท์และ โซดาไลท์ผสมเพิ่มขึ้น ส่งผลให้พื้นที่ผิวเฉพาะและปริมาตรรูพรุนลดลง เนื่องด้วยพื้นที่ผิวจำเพาะและปริมาณรูพรุนมีขนาดใหญ่มีบทบาทสำคัญในการทำปฏิกิริยาต่อซีโอไลต์ สภาวะที่เหมาะสมที่สุดเพื่อใช้ในการดูดซับจึงพิจารณาจากพื้นที่ผิวสูงสุดของซีโอไลต์ที่ถูกสังเคราะห์ การกำจัดซัลเฟตอยู่ที่พีเอช 6 ประสิทธิภาพการดูดซับสูงถึง 80.43 % ด้วยปริมาณตัวดูดซับ 2 กรัมต่อลิตร โดยมีอัตราการเกิดปฏิกิริยา 0.0005 ต่อนาที และความสามารถในการดูดซับ 14.26 มิลลิกรัมต่อกรัมที่อุณหภูมิ 27 องศาเซลเซียส การดูดซับแบบชั้นเดียวโดยเข้ากับโมเดล Langmuir (R^2> 0.9) สุดท้ายนี้ปรากฏการณ์การดูดซับถูกอธิบายด้วยปฏิกิริยาเทียมอันดับสอง (R^2> 0.9) ประสิทธิภาพการดูดซับไอออนของซีลีเนียมมีค่า 36.47 % ที่พีเอช 6 ใช้เวลาดูดซับ 1 ชั่วโมง

Thesis Title	Sulfate and Selenium (IV) Adsorption by Hydrothermal Activated Coal Fly Ash based Synthesized Zeolites
Author	Miss Anis Usmani
Major Program	Chemical Engineering
Academic Year	2017

ABSTRACT

Coal is generally composed of inorganic matters and minerals. The utilization in coal fired generating plant releases SO_x, NO_x, and other heavy metals which produces severe problems to the environment. In coal combustion process, fly ash was considered as a major solid waste enriched of SiO_2. There have been attempts on value adding these waste utilization, the applicability as an adsorbent has been interesting. However, the challenge is a high CaO composition of this fly ash which impacts on high crystallinity formation. This study was aimed to develop a functional zeolite material from alkali activated coal fly ash through hydrothermal treatment without purification. As being a porous and small feature size material of synthesized zeolite, it is subjected for sulfate adsorption. Since sulfate behaves highly toxic when overdosing in living organism and it is dissolved in high amount around coal mining area. The zeolite synthesis was carried out via hydrothermal method (105-180°C, 6-72 hours). Different instrumental techniques were used to characterize instance XRF, XRD, FTIR, BET, and zeta potential. The XRD patterns reveals the mineralogical phase of Na-P1, sodalite, and cancrinite. FTIR spectra confirm the present of functional group of aluminosilicates connected into tetrahedral/hexagonal, with the hydrate groups. In addition, particle size of synthesized zeolite was 0.3-0.15 μm diameter. The BET specific surface area and pore

volume were 65.38 ± 0.27 m^2/g and 15.02 cm^3/g, respectively. The zero point charges obtained between 6-8 of pH solution, a decreasing pH solution results higher zeta potential while an increasing pH solution results lower zeta potential. At higher temperature and longer hydrothermal time, cancrinite and sodalite phases were increased, however lower in specific surface area and pore volumes. Since the larger specific surface area and pore volume play an important role in influencing reactivity of zeolite. The optimal condition was selected based on the maximum surface area, pore volume, and product yields. Sulfate was adsorbed at pH 6 with 0.0005 min^{-1} reaction rate, the efficiency of synthesized zeolite 80.43 % with adsorbent dosage 2 g/L., and 14.26 mg/g of uptake capacity at 27 ℃. It is implied as monolayer adsorption fitted well by Langmuir model (R^2 > 0.9). Lastly, the adsorption phenomena described by Pseudo second order reaction (R^2 > 0.9). The removal of selenium ions is reported as 36.47% efficiency at pH 6 for 1 hour.

ACKNOWLEDGMENTS

I would like to express my special thanks with gratitude to my advisor firstly, Assoc. Prof. Dr. Lupong Kaewsichan, who gave me the opportunity, knowledge and stimulate throughout the Master degree study. Special thanks with great gratitude to Assoc. Prof. Dr. Nurak Grisdanurak, who encourages, opens my perspective of both knowledge and life, disciplines, provide thoughts, motivation, and inspirations. I am very grateful to be a part of their students.

I would like to thank to Miss Kwannapat Sorachoti, Miss Kanogwan Tohdee, Dr. Sattrawut tulaphol, and Dr. Ekkachai Kanchanathip, who help and guide me during a year conducting the experiment. I would like to thank also my committee members, who sacrifice their time and give me the guidance for my research.

Million thanks to my beloved mother and father, who fully support me throughout my life, with love, patience and encouragement.

Finally, I would like to forward all my appreciation to almighty ALLAH who guides those people who supported and helped me through my research.

Anis Usmani

CONTENTS

CONTENTS (Continue)

CONTENTS (Continue)

LIST OF FIGURES

LIST OF FIGURES (Continue)

LIST OF FIGURES (Continue)

LIST OF TABLES

CHAPTER 1

INTRODUCTION

1.1 Background

Sulfate is a primary contaminant in industrial wastewater, the industries such as fertilizer production, pesticide production, paper mills, and root crop processing mainly generates pollutants into both air and water sources. For coal electricity generating plant, process of coal combustion releases Co_x, So_x and NO_x as its main by-product compounds, particulate matters, and heavy metals in trace amounts [1]. Sulfur can be leached to the environment by either emission, wastewater discharge or solid waste disposal. Several forms of sulfate in aqueous system appears predominantly depending on pH. There are six oxidation states of sulfur seems in various sulfur compounds; sulfate ion is an oxidized form with +6 of sulfur. Sulfur oxidation can be stimulated by both chemical and enzymatic reaction [2] forming into sulfate. Sulfate contamination in disposed water pond has been experienced in the range of 500-2000 ppm concentration. Sulfate is a mild hazardous compound, there is no strict regulation in many countries. The excessive contamination causes taste change and the laxative effects for a human at above 600 mg/L.Sulfate standard level in industrial wastewater has been set about 500-1000 mg/L [3, 4]. In Thailand, sulfate contamination has been found mostly in mine activity wastewater and water discharge from electricity generating processes (Lampang, Thailand). Several issues of contaminated water have been interested, with costly technology and difficulty of contaminants removal from

streams affected by surface mining high selenium are focused to be solved. Domestic area is possibly facing the increments of water pollution in groundwater, the EPA enforces to include selenium standards on pollution discharge permits, so that water quality is adequately protected. Since selenium species are oxyanions. Adsorbents with surface positive charges are expected to perform better for selenium ions removal. In addition, the specific pH conditions for obtaining maximum selenium (IV and VI) removal will also be determined. The performance of the adsorbents is directly proportional to the amount of positive surface charges present at a certain pH. As selenium species are negative charged anions, it is expected that adsorbents surface displaying opposite charges would provide better attraction of selenium ions and thereby increase removal.

1.2 Contaminants remediation

Both chemical and biological route applies sulfate treatment methods. For chemical treatment method, Calcium is a content to bind sulfate, as a sequent, the remaining sulfate in the reservoir is reduced. Lime or limestone often used for precipitation gypsum. Barium sulfate precipitation is another method for sulfate elimination in an acidic region with low residual sulfate. However, it is toxic, expensive and capable to remove the ions approaching the regulatory limits. Ettringite formation, it requires alkalinity for active sulfate uptake[4]. Metal cations or iron (Fe) can also precipitate with sulfate and reaction in the gas stream for sulfide removal in the scrubber, and the response in a packed bed with iron or zinc [5]. Amongst various treatment techniques, adsorption is a cost- effective and straightforward for the

reaction with an adsorbent. The adsorbent is mainly synthesized resulting high surface area with surface modification and charge which enhance the removal.

1.3 Coal fly ash

Coal as an energy enriched material has become a major source for electricity generation owning to the lowest operating cost compared to other alternative sources. Natural gas operating cost is about 3.96 B while using coal is only 2.7 B. However, utilizing coal has gained lots of attention in public, since coal generally contains sulfur and heavy metals. Processing water, and by-products discharged during combustion certainly leaches pollutants more unfriendly like SO_2 and particulates. Severe environmental problems have been experienced from the existing plant particular to highly toxic wastewater, prior remediation process is recommended before the discharge. Combustion of lignite coal releases ashes as by-products called fly ash, and bottom ash. Interestingly, Coal ashes utilization has diversely advantages. Coal fly ash (CFA) has been emerged as a promising material playing a crucial role in geopolymer, cement, wastewater remediation and stabilization, and catalyst [6]. CFA consists of aluminosilicate amorphous and crystalline phases, generally quartz (SiO_2), mullite ($3Al_2O_3{\cdot}2SiO_2$), hematite (α-Fe_2O_3), and magnetite (Fe_3O_4). These compounds allowed the conversion of CFA into zeolites via hydrothermal method.

Zeolites are minerals generally composed of silicon, aluminum, and oxygen [1] with three-dimensional framework of interconnected tetrahedra. Crystalline structure generated from $[AlO_4]^{5-}$ and $[SiO_4]^{4-}$ bonded Al and Si as a central atom surrounded by four oxygen atoms in the corner sharing with each tetrahedron in adjacent tetrahedron

crystals. Depending upon the resource, types of raw material, synthesis method and condition, the material applications would be varied based on their properties. Synthesis of porous material requires NaOH solution used in Na-P1zeolite synthesis is in the range of 2.5-2.9 M in pressurized reactor at 150℃. Theses synthesized material were efficiently remove the contaminants in acid mine drainage with 10 gL^{-1} adsorbents [7]. Nano-scale material has been emerged as multi-functional material in diverse applications i.e. catalyst, sensing, electronics, and etc. It is interesting to modify this solid waste material into high small particles possessing large porosity. CFA modification with agitated alkali-hydrothermal treatment under high temperature and pressure can enhance specific surface area and porosity of materials. However, not only being a silica and alumina source, the presented impurities of coal fly ash depending on types of coal such as anthracite, subbituminous, bituminous, and lignite, combustion method, and heating and cooling in the coal-fired boiler can affect the chemical composition and types of produced zeolites [3].

1.4 Zeolite via hydrothermal synthesis

Hydrothermal synthesis is known as a simple and cost effectiveness method of zeolite synthesis. With less energy consumption, fast kinetics reaction and etc., hydrothermal synthesis became an attractive method amongst pioneering techniques. The synthesis method involving the Si/ Al composition with other elemental composition which mainly influences microporous crystalline surface. Molecular structure of Si and Al particles undergoes the modification with the existence of alkali-supersaturated solution. The crystallization and reaction mechanism has been

predicted [6]. The Hydrothermal phenomena generated inside the autoclaved has been predicted and designed. The autoclave equipped with thermal control system including thermocouple, heating jacket. Hence, temperature in the system is accurate and effective to desired structure. The pressure was arisen regarded to the vapor pressure of NaOH solution. The solution starts to vaporized as the temperature inside autoclave approaches 100°C and continuously increases. The characterization results have sustained with previous studies that sodalite formed at low temperature. The increasing temperature produces more sodalite and cancrinite phases obviously identified by XRD patterns and SEM. The hydrothermal synthesis is described as the amorphous reactants constitutes of silica and alumina by mixing into aqueous mixture.

Zeolites are widely used in various applications i.e. catalysis, ion exchange, separation and adsorption, because of being a high specific surface area, uniform microporous material, and high thermal stability. Amongst several types of zeolites, sodalite is a zeolite having ultra- micro pore size and is commonly used as a heterogeneous basic catalyst in fine chemical production, which is typically prepared via hydrothermal synthesis, under autogenous pressure. As a catalyst support, the prevailing catalyst carrier is alumina. It acts as inert to reacting system, structurally stable to relatively high temperatures and is available in various forms with surface areas ranging from 1-300 m^2/g, approximately. Addai-Mansah Barnes et al. [8] studied on sodalite to cancrinite conversion mechanism preparing from Kaolin [$Al_2Si_2O_5(OH)_4$], reaction was carried out at 90 and 160 °C for 21 days. An amorphous type phase primarily occurs in a minute, zeolite A formed in 2 hours synthesis, transformed into sodalite after 2 days then remained until 21 days, cancrinite phase finally presented.

In this work, sodalite were obviously achieved at 12 hours synthesis, at 105℃ via hydrothermal treatment in closed system. By varying synthesis condition, different portion of sodalite, cancrinite, Na-P1, and amorphous phases are also observed. Typically, mineralogical zeolites contain silicon, aluminum, and oxygen with three-dimensional framework of interconnected tetrahedra. Crystalline structure generated from $[AlO_4]^{5-}$ and $[SiO_4]^{4-}$ bonded Al and Si as a central atom surrounded by four oxygen atoms in the corner sharing with each tetrahedron in adjacent tetrahedron crystals. Depending upon the resource, types of raw material, synthesis method and condition, the material applications would be varied based on their properties. Synthesis of porous material requires NaOH solution, Na-P1zeolite is in the range of 2.5-2.9 molar in an autoclave at 150℃. These synthesized materials plays a crucial role on contaminants removal in acid mine drainage with 10 g/L adsorbents [7]. CFA modification with agitated alkali-hydrothermal treatment under high temperature and pressure can enhance specific surface area and porosity of materials. However, not only being a silica and alumina source, the presented impurities of coal fly ash depending on types of coal such as anthracite, subbituminous, bituminous, and lignite, combustion method, and heating and cooling in the coal-fired boiler can affect the chemical composition and types of produced zeolites

1.5 Aims and Objectives

This research is aimed to solve the existed problem of sulfate accumulation in industrial and coal mining water discharge by developing materials to function in the plant and to enhance on material and adsorption engineering perspectives.

Development of porous materials by major solid wastes obtained from coal fired generating plant purposes water remediation. The study involves the zeolites synthesis as molecular sieve via two steps synthesis; dissolution and hydrothermal process.

1.6 Scopes of this study

This study is emphasized on the adsorption of contaminated sulfate and selenium in synthetic water by initially examine chemical and physical properties of synthesized materials. Lignite coal fly ash obtained from Mae Moh power plant was used as the raw material. The research scope is described as followed;

1.6.1 To modify surface and structure of coal fly ash via highly alkali-hydrothermal treatment.

1.6.2 To investigate the effects of hydrothermal temperature and time on zeolite by various instrumental characterization techniques including mineralogical analysis though X-ray diffraction (XRD), functional groups by Fourier transform Infrared spectrometer (FTIR), elemental analysis by electron dispersive spectroscope (EDS), specific surface area analysis by Bruneaur- Emmett- Teller (BET), and surface morphology by scanning electron microscope (SEM).

1.6.3 To evaluate the synthesized materials in sulfate and selenium contaminated water.

1.6.4 To study the adsorption performance of synthesized zeolites and the raw material using Langmuir and Freundlich isotherm models.

1.6.5 To investigate the adsorption behavior through kinetics study of the synthesized materials and coal fly ash.

CHAPTER 2

LITERATURE REVIEW

2.1 Sulfate

Sulfate (SO_4^{2-}) is a polyatomic anion with 96.06 g/mol molecular weight. A description involving the chemical structure, the model proposed by D.W.J Cruickshank indicated that fully occupied p orbitals on oxygen overlap with empty sulfur orbitals, the bond has significant ionic character. The structure obeys the octet rules and the electronegativity plays a key role for charge distribution. The dislocation between the S-O length in the sulfate is described by donation of p-orbital electrons from the terminal S=O bonds [9].

2.1.1 Sulfate contamination

Coal mining effluent regulations covering the discharged wastewater from mine drainage, coal storage facilities, and coal preparation plants. Sulfate is often contaminated from mine activity at 500-2,000 mg/L as illustrated in Figure 1. The world health organization (WHO) set the standard sulfate concentration in drinking water at 250 mg/L. Sulfate removal technology includes lime precipitation, the simplest method with the presence of calcium reduces sulfate by sulfur capturing mechanism. Independent parameters affecting the sulfate removal mechanism has been studied in fluidized bed reactor; temperature and concentration of limestone which determines limestone conversion, heat transfer, attrition, sulfur capture mechanism, etc [10]. Benatti, T. et al [11] studied the effects of pH on sulfate removal

onto calcium and barium in non-treated wastewater, pH was varied from 2-8. The results show that calcium is higher induced sulfate removal than barium at pH 5 which obtains 20% removal from 200 g SO_4^{2-} per liter. Excess sulfate intake causes dehydration on human and lead to diarrhea [12] in infants. Mine water typically was contaminated by various pollutant such as SO_4^{2-}, CaO, Mg, Mn, Fe, and Zn. Table 2.1 shows concentration of contaminant in mine water source in US, it was found that SO_4^{2-} is polluted in highest amount.

Table 2.1: Concentration of Mine water contaminants [4]

Mine Water	Elements	Concentration (mg/L)
Sample I	SO_4^{2-}	588.0
	Ca	132.9
	Mg	48.0
	Mn	45.0
	Fe	2.4
	Zn	0.15

2.1.2 Removal of Sulfate

Both chemical and biological methods have been applied for sulfate remediation. One of the various treatment methods is adsorption, the cost effective and high efficiency. The common industrial process for sulfate removal involves lime or limestone precipitation, Figure 2.1 illustrate the process flow diagram, wastewater inlet undergoes 2 stages lime softening clarifier and re-carbonation before discharge, the sludge from these processes filtered out before disposal.

The general reaction takes place in this process can be described as in the reaction (1); calcium ions binds to sulfate ions yields calcium sulfate and sodium hydroxide. Hence, the pH is increased respected to the Rxn (1).

$Ca(OH)_2 + Na_2SO_4 \quad => \quad CaSO_4 + NaOH$ Rxn. 1

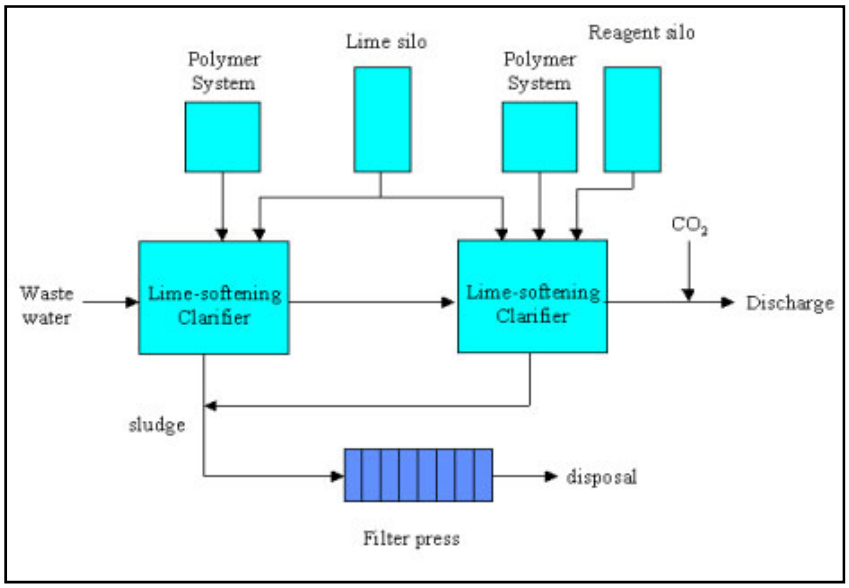

Figure 2.1: Process flow diagram of sulfate remediation by lime precipitation method [13]

List of various sulfate treatments review is illustrated in Table 2. 2. Precipitation, crystallization, and adsorption techniques for sulfate treatments are frequently studied utilizing original available source in natural and modified these natural sources such as barium and calcium, gypsum, modified rice straw, modified washed analcime, alpha-alumina and etc [11, 14-17]. The pH of solution is mostly studied at the mild acidic to neutral. The optimal treatment time was 2 hours, longer treatment time resulting less uptake capacity such alpha alumina with 7.7 mg/g uptake at pH 5.7 for 24 hours.

Table 2.2: Literature Review of sulfate treatment

Materials	Method	Condition	Results	References
Barium and calcium	Precipitation	Fenton Oxidation pH adjusted with sulfuric acid and NaOH pH = 4 Dosage = 80 g/L	Barium remove 61.4% Calcium remove 99%	[11]
Gypsum seed	Fluidized bed crystallization	pH = 7 – 8 Silica carrier 0.45 μm syringe filters	Removal = 65.08 %	[15]
Modified Rice straw	Adsorption	Dosage = 0.1 g in 50 mL Temp = 25 °C pH = 6.4 Contact time = 120 mins UV-Vis at 420 nm	q_{max} =74.76 mg/g	[14]
Barium-modified acid-washed analcime	Adsorption	Temp = 25 °C pH = 3-6 Contact time = 120 mins Dosage 5g/L	q_{max} =13.7 mg/g	[16]
γ-Al_2O_3	Adsorption	pH 5.7 Initial Conc. = 20-40 mg/L Contact time = 24 hrs	q_{max} =7.7 mg/g	[17]

Sulfate treatment has been studied using various types of adsorbent, either by natural material or modified materials as reported in Table 2.2. The adsorbent should be characterized in order to easily identify causes of uptake as well as enhanced factor in sulfate treatment process.

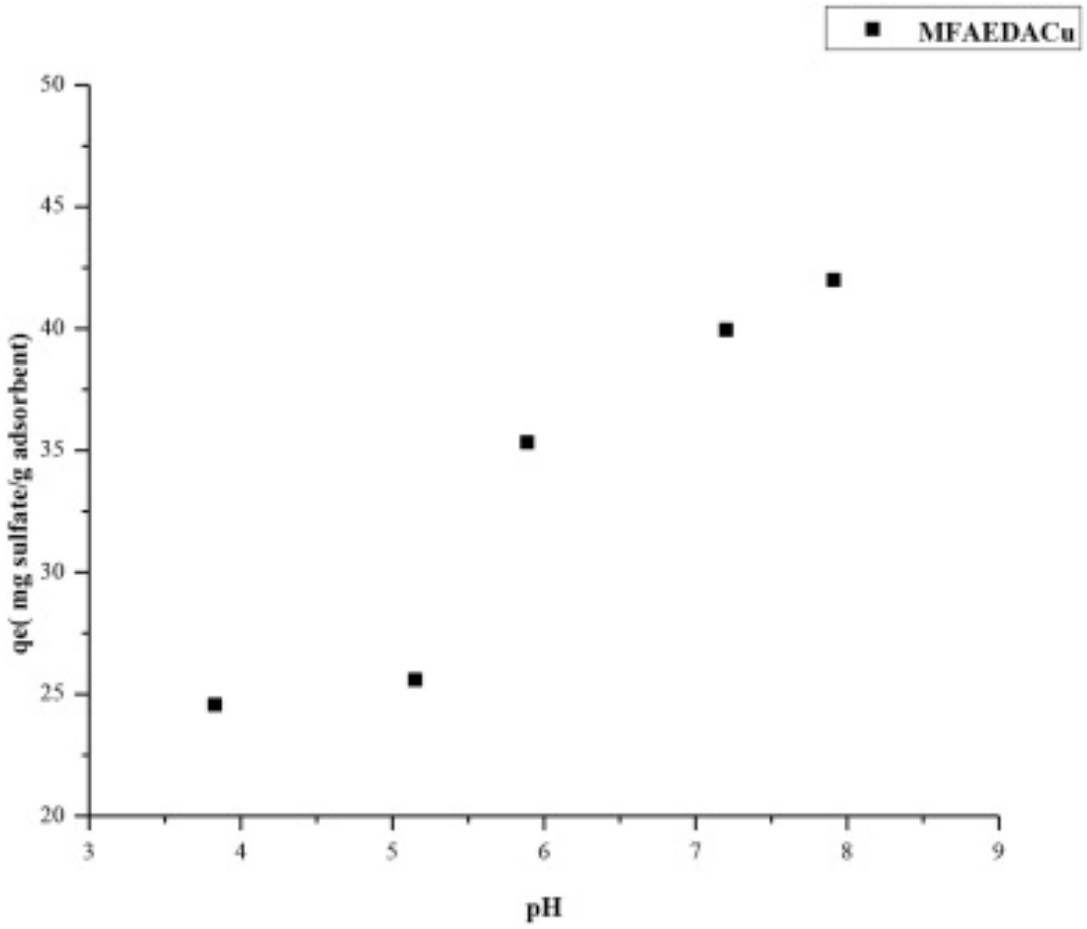

Figure 2.2 Effects of pH on sulfate adsorption capacity by copper modified mesoporous material (MFAEDA-Cu) [18]

Figure 2.2 shows the sulfate adsorption results on copper modified mesoporous material at different pH value. The ultimate uptake capacity is observed within pH 6-8 range, varying between 57% and 68% of sulfate uptake (35-42 mg/g). Its attribution has been predicted as the possible replacement of ethylene diamino ligand from the

octahedral ethylene di-amino complex that allow a change in cation coordination number [18].

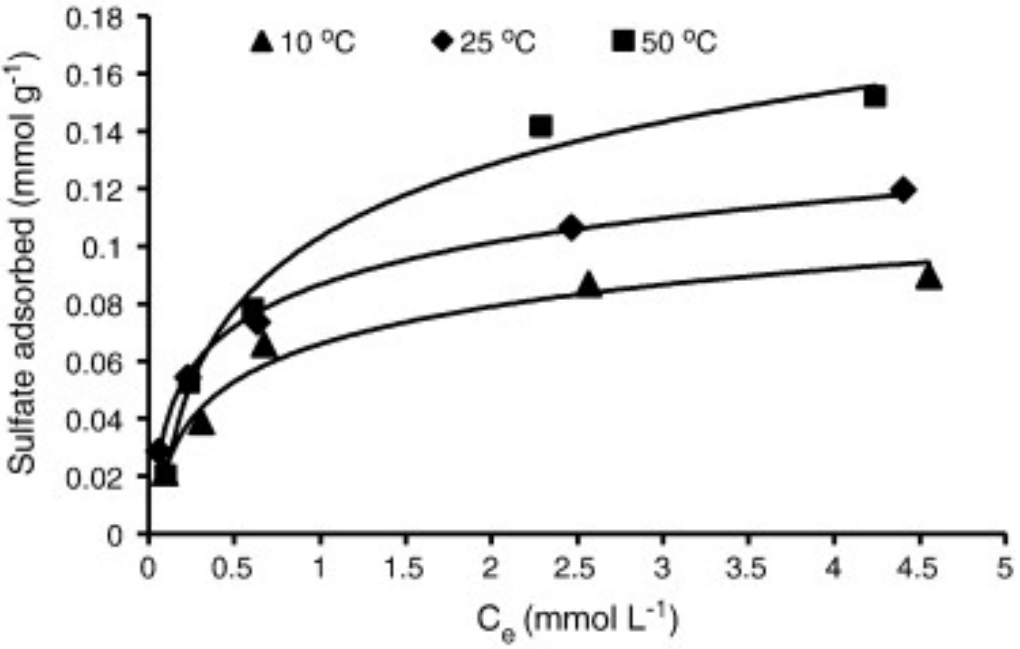

Figure 2.3 Equilibrium isotherm of sulfate removal on LDH at different temperature at pH =7 [19]

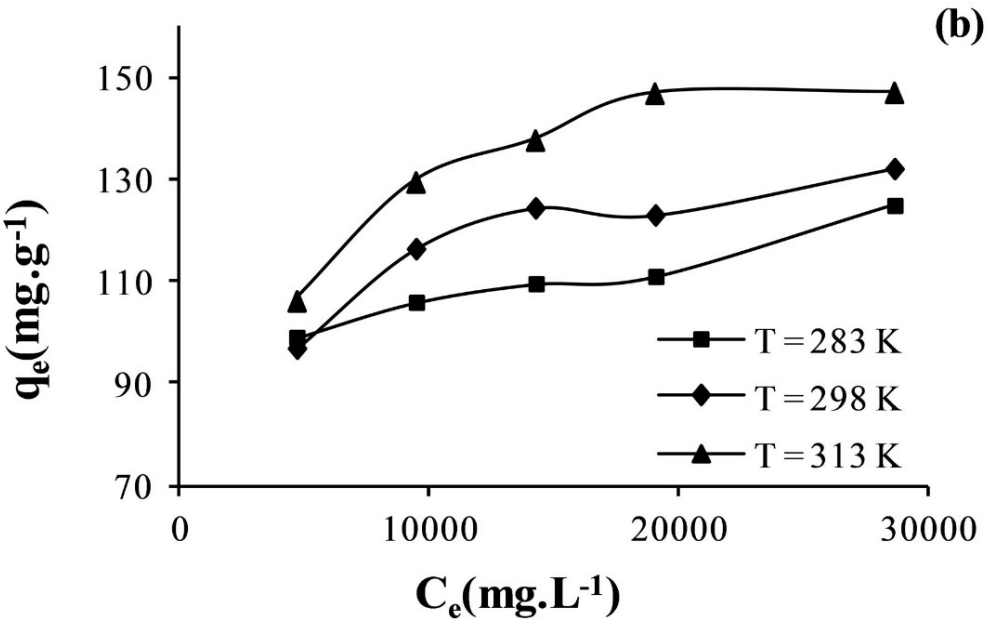

Figure 2.4 Adsorption of sulfate with three different temperature [20].

Figure 2.4 shows the adsorption capacity versus concentration at equilibrium point curve. Sulfate could be adsorbed at maximum capacity at 313 K (40°C) utilizing anion membrane which produced from base polymers; styrene and divinylbenzene and ammonium groups which considered as a strong anion exchanger [20]. The certain and high temperature can enhance the sorption capacity for sulfate uptake.

2.2 Selenium

Selenium (Se) is an inorganic colorless salt with atomic mass of 78.96 u ± 0.03 u, typically dissolved in water consisting 4 oxidation states which is +6, +4, 0, and -2. It possesses atomic radius of 120 pm of atomic radius, 120 ± 4 pm covalent radius, and 190 pm of Vander Waals radius. Selenite (SeO_3^{2-}, Se(IV)) and selenate (SeO_4^{2-}, Se(VI) mostly formulated in aqueous system (Daniel Strawn et al., 2004). As being dual characters trace element, it performs both as a toxic to environment and a micronutrient to human regarding the apparent species and quantity. Se(IV) and Se(VI) are toxicant species which contrast to Se (0) and Se (-II).

Se (IV) and Se (VI) formulates in natural water. Elemental Se and Se (-II) are mostly predominant in fresh water and estuary ecosystem [21]. The existent of Se (IV) and Se (VI) in wastewater is especially concerned due to the toxicity to human, and ecosystem at high exposure. While elemental Se and Se (-II) are predominantly presented in natural water. The minimum and maximum amount containing in drinking water was set at 10 and 50 µg/L by WHO [22]. The excess consumption of selenium causes illness and disease to vectors and other living organism. Selenium is about 0.7 ppm concentration of the earth's crust, concentrated in various material such as

plants, sulfur deposits, mineral sulfide of copper and molybdenum, and fossil fuels [23].

Excessive consumption of selenium causes illness and disease to vectors and other living organism. Selenium is about 0.7 ppm concentration of the earth's crust, concentrated in various material such as plants, sulfur deposits, mineral sulfide of copper and molybdenum, and fossil fuels (M. Dubrovsky, 2005). Selenium can be found in waste streams of copper refining, acid coal mine drainage, coal-fired power plants, and petroleum refining. A number of environmental impacts was attained regarding to these activities which heavy metal, and non-metal elements including selenium can be leached into soil layers and contaminate into groundwater. As industrial revolution arisen, the following massive impacts have been concerned. Therefore, selenium removal becomes a major issue on developing a new remediation technology.

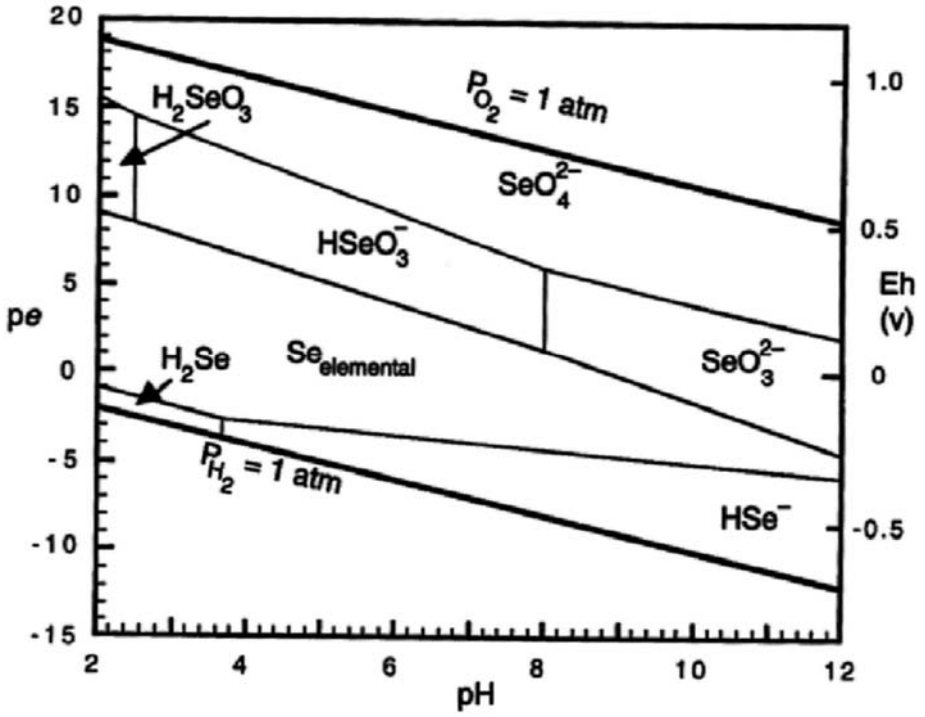

Figure 2.5 Pourbaix diagram for selenium predicting of thermodynamic stability

Thermodynamic stability as a function of pH is predicted employing pourbaix chart as illustrated in Figure 2.5. Measurement of redox (oxidation-reduction) reaction, Se (IV) in oxyanion form of $HSeO_3^-$ is penetrated in positive Eh region range from 0-0.75 V. To control SO_x pollution in coal electricity generating plant, flue gas desulfurization (FGD) systems can be done by using wet scrubbing which could remove sulfur up to 69% of coal-fired capacity. Wastewater from FGD contains metalloid including total dissolved solids (about 50,000 mg/L) and Se. They will negatively affect quality of water [24]. In FGD process, there are inhibited oxidation, natural oxidation, and forced oxidation which is the main constructed type. With the force oxidation type, air is pumped to oxidize SO_3^{2-} into SO_4^{2-} to be precipitated as gypsum ($CaSO_4 \cdot 2H_2O$) applicable products for soil improvement or board. In the air of force oxidation, metals and metalloids including Se are also oxidized.

Table 2.3 Standard quality of industrial wastewater

	Standard level	Measurement Techniques
pH	5.5 – 9.0	pH meter
Temperature	40°C	Thermometer
Sulfide (as H_2S)	≤ 1 mg/L	Titration
Heavy metal (Se)	≤ 0.02 mg/L	Hydride-Generation Atomic Absorption Spectrophoto-metrer

Standard level of industrial wastewater properties is shown in Table 2.3, pH value presented in mild acidic to basic condition, at 40°C. The sulfide as a sulfur source should be limited below 1 mg/L and selenium content should be below 0.02 mg/L.

2.2.1 Removal of Selenium

Selenium can be found in waste streams of copper refining, acid coal mine drainage, coal-fired power plants, and petroleum refining. A number of environmental impacts was attained regarding to these activities which heavy metal, and non-metal elements including selenium can be leached into soil layers and contaminate into water source. One more research reveals the removal mechanism of zero valent iron in selenium adsorption. The reductive precipitation has been investigated following by sorption on the corroded iron surface.

Zero valent iron is an attractive alternative for selenium removal from water via reduction of selenium oxyanions to elemental selenium (Se^0). In redox reaction, selenate (SeO_4^{2-}) acts as an electron acceptor, the Fe metal is the electron donor. reaction 2 and 3 [25] indicated possible reactions for the reduction and deposition of selenium on iron surfaces.

$$SeO_4^{2-} + Fe^0 + H_2O \Rightarrow SeO_3^{2-} + Fe^{2+} + 2OH^- \quad \text{Rxn. 2}$$

$$SeO_4^{2-} + 3Fe^0 + 4H_2O \Rightarrow Se^0 + 3Fe^{2+} + 8OH^- \quad \text{Rxn. 3}$$

SeO_4^{2-} is initially adsorbed onto surface and electrically reduced by Fe (0) which is transported from the oxide over the adsorbent layer to its solid-liquid interface. The electron transport mechanism of electron has not been studied, the movement of electron was implied to occur since thermal electrons such as those involved in

chemical reaction, has ability to transport longer distance within a solid than photoelectrons. Fe (II) created in no dissolving oxygen region was consequently appeared in the solution. Once electrons are unleashed from Fe (0) forming onto Fe (II) at Fe metal interface. Then, the Fe layer becomes thicker till the it is inhibited from electron transportation thereby the SeO_4^{2-} reduction at the surface is then deterred. Accordingly, fewer adsorbates are deposited in the presence of atmospheric region. For this reason, fine iron particles with large surface area to volume ratios are preferable [26].

Table 2.4 Literature Review of selenium adsorption

Adsorbents	Condition	Maximum Capacity (mg/g)	References
$Fe(OH)_2$ impregnated CNTs	pH = 6 Initial concentration = 1 mg/L Time = 6 hours Dosage 25 mg Rotation speed 150 rpm	111	[27]
Iron oxide nano particle	pH = 4 Initial concentration = 0.01 mg/L	15.1	[28]
Chitosan-clay composite	pH = 4 Initial concentration = 0.1 mg/L Temperature = 30 °C	18.4	[29]
Iron-coated GAC	pH = 2-8 Initial concentration = 2 mg/L Temperature = 30 °C	2.89	[30]
Nanocrystalline hydroxyapatite	pH 5 Initial concentration = 0.01 mg/L Temperature = 30 °C	1.94	[31]
Aluminum oxide coated sand	pH 4.8 Initial concentration = 1.2 mM	1.08	[32]
Sulfuric acid treated rice husk	pH = 1.5 Initial concentration = 100 mg/L Temperature = 45 °C	40.92	[33]

Table 2.4 shows list of selenium (Se IV) treatments review which utilizing various types of adsorbents. All pH values were studied at acidic region with ultimate low initial concentration since Se (IV) is generally presented at very low amount in contaminated water. However, Se (IV) needed to be treated as it is a heavy metal which is toxic to

human and environment. Most of the adsorbents in Table 2. consist of high crystallinity surface which is beneficial to adsorb and attract ion of Se (IV) [31].

2.3 Zeolites

Zeolite is an aluminosilicate material enriched of silica and alumina sources with microporous which typically applied as a molecular sieve. The unique properties of the material such as large specific surface area and porosity, ion exchange capability, and high thermal stability enable the catalysis reaction with shape selection and surface charge attraction that enhance application efficiency. Molecular structure of cancrinite is connected by tetrahedra of double 6 membered ring in hexagonal prism [34] as illustrated in Figure 2.6. Both sodalite and cancrinite minerals possess hexagonal shape with 20-30 μm particle size. Na-P1 presented as a fibrous shape. Its particle size is unavailable [35]. Sodalite has been prepared at 100°C for 24 hours. It is widely used as a catalyst in transesterification [36].

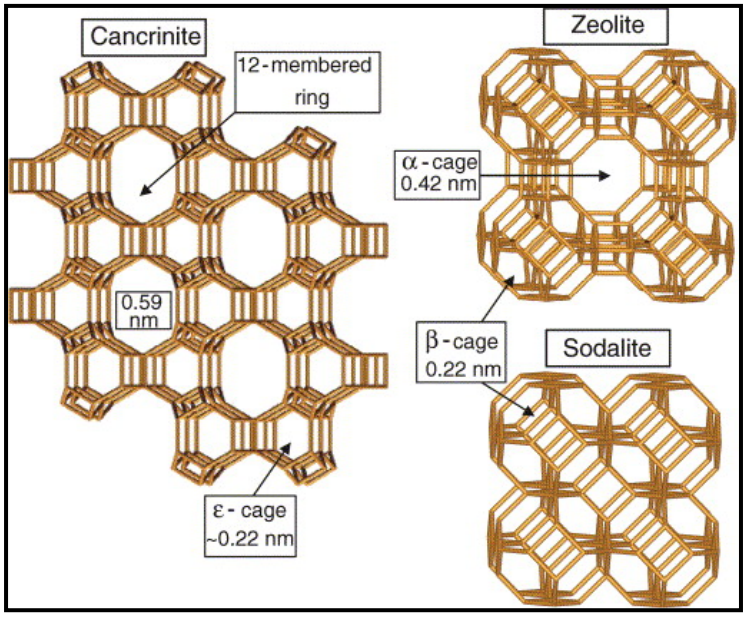

Figure 2.6 Molecular structure of zeolites, sodalite, cancrinite [37]

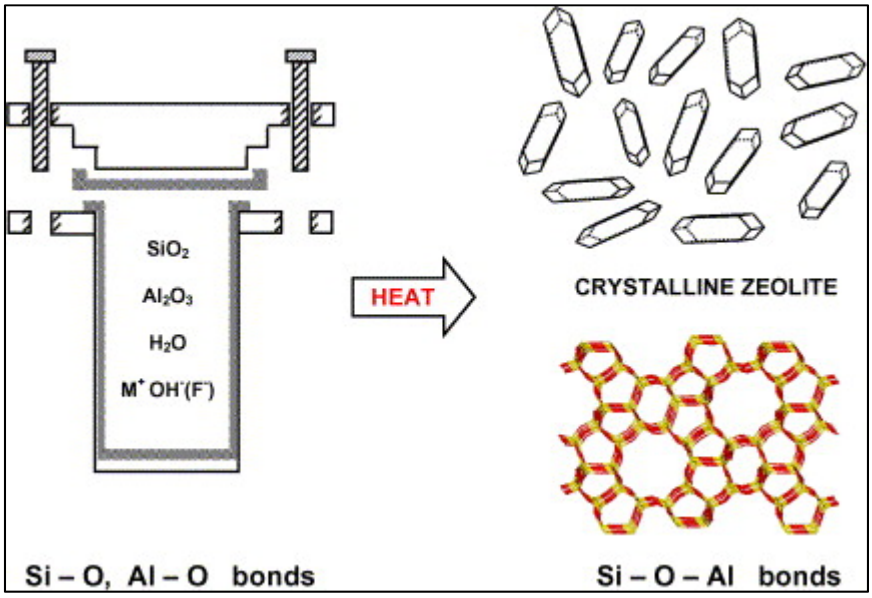

Figure 2.7 Hydrothermal synthesis of zeolites in an autoclave [38]

SiO_2, Al_2O_3, H_2O and alkaline mixed and heated in a pressurized sealed autoclave can generate crystalline zeolite, and zeolite frame work (Si-O-Al) as illustrated Figure 2.7. In order to clearly understand the fundamental of zeolite formation, Colin S. et al [38] reported a general hydrothermal zeolite synthesis which can be explained as follows;

1. Amorphous material containing silica (SiO_2) and alumina (Al_2O_3) are mixed together with a cation source, usually in a high basicity.
2. The mixture is heated in a closed autoclave (reaction temperature is usually above 100^{o}C).
3. The reactant materials remain amorphous after increasing temperature.
4. Crystallinity on zeolite product can be found, after the “induction period”.

5. The essential amorphous phase is replaced by crystals of zeolites which approximately has equal mass (this can be recovered in filtration, washing, and drying step.

Zeolites synthesis mechanisms are summarily described in Figure 2.8, SiO_2 and Al_2O_3 sources with present of alkali solution are partly reacted into heterogeneous non-equilibrium mixture contained solution and solid which is initially generated as a primary amorphous phase. Reaction time and temperature are one of key factors in zeolite framework formation, the equilibrated solution in terms of ionization into monomers and polymers assisted by the present of water content can generate the colloidal and gel silicates or aluminosilicates which known as the secondary amorphous [38].

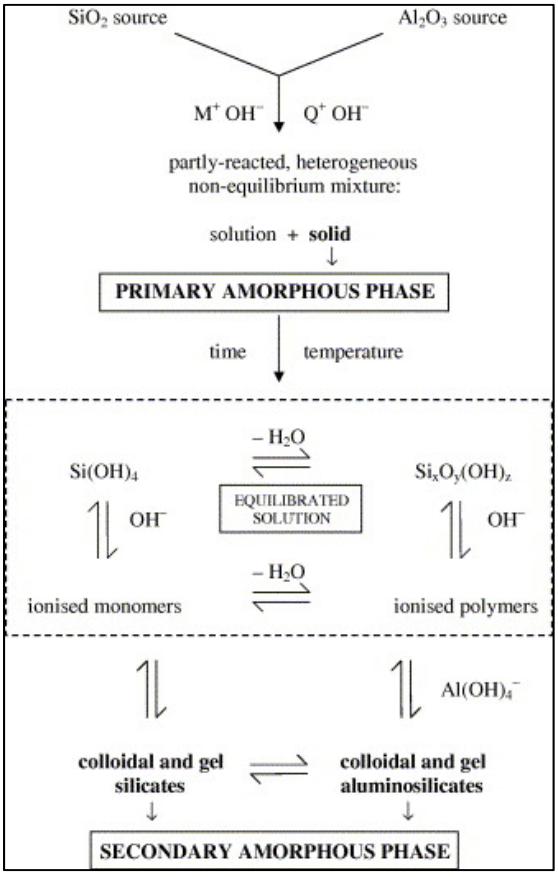

Figure 2.8 Synthesis mechanism of zeolite [38]

Synthesized zeolites as micromaterials have widely been evidenced by SEM analysis to investigate predicted physical properties by relating available chemical composition, x-ray diffraction, or surface potential data.

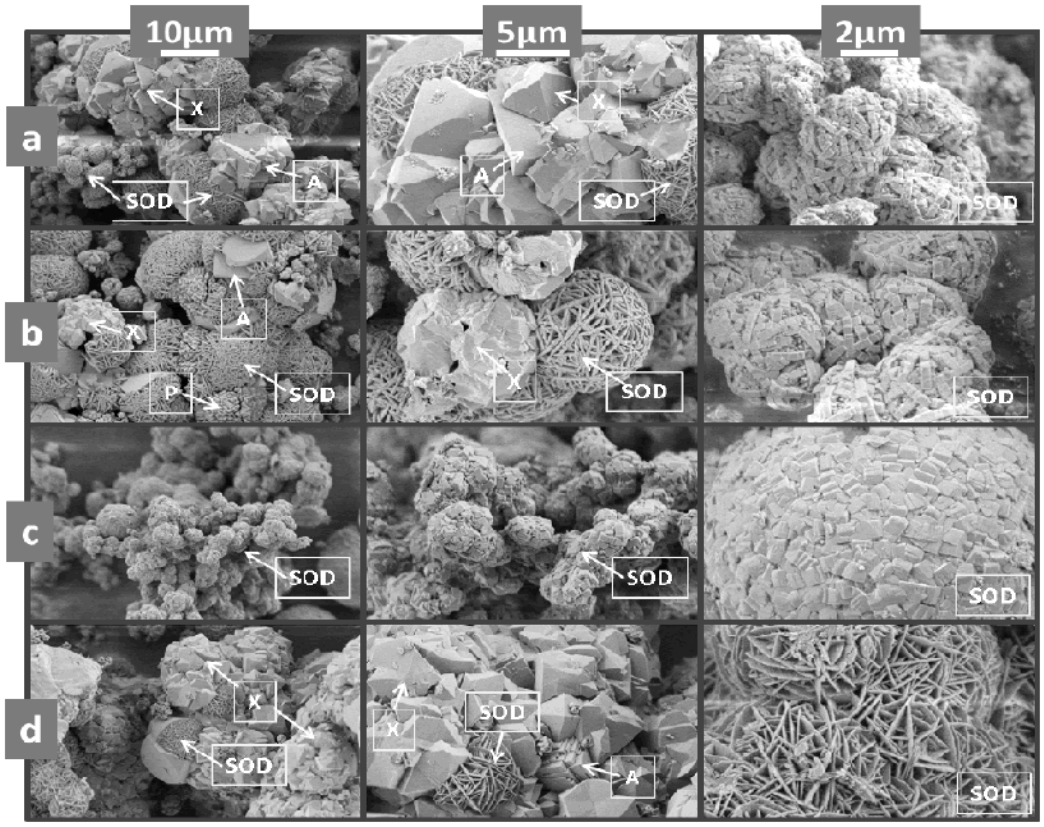

Figure 2.9 SEM images of the materials synthesized at 80°C after (a) 25 hours and (b) 48 hours, (c) at 90°C after 25 hours and (d) 70°C and after 48 hours [39].

According to Figure 2.9, morphology and surface properties of synthesized materials at various conditions have been investigated by scanning electron microscope (SEM) at 2, 5, and 10 µm magnification. Sodalite was mostly presented with different morphologies at different synthesized conditions [39]. At lower temperature and longer aging time providing sharper edge on its surface, it is formed un-uniformly which might

be affected by impurity, non-homogeneous mixing, or zeolites dissolution/ formation steps.

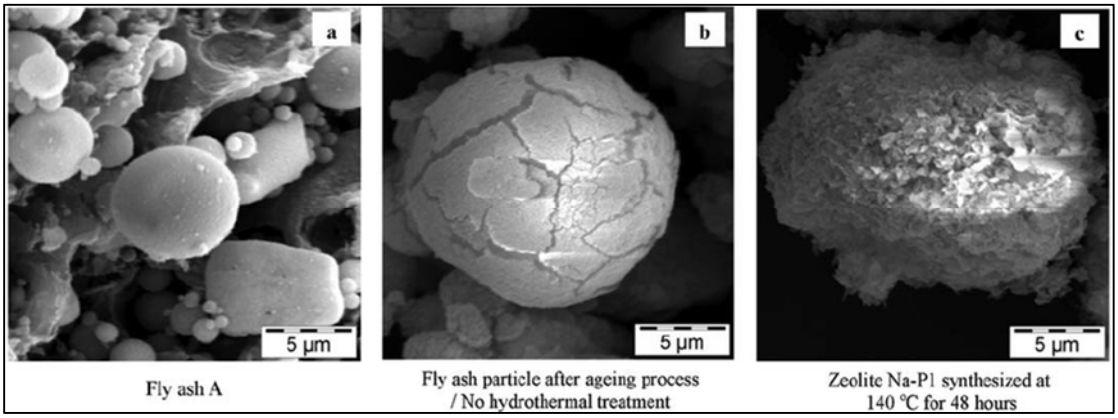

Figure 2.10 SEM images of example fly ash (a), fly ash particles after aging process (b), and zeolite of hydrothermal [40]

The previous study has reported physical change of synthesized zeolite in each step as shown in Figure 2.10, raw material fly ash, aged fly ash, and zeolite Na-P1 product surface and morphology were investigated. It is started with smooth surface of spherical fly ash then cracked under aging step without hydrothermal treatment, finally its product was completely modified resulted as like-flakes covering particles [40].

2.4 Hydrothermal synthesis

Hydrothermal synthesis is known as a simple and cost effectiveness method of zeolite synthesis. With less energy consumption, fast kinetics reaction and etc., hydrothermal synthesis became an attractive method among pioneering techniques. The synthesis method involving the Si/ Al composition with other elemental composition which mainly influences microporous crystalline surface. Molecular

structure of Si and Al particles undergoes the modification with the existence of alkali-supersaturated solution. The crystallization and reaction mechanism has been predicted [6].The Hydrothermal phenomena generated inside the autoclaved has been predicted and designed. The autoclave equipped with thermal control system including thermocouple, heater, and electric circuit. Hence, temperature in the system is accurate and effective to desired structure. The pressure was arisen regarded to the vapor pressure of NaOH solution. The solution starts to saturate as the temperature inside autoclave approaches 100°C and continuously increases. The characterization results have sustained with previous studies that sodalite formed at low temperature. The increments of temperature produce more sodalite and cancrinite phases obviously identified by XRD patterns and SEM.

2.5 Adsorption

Adsorption describes the phenomena between adsorbent surface and the adsorbate ion which is to be adsorbed onto active site. The adsorption is generally get to know as the one or more components in the region between two bulk phases including interfacial layer and adsorption area. In this context, one of these phases is necessarily a solid and the fluid (i.e. gas or liquid). With certain systems (e.g. some metals exposed to hydrogen, oxygen or water), the adsorption process is accompanied by absorption, that is the penetration of the fluid into the solid phase. Adsorption and desorption are often used to indicate the direction from which the equilibrium states have been approached. Adsorption hysteresis arises when the amount adsorbed is not brought to the same level by the adsorption and desorption approach to a given ‘equilibrium’ pressure or bulk concentration. The relation, at constant temperature,

between the amount adsorbed and the equilibrium pressure, or concentration, is known as the adsorption isotherm.

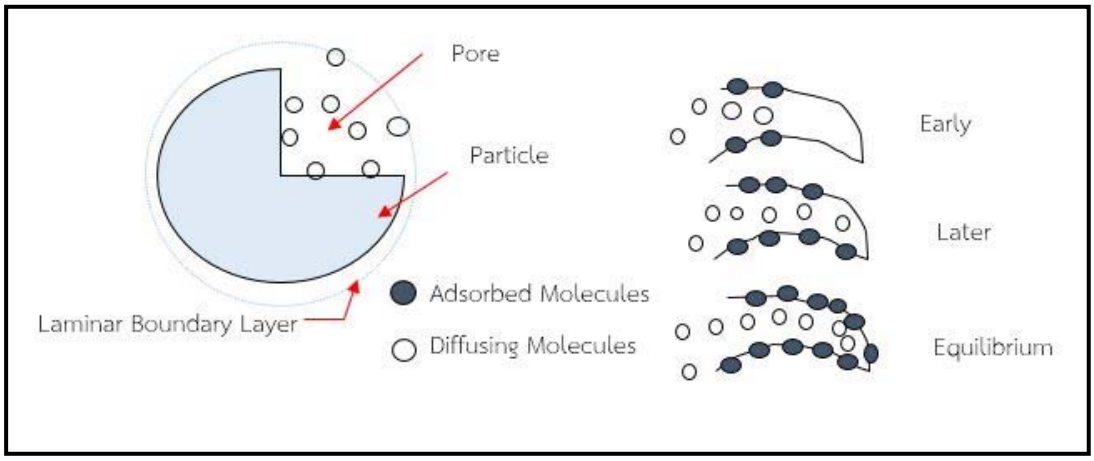

Figure 2.11 Adsorptive Equilibrium of particle

The surface area is frequently used in the current literature in an ambiguous manner. In principle, we can identify an experimentally accessible surface area, which is available for the adsorption of certain adsorptive as graphically described in Figure 2.11. The adsorbate encounters to the material active site until saturation point is achieved.

2.5.1 Types of adsorption

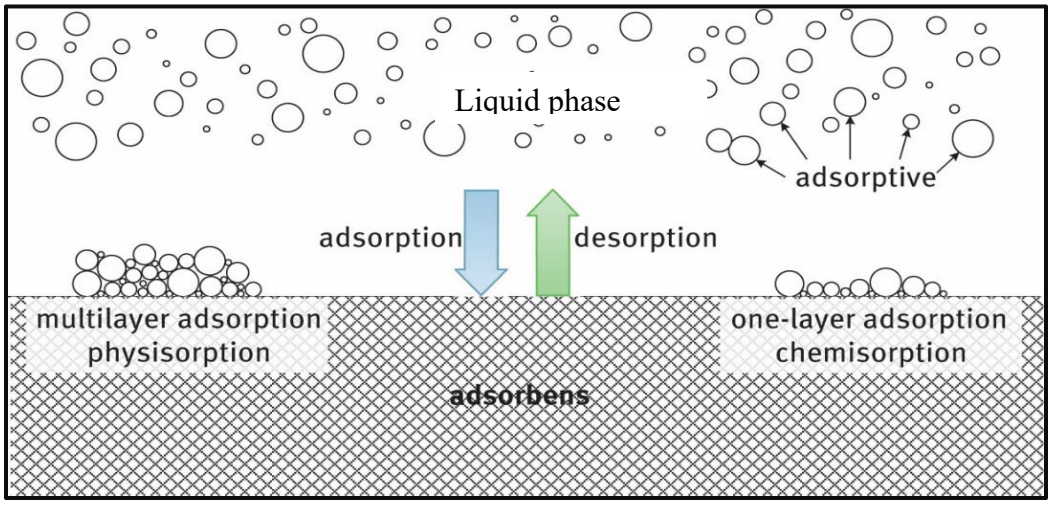

Figure 2.12 Adsorption behavior

Forces of attraction are existed between adsorbate and adsorbent. The forces of attraction that is occurred on adsorbent surface, might be either the Vanderwaal forces which are weak forces or the chemical bond which are strong forces. Figure 2: shows the differences of adsorption types which adsorptive accumulated on adsorbent surface. On the types basis of attraction force between adsorbate and adsorbent, the adsorption can be distinguished into two types which is physicochemical and chemical adsorption as follows;

1. Physical Adsorption

Physical Adsorption or physi- sorption is defined when force of attraction existing between adsorbate and adsorbent are weak Vander Waals forces of attraction. The physisorption typically takes place with formation of multilayer of adsorbate on adsorbent. No chemical was changed on adsorbent.

2. Chemical adsorption

Chemical adsorption or chemisorption is defined when force of attraction existing between adsorbate and adsorbent are chemical forces of attraction or chemical bond. Surface compound is formed when the chemisorption takes place on adsorbent. Its heat of adsorption is higher than physisorption which is 20-400 kJ/mol and has positive effect on temperature. The adsorptive was accumulated into monolayer. The adsorption process is irreversible which has strong attraction on adsorbate and adsorbent [41]. Two types of adsorption is obviously differentiated as shown in Table 2.5.

Table 2.5 Differences between physisorption and chemisorption [41]

	Physisorption	Chemisorption
Bonding force	Van der Waals	Chemical bond (similar)
Chemical change of adsorbate	None	Surface compound Formation
Heat of adsorption	Low, 10-40 kJ/mol	High, 20-400 kJ/mol
Effect of Temperature	Negative	Positive (some extent temperature); activated adsorption
Reversibility	Reversible process[1]	Irreversible
Layer Formation	Multilayer	Monolayer

[1] Desorption occurs when decreasing the adsorption activity in fluid surrounding surface

2.5.2 Adsorption Isotherms

To predict the adsorption behavior between adsorbent and adsorbate, two adsorption Isotherm models have been proposed in this study as follows;

1. Langmuir Model

Langmuir isotherm model is the simplest model describing coverage behavior between adsorbed molecules to active sites, can be obtained from equation 1. Its linearized form is illustrated in Eq. 1. [42].

$$q = q_{max}\frac{K_L C}{1+K_L C} \qquad \text{Eq. 1}$$

$$\frac{C_e}{q_e} = \frac{1}{q_m K_L} + \frac{C_e}{q_m} \qquad \text{Eq. 2}$$

Where; C_e represents concentration at equilibrium (mg/L), q_e is adsorbed capacity at equilibrium (mg/g), q_m is maximum capacity (mg/g), and K_L is adsorption constant or energy of adsorption (L/mg).

2. Freundlich Model

Another simple adsorption model which frequently used is Freundlich isotherm. It is an empirical model which implies the fitted experimental data as a multilayer sorption occurred onto a heterogeneous surface. The model is described following Eq. 3, and Eq. 4 indicates its linearized form.

$$q = K_f C_e^{\frac{1}{n}} \qquad \text{Eq. 3}$$

$$\ln q_e = \ln K_f + \frac{1}{n} \ln C_e \qquad \text{Eq. 4}$$

Where; K_f indicates sorption capacity per unit mass sorbent (mg/g), 1/n represents sorption intensity. The 1/n value allows predicting sorption phenomena. The slope between 0-1 correlates to a chemisorption process; it is more heterogeneous as the value get closer to 0. The obtained slope is above 1, that it is consistent with multi-adsorption [43, 44].

2.5.3 Adsorption Kinetics

Adsorption behavior typically involves thermodynamics and kinetics performance of adsorbent, sorption capacity is a great significance factor for large scale applications. Generally, kinetics models have been applied to determine rate constant or residence time relevance to adsorption performance in fixed bed or design flow in the system. Several mathematical models have been proposed to explain the adsorption data. These models of adsorption can imply the adsorption reaction, describe the adsorption diffusion. The diffusion controlled process is predicted based on three coherent steps;

firstly, external diffusion which is defined as the diffusion across the liquid film surrounding the adsorbent particles, secondly internal diffusion which is referred to the diffusion in the liquid contained in the pores/along the pores wall, also called as intraparticle diffusion, and lastly adsorption and desorption between the active sites and adsorbing molecules.

1) Pseudo First Order

The earliest model describes the adsorption behaviors (chemisorption/physorption) between solid and liquid phase based on the adsorption capacity, as presented in Eq.5

$$\frac{dq_t}{dt} = k_2(q_e - q_t) \qquad \text{Eq. 5}$$

$$q_t = q_e(1 - e^{-k_1 t}) \qquad \text{Eq. 6}$$

$$\log(q_e - q_t) = \log q_e - \frac{K_{pt}}{2.303} t \qquad \text{Eq. 7}$$

Where; q_e and q_t indicate the adsorption capacities at equilibrium and time t (min), respectively. K_{p1} is the pseudo first order rate constant (min^{-1}). Integrating Eq. 5 requires substituting $q_t = 0$ at $t = 0$ and $q_1 = q_t$ at $t = t$ boundary condition [45], the kinetics parameters can be obtained from log (qe- qt) versus t plot. Non-linearized and linearized form are indicated in Eq 6 and Eq 7, respectively.

2) Pseudo Second Order

The basic assumption for pseudo second order kinetic model (Eq. 8) is reported that adsorption reaction on adsorbent surface is rate controlling step [46]. Based on the literature, once the pseudo second order model is applicable, the adsorption rate is found to respect to the availability of adsorption sites rather than the concentration of adsorbate in bulk solution. The model is expressed as the adsorption sites availability on adsorbent surface at time (t).

$$\frac{dq_t}{dt} = k_2(q_e - q_t)^2 \qquad \text{Eq. 8}$$

$$q_t = \frac{k_2 q_e^2 t}{1 + k_2 q_e t} \qquad \text{Eq. 9}$$

$$\frac{t}{q_t} = \frac{1}{k_2 q_e^2} + \frac{1}{q_e} t \qquad \text{Eq. 10}$$

Where; q_e and q_t indicate the adsorption capacities at equilibrium and time t (min), respectively. K_{p2} is the pseudo second order rate constant (min^{-1}). Integrating Eq. 8 requires substituting q_t=0 at t=0 and q_1=q_t at t=t boundary condition [45], the kinetics parameters can be obtained from t/q_t versus t plot. Non-linearized and linearized form are indicated in Eq 9 and Eq 10, respectively. The rate law is originally complexed, however it can be derived and transformed into a simple hyperbolic plot and clearly identify using mathematical forms (Eq. 9). The kinetics parameters can be obtained from its linear equation (Eq.10).

CHAPTER 3

MATERIALS AND METHODOLOGY

In this chapter, the methodology is divided into three main parts. Firstly, synthesis of zeolite via hydrothermal method has been focused on the effects of temperature and time on crystallites formation. Secondly, characterization of material; raw fly ash, and synthesized zeolites. Lastly, the synthesized zeolites compared with raw fly ash were evaluated in sulfate and selenium sorption with the statistical analysis. The experimental procedure is described in the Figure 3.1;

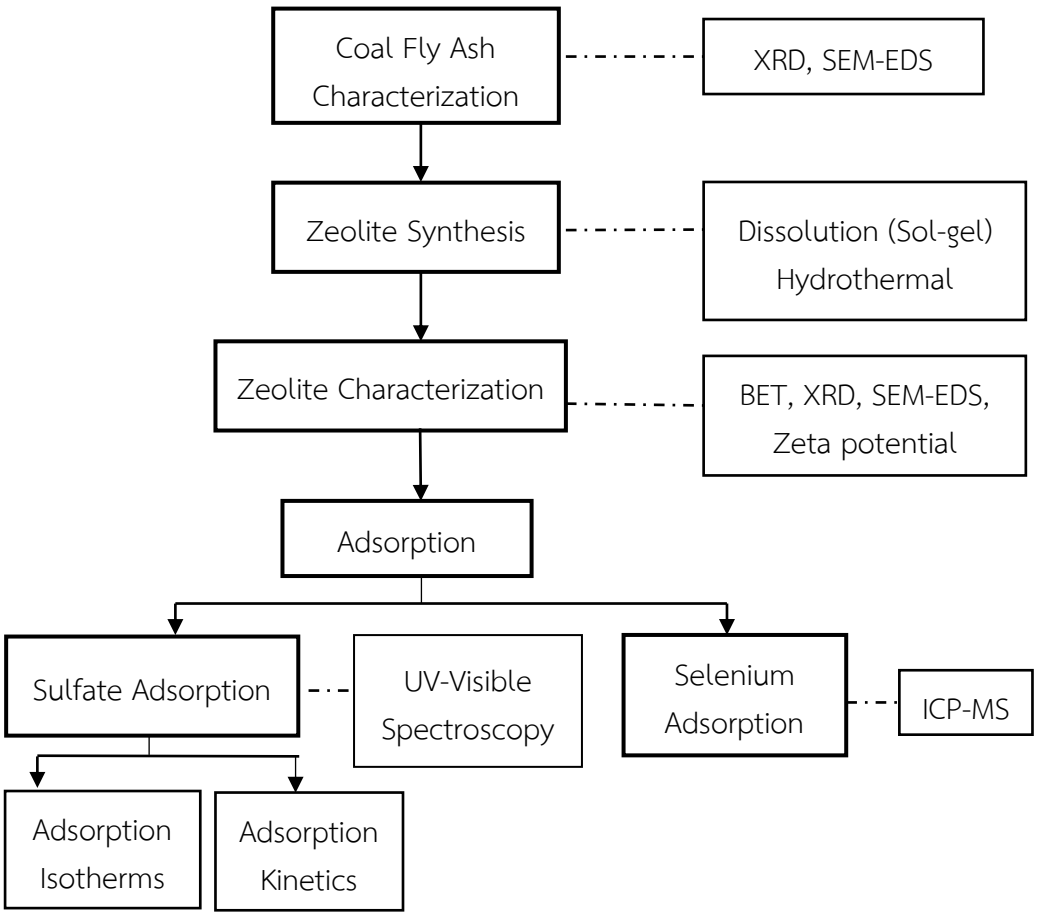

Figure 3.1 Experimental flowchart

3.1 Materials

3.1.1 Chemicals

1) Coal fly ash (Mae Moh electricity generating plant, Lampang, Thailand)

2) Sodium Hydroxide (NaOH, Merck Chemical, Germany)

3) Sodium Selenite (Na_2SeO_3, 44%, Acros organics, Belgium)

4) Sodium Sulfate (Na_2SO_4, Carlo Ebra Reagents, S.A.S.)

5) Magnesium Chloride ($MgCl_2 \cdot 6H_2O$, Carlo Ebra Reagents, S.A.S.)

6) Sodium Acetate (CH_3COONa, Carlo Ebra Reagents, S.A.S.)

7) Potassium Nitrate (KNO_3, Carlo Ebra Reagents, S.A.S.)

8) Acetic Acid (CH_3COOH 99%, Carlo Ebra Reagents, S.A.S.)

9) Barium Chloride ($BaCl_2$, Carlo Ebra Reagents, S.A.S.)

3.2 Methodology

3.2.1 Zeolite synthesis

Coal fly ash, a by-product from lignite coal combustion process was collected from Mae Moh coal fired electricity generating plant (Lampang, Thailand). In preparation procedure, concentrated NaOH solution of 2.8 M was used as a leaching solvent. Zeolite synthesis was conducted in a 400ml stainless steel autoclave equipped with proportional integral derivative (PID) control of temperature consisting of heating jacket, and thermocouple which pressurize due to the heat inside the closed system. This pressurized autoclave enhances crystallization phenomena, and surface cracking onto particles.

Mae Moh coal fly ash as a raw material was utilized undergone hydrothermal treatment for zeolites. Zeolite synthesis was carried out in a 400ml stainless steel autoclave equipped with heating jacket and thermocouple which pressure was arisen due to increasing temperature inside a closed system, design system is as shown in Figure 3.2. In this study, the methodology was modified from previous research [47] by dissolving 10 g of NaOH into 30.25 g of deionized (DI) water, and adding 16.86 of CFA into 250 ml beaker, then they were vigorously mixed by a magnetic bar on hotplate stirrer. Then, ten grams of the mixture was transferred into NaOH solution consisting of 61.2 g DI water and 5.61 g of NaOH anhydrous, named as seed gel. The mixture was vigorously mixed for 30 minutes at 95°C. Next step, mother gel was prepared by dissolving 8.27 g of NaOH into 75 g of DI water, adding 7.98 g of CFA. All mixtures, seed gel and mother gel were mixed for 3 hours at 100°C. The mixture was transferred into the autoclave. The operating temperature was varied by varied by at 105, 130, 155, and 180 °C and aging for 6-72 hours.

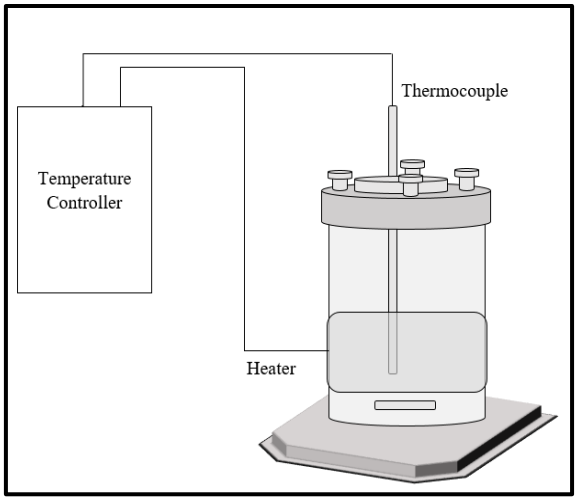

Figure 3.2 The autoclave equipped with heating jacket and thermocouple controlled by proportional integral derivative (PID) system

3.2.2 Characterizations

1) X-ray Diffraction (XRD)

Synthesized zeolite powder was characterized via instrumental techniques; x-ray diffraction (XRD, D8 advance Bruker, Germany) with Cu-Kα radiation, wavelength of 1.5406 Å, data collected at 0.02 steps within 10-50° of 2theta.

2) Fourier Transform Infrared (FTIR)

Functional groups of synthesized zeolites were determined using KBr-FTIR Spectrometer (EQUINOX 55, BRUKER, Germany) at 400-4,000 cm^{-1} wavelength.

3) Scanning Electrode Microscope (SEM) and Energy Dispersive Spectroscopy (SEM-EDS)

Particles surface was analyzed by SEM (SEM-EDS, JEOL 6110LV, USA). Small portion of samples take place onto tape coated on aluminum holder. EDS analysis, aluminum holder painted by silver to electrically enhance image resolution.

4) Zeta Potential

Zeta potential and particle size measurement, 0.5% weight of zeolite powder was dispersed using ultrasonic bath (Telsonic, UK) in deionized water. The solution was inserted into the cell and measured by zeta potential analyzer (Malvern, Germany), pH 2-12 auto-titrated with 0.5 M NaOH and 1 M HCl. Specific surface area of a material is determined by Nitrogen physisorption technique.

5) Bruneaur-Emmett-Teller (BET)

Bruneaur-Emmett-Teller (BET) is a common instrumental technique for specific surface area determination. Surface material was assumed as homogeneous. In this work nitrogen adsorption was performed at 573 K for 3 hours.

3.2.3 Sulfate Adsorption

Batch adsorption experiments were carried out at ambient condition. Synthetic sulfate solution was prepared by weighing Na_2SO_4 1.4878 g, then added up deionized water to 1000 ml. The calculated concentration was controlled at 1000 mg sulfate/L, dilution factor 10-100x. The plot between reading absorbance versus concentration of sulfate for calibration curve was prepared within the range of 0- 40 mg/ L. The synthesized zeolite of 50 mg was added into 50 ml of synthetic solution under constant agitation by magnetic stirrer. Then, the suspension was filtered through Nylon filter 0.45 μm. Sulfate measurement using spectrophotometer (Jasco 730V, Japan) at 400 nm wavelength, the method is involved sulfur determination in solution, barium chloride ($BaCl_2$) was precipitated with sulfur in acidic solution resulting as white precipitates of barium sulfate (BaSO4). The remaining sulfate in adsorbed solution was determined by calibration curve preparation with the range of 0-40 mg/L sulfate. Above 40 mg/L is the beyond detection limit, hence the reading value will be less accuracy. The adsorption capacity and percent removal of the materials were calculated using equation 5 and 6, respectively.

$$q_t = \frac{C_0 - C_t}{M} V \qquad (5)$$

$$\text{Removal (\%)} = \frac{C_0 - C_t}{M} \qquad (6)$$

Where; q_t exhibits the sorption capacity (mg/g), C_0 and C_t represent initial concentration and concentration at certain time (mg/L), respectively. V indicate volume of solution (L). Lastly, M is the mass of adsorbent (g)

3.2.4 Selenium Adsorption

The experiment was carried out in a batch system at ambient condition. The synthetic sulfate contaminated water was prepared by measuring 2-12 mg of Na_2SeO_3 which is 2.887-46.23 µmol Se/L. The 50 mg of synthesized zeolite III (SZ III, 105°C, 12 hours) was added into 50 ml of synthetic solution at stirring speed 150 rpm for 1 hours. Initial concentration, contact time and pH solution were the independent factors. After the adsorption complete, SZ III as the adsorbent was filtered out through filter paper 0.25 µm equipped with vacuum pump. The solution was kept in the bottle, the pH was measured and adjusted to 2. The remaining Se in adsorbed solution was measured by inductively couple plasma (ICP).

CHAPTER 4

RESULTS AND DISCUSSION

Throughout the experiment, coal fly ash as a main role, undergoes in the structure and surface modification via hydrothermal technique and utilizes in wastewater treatment, particular to coal-fired wastewater problems. The chapter is divided into three sections, including synthesis of zeolite, characterization of obtained materials and the reduction of sulfate and selenium contaminated in wastewater (synthetic one).

4.1 Synthesis and characterization

Prior to the synthesize the zeolite using CFA, the CFA was characterized for its chemical species. Si and Al generally play a crucial role in zeolite synthesis, CFA as a raw material composed of O, Si, Al, Ca, and Fe as the main component with 17.7, 12.4, 11.86, and 12.70 % weight, respectively. In oxide forms of SiO_2 and Al_2O_3 contribute appropriate structure with ultrafine pore sizes, beside these silica and alumina possess high porosity and large surface area. The amorphous silica properties provide high surface area, with small particles features to macroscopics gels depends largely on its surface properties. However, the present of calcium having 839 °C of melting point, and crystalline in the faced center cubic is able to inhibit the porous generating surface onto synthesized zeolites. Zeolite often gains cations during synthesis like Na^+ and K^+. This synthesized material was categorized into low silica zeolite grade due to Si/Al obtained as 1.27 which is below 2. The common mineralogical phase of low silica

zeolite that can be transformed includes cancrinite (CAN), sodalite (SOD), Na-X, analcime, natrolite, and philipsite phase [35]

CFA and synthesized zeolite elements have been analyzed by EDS. Table 2 illustrated the elemental composition of CFA and selected synthesized zeolite based on highest S_{BET}. Si, Fe, Ca, and O are the main elements composed in CFA, and synthesized zeolite. Sol-gel preparation, hydrothermal treatment and filtration procedure influences the reduction of Ca and Fe weight and the increasing of Si and Al content. Silica (SiO_2), alumina (Al_2O_3), and iron oxide have significant effect on adsorption, this is to be further explained in adsorption part.

CFA categorized into class F Fly ash, C316 ASTM standard. undergoes dissolution process with high alkalinity hydrothermal treatment. Several trace elements composed in coal fly ash are subjected to be eliminated. Seed gel and mother gel preparation is a pretreatment to dissolve amorphous phases CFA. Stirring speed has significant effect on increasing Si and Al which enhance SiO_2/Al_2O_3 ration in the product [48]. In this study, CFA undergoes pretreatment by 2 gels preparation at 100 °C for 3 hours, and vigorously agitation using magnetic stirrer. As a result, calcium is found decreased in the product obtained by 105 °C, 12 hours hydrothermally synthesis. Calcium and trace elements dissolution are the effect of highly alkaline and agitation during pretreatment, consequences surface cracking in hydrothermal process.

4.1.1 SEM-EDX analysis

Elemental composition of coal fly ash and synthesized zeolite were tabulated in Table 4.1. The Si/Al ratio was 1.428 reduced into 1.268. CFA composed of calcium and iron as 11.86 and 12.7 respectively, was undergo highly alkali treatment (NaOH 12.8 M). After aging during dissolution and hydrothermal process under vigorously mixing, zeolites particles size was reduced, this can be observed by SEM along with the reduction Fe and Ca contents. Since lime ($Ca(OH)_2$) cannot tolerate with high alkalinity, thus it dissolves. Influencing of temperature and pressure in a closed reaction can crack the surface of raw fly ash and generate porous structure with crystallization, hence increase in specific surface area.

Figure 4.1(a) and (b) illustrates the elements reflected on the energy distributed on respected to the existing elements of CFA and synthesized material (105 °C, 12 hours). The highest intensity of oxygen presented at 0.5 keV of both materials. Ca with lowest energy evidently reduced at 0.3 keV after treatment. Al and Si obviously increased at 1.5 and 1.75 keV which are the highest energy of element.

Effects of hydrothermal treatment on elemental composition of coal fly ash, analyzed by EDS. Table 4.1(a) shows that CFA contains calcium as the highest element. While SiO_2/Al_2O_3 of 1.87 was increased into 2.13, ferric oxide 11.6 % and higher. Specific surface area is not only depended on the hydrothermal temperature and aging time but also Si/Al ratio and Na^+ from alkali solution. This research achieved sodalite as a main product integrated with cancrinite phase, Na-P1 presented in less amount. It assumed that calcium content could not be dissolved during sol-gel preparation that inhibits crystallites growth in hydrothermal process.

Table 4.1 (a): Elemental composition of CFA analyzed by SEM-EDS

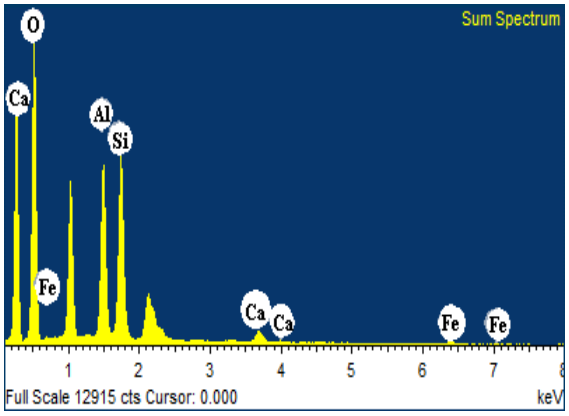

Element	Weight (%)	Atomic (%)
O K	46.09	64.49
Al K	12.04	9.99
Si K	17.31	13.80
Ca K	11.86	6.63
Fe K	12.70	5.09

Figure 4.1 (a): Energy distributed spectroscopy of CFA analyzed by SEM-EDS

Table 4.1 (b): Elemental composition of synthesized zeolite (105°C for 12 hours) analyzed by SEM-EDS

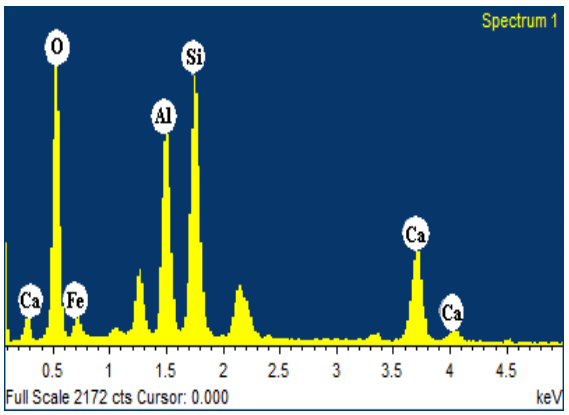

Element	Weight (%)	Atomic (%)
O K	61.56	74.22
Al K	15.02	10.74
Si K	19.40	13.32
Ca K	2.43	1.17
Fe K	1.59	0.55

Figure 4.1 (b): Energy distributed spectroscopy of synthesized zeolite (105°C for 12 hours) analyzed by SEM-EDS

4.1.2 XRD analysis

. The common mineralogical phase of low silica zeolite that can be transformed includes cancrinite (CAN), sodalite (SOD), Na-X, analcime, natrolite, and philipsite phase [35] corresponding to the obtained XRD pattern, sodalite is strongly present and consistently decreased as other phase formed. Figure 4.3 illustrates the mineralogical composition in CFA, the sharpest peak of quartz presents at 25.5° as the main phase, with minor peaks of anhydrite, calcite, magnetite, and hematite.

For mineralogical analysis, based on Joint Committee on Powder Diffraction Standard (JCPDS) database, XRD spectra of CFA exposed crystal structures of the quartz [SiO_2 (pdf 83-2456)], anhydrite [$CaSO_4^{2-}$ (pdf)], calcite [$CaCO_3$ (pdf 01-0837)], magnetite [Fe_3O_4 (19-0629)] and at two theta(s); 25.5°, 31.4°, 33.3°, 35.6°, 37.5°, 40.9°, respectively [49]. Anhydrite is typically less soluble, and stable at high pressure and temperature. However, it could not handle the high alkalinity.

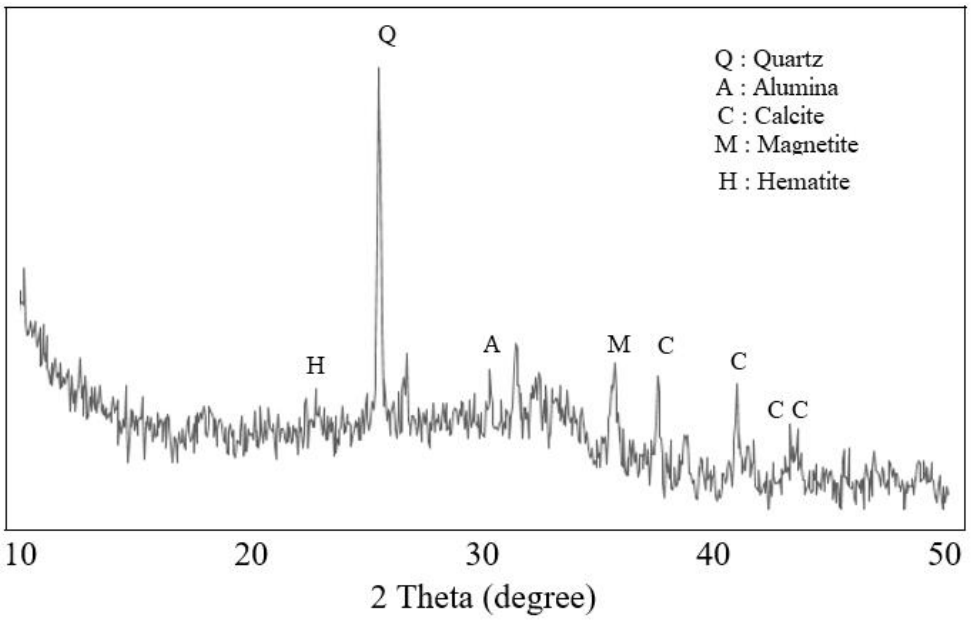

Figure 4.3 XRD pattern of Mae Moh coal fly ash

In this study, XRD analysis were made only on hydrothermal synthesis as a function of temperature within the range 105-130 ℃. Hydroxy-sodalite (JCPDS: 81-0704), cancrinite (JCPDS: 752318), and Na-P1 (JCPDS: 39-0219) [49] phases were presented at 2theta of 13.9 (6.3977 Å), 24.3, 28.92, 29.97, 33.08, 34.48, 39.61, and 40.11, and 45.84°, respectively. Crystallographic data indicates lattice vectors and plane of mineral structure. Sodalite has 110 and 211 of d_{hkl} presented at 14.01 and 24.36°, respectively. According to Figure 5, Na-P1 peak sharply presents at 33.28° with high intensity, and 39.87°. Sodalite favors to form under mild condition. However, Na-P1 has been reported to be gradually decreased because of sodalite formation [50]. This can be implied that sodalite phases with meso-porous surface can be formulated in high intensity at 105-130 ℃, the elevating temperature will induce cancrinite and the other amorphous phase. However, not only crystallization temperature and time have significant impacts on crystallite surface but also Na_2O concentration, and Si/Al ratio.

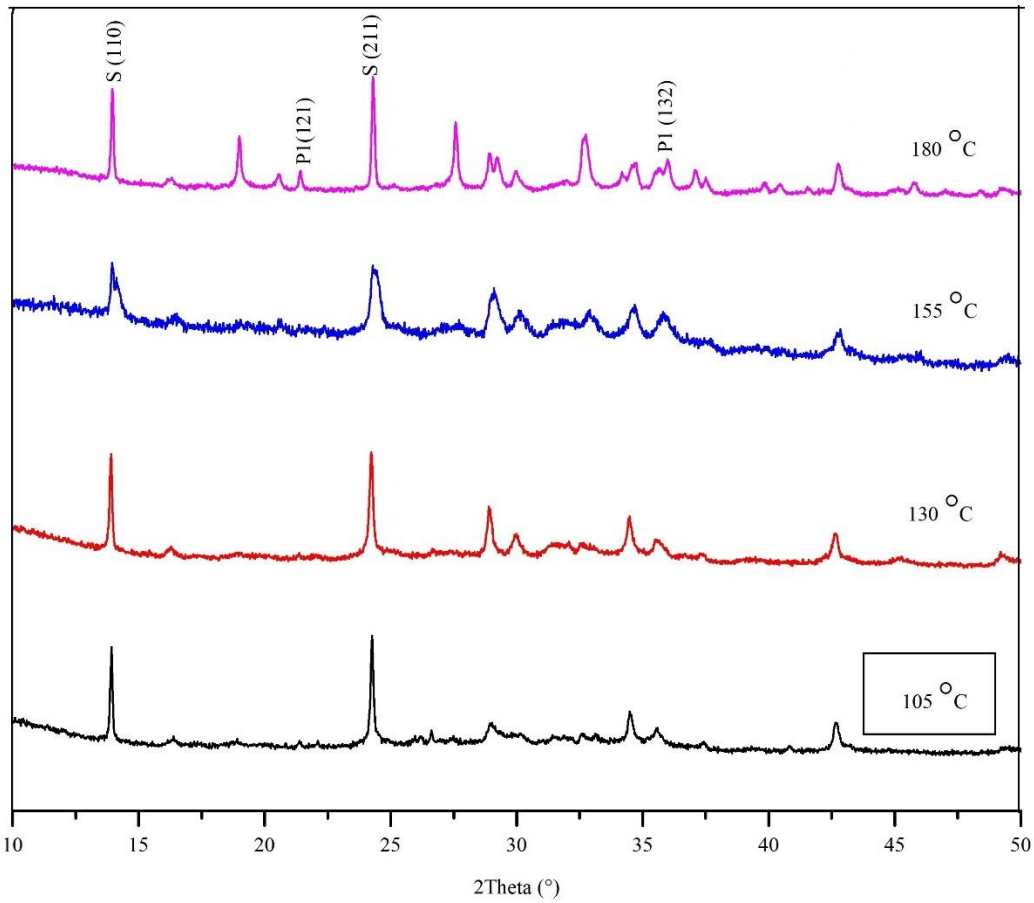

Figure 4.4 XRD patterns of synthesized zeolite at 105°C, 130°C, 155°C and 180°C

Cancrinite peak at 28.92° evidently grows sharply at 130 and 155 °C, Na-P1 presented at 180 °C as in Figure 4.4. Sodalite and cancrinite are existed in similar 2theta position. Peak intensity belonging to Na-P1 yields broader and higher in zeolite sample of 180°C synthesis. This synthesis condition was simulated as natural zeolite formation under the surface's earth. Zeolite transformation mechanism has been previously suggested that it occurs in four stages; amorphous phase or zeolite A dissolution, supersaturation of hydroxysodalite, sodalite or Na-P1 nucleation, and subsequently nuclei growth [51] which corresponds to xrd patterns, zeolite A, and Na-P1 were formed at mild condition.

4.1.3 Specific surface area analysis

For Bruneaur-Emmett-Teller specific surface area (S_{BET}), within temperature range of 105-180℃ at 12 hours, S_{BET} results as 65.38 ± 0.27 to 25.22 ± 0.1 m^2/g. Independent of aging time 6-72 hours at constant 130℃, the S_{BET} was found at 52.9492 to 36.4706 m^2/g (Table 4.2). The results show that the maximum S_{BET} (65.38 m^2/g) obtained at 105℃ synthesis.

Table 4.2 Physical properties of coal fly ash and synthesized zeolites

Adsorbent/Condition	S_{BET} (m^2/g)	Pore volume (cm^3/g)	Bulk density (g/cm^3)	pH_{zpc}
CFA	0.16	N.A.	1.307	N.A.
105 ℃, 12 hrs	65.38	15.02	0.366	7.4
130 ℃, 12 hrs	45.24	12.165	0.408	3.58
155 ℃, 12 hrs	40.70	9.35	0.4201	6.87
180 ℃, 12 hrs	25.22	5.80	0.352	7.57
130 ℃, 6 hrs	52.95	12.165	0.235	6.97
130 ℃, 24 hrs	42.95	9.175	0.484	6.34
130 ℃, 48 hrs	39.94	8.38	0.452	3.21
130 ℃, 72 hrs	36.47	9.65	0.387	7.13

The increasing temperature induces cancrinite and sodalite phases which typically possesses the small pore sizes and less specific surface area. The significant condition yields the highest BET specific surface area at 105℃ aging for 12 hours. Table 2 shows

that zeolites synthesized at 105°C, 12 hours has highest specific surface area, pore volumes, and recovery (65.28 m^2/g, 15.0212 cm^3/g, and 87.06%). The increment of temperature decreases BET specific surface area, pore volumes, and %recovery values. The temperature of 130°C was chosen to further determine the optimal aging time, the results show that the responses were decreased with longer aging time. In conclusion, characterization of synthesized zeolites, it was investigated that high temperature with constant pressure built up inside the reactor can deteriorate the CFA particles physicals resulting in less responses on BET, pore volume, and recovery. However, S_{BET} is not only depended on temperature and time but also NaOH and Si/Al ratio.

4.1.4 FTIR analysis

Synthesized zeolites with different hydrothermal temperature and time resulted in various minerals composition, these were confirmed by short range FTIR spectrum and XRD, the infrared refraction on the material which disclosed functional groups in each band. The band positions correspond the presence of samples structure. According to Figure 4.5 and 4.6, eight samples similarly attributed bands at 450-460 cm^{-1}which represents Si/Al-O bending, 550-580 cm^{-1} of tetrahedral or octahedral ring, 950-1250 of internal tetrahedra vibration of Si/Al-O stretching, and 3450 cm^{-1} of Si/Al-O-H stretching indicating water inside the molecules [52]. Peaks at 436 and 1105 cm^{-1} wavenumber synthesized zeolite at 180°C are presented. Similarly, the band at 439 was attributed in the synthesized for 72 hours. The higher temperature and time increases the peak of Si/Al-O stretching.

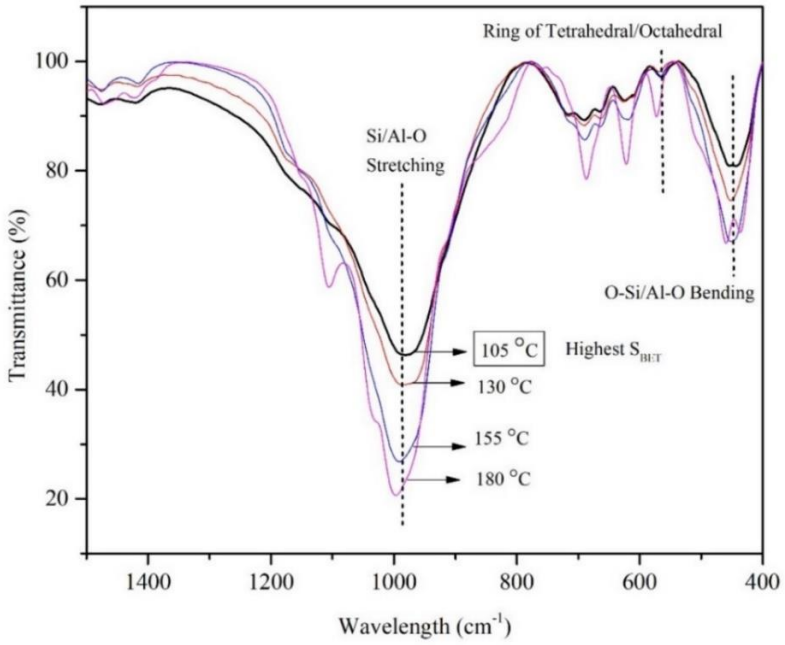

Figure 4.5 FTIR spectra of synthesized zeolites at 105, 130, 155, and 180° C aging for 12 hours

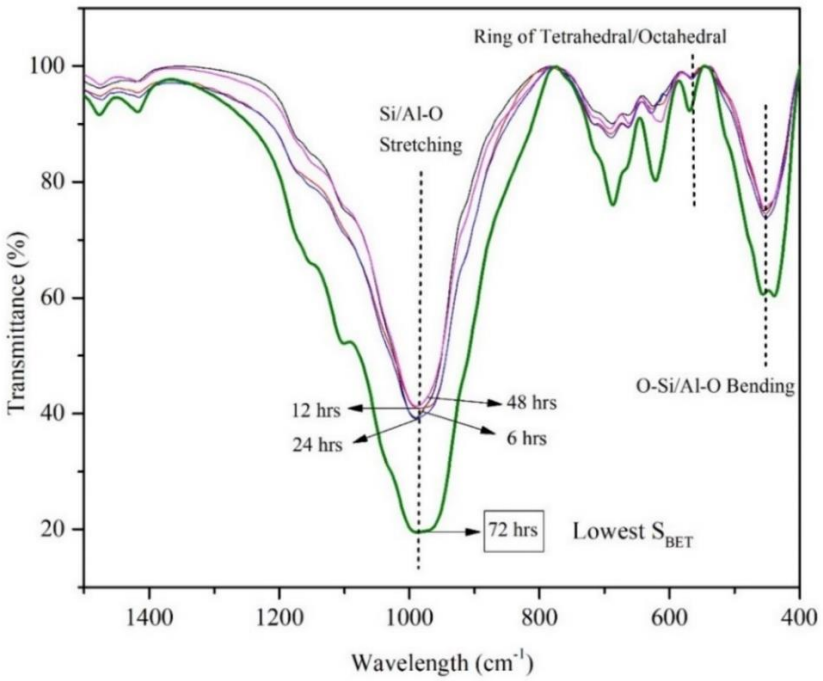

Figure 4.6 FTIR spectra of synthesized zeolites aging for 6, 24, 48, and 72 hours at 130° C

The spectrum attributed around 605 cm^{-1} was examined to be double ring in the GIS-NaP1 zeolite phase [53]. The wavelength at 420-500 cm^{-1} was examined as tetrahedron vibration of Si-O and Al-O of Sodalite (Si/Al-O-Si/Al) bending modes of sodalite confirmed from Flaningen et al [54] study. The cancrinite phase was exhibited on the bands of 622 and 686 cm-1 with high intensity (low % transmittance). These functional groups support XRD and XRF reveals that cancrinite and sodalite were well grown at elevated temperature and time.

4.1.5 Zeta potential analysis

The point of zero charge (PZC) or isoelectric point (IEP) refers to pH at which no electrical charge on particle surface to determine the adsorption phenomena through adsorbent surface. When the particles dispersed in the pH lower than PZC values, protons donated more than hydroxide groups. Particles surface typically constitutes positive charges which is capable to attract anions onto surface of synthesized zeolites [55]. The positive region response of zeta potential indicates that particles surface possesses positive charge on material's surface which attracts the negative ion to be adsorbed on their sites. The PZCs of zeolite synthesis by varying temperature (105, 155, 180°C) were 7.4, 6.87, and 7.57 mV, respectively while at 130°C has 3.58 mV. By varying aging time (6, 12, 24, 48, 72 hours), PZCs were at 6.97, 6.34, 3.21, and 7.31 mV, as illustrated in Figure 4.7 and 4.8. Based on chemical composition and pH value which has significant interactions and effects on adsorption process, can influence and performs attraction and repulsion of material surrounding ionic. In this study, the materials are mainly composed of Si, Al, and O which provides IEP at neutral region. The oxygen is predicted to bond completely with either Si or Al generating into various zeolitic frameworks.

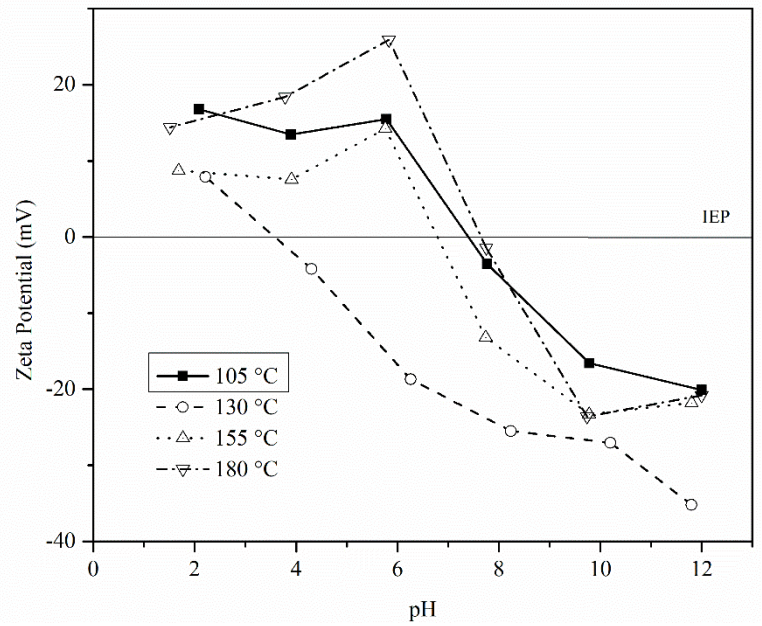

Figure 4.7 Zeta potential of synthesized zeolites as a function of hydrothermal temperature

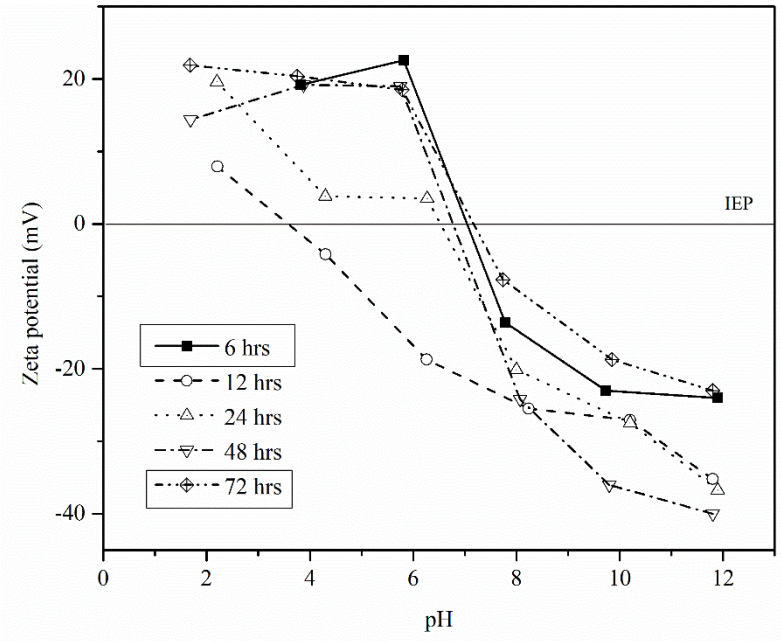

Figure 4.8 Zeta potential of synthesized zeolite as a function of hydrothermal time

4.1.6 SEM analysis

Figure 4.9 shows the particle surface results from 10,000 magnificent resolution including CFA, the synthesized zeolites at 105℃ for 12 hours; 180 ℃ for 12hours; 130 ℃ for 6 hours; and 130℃ for 72 hours. Higher temperature and longer time yields. CFAs has spherical shape, and less porous surface, covered by quartz content as shown in Figure 4.9(a), Figure 4.9(b) shows sodalite phase with porous surface, larger size with aggregation, and cubic wall with channels connecting on the surface. Because this lignite Mae Moh CFA was classified as a low silica zeolite as mentioned in SEM-EDS analysis with NaOH 2.8 M, sodalite cubic structure generated after the treatment.

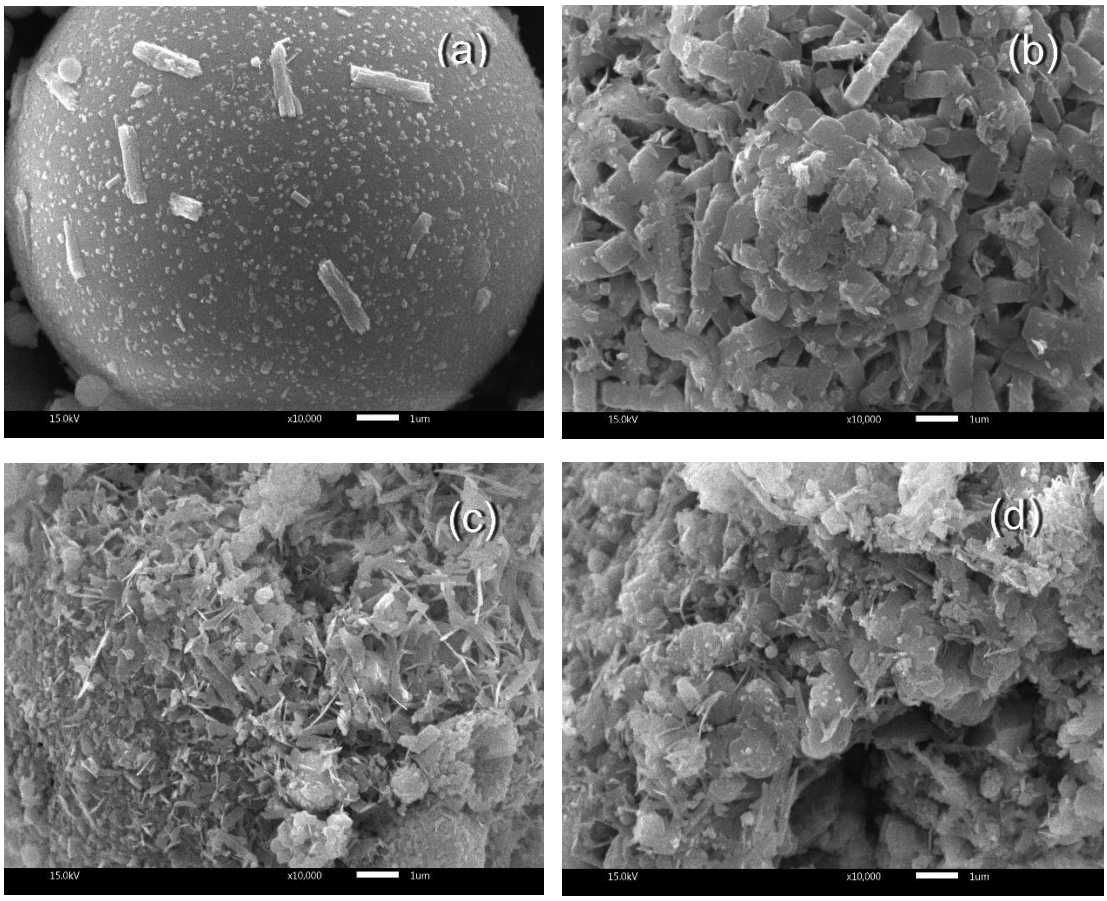

Figure 4.9 Morphology of CFA (a), zeolite synthesized at 105 ℃, 12 hours (b); 130 ℃, 6 hours (c); and 130 ℃, 72 hours (d).

The fibrous surface as illustrated in Figure 4.9(c) exhibits the particle surface like sodalite grown along with cancrinite, this confirmed by the previous studies [35, 55]. Generally, sodalite and cancrinite has hexagonal shape sizing of 20-30 μm, while Na-P1 with fibrous morphology [35]. The fly ash particles might be affected by several factors; chemical composition, high alkalinity, temperature, pressure, and stirring speed. consequently, structural and surface were modified as described previously.

Elemental distribution of two materials; CFA and synthesized sodalite (defined as sodalite) is illustrated in Figure 4.10 (a-b). These contributions correlate to the elemental Silicon (Si) and alumina (Al) were distributed along particles. Elemental mapping reveals that Si and Al content were interacted each other throughout particle not only certain position, they were dissolved and leached in concentrated NaOH solution in the synthesis, therefore porosity generated in particle.

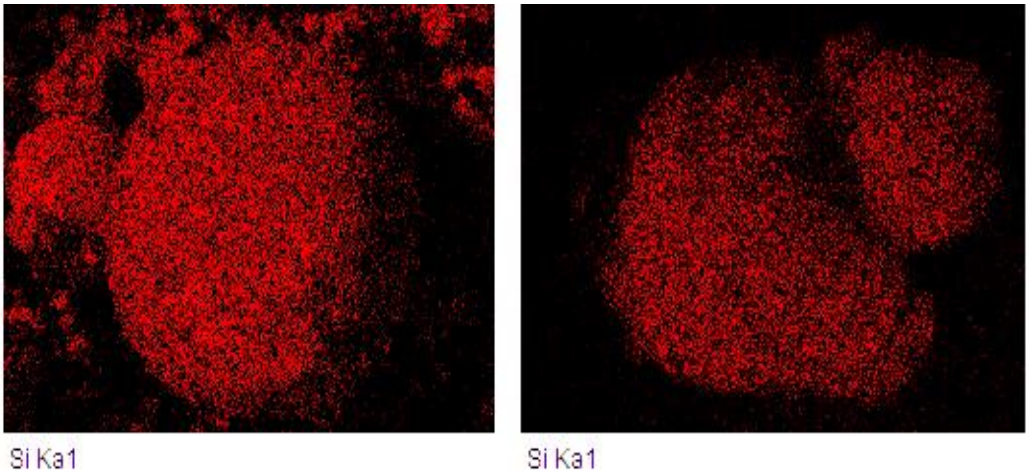

Figure 4.10 (a) Elemental mapping of coal fly ash and synthesized zeolite at 105°C, 12 hours analyzed by SEM-EDS (Si Ka)

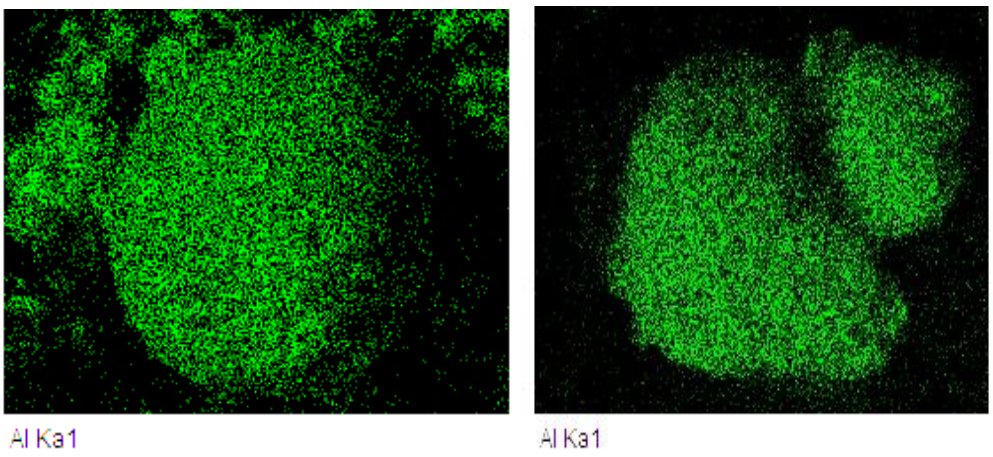

Figure 4.10 (b) Elemental mapping of coal fly ash and synthesized zeolite at 105°C, 12 hours analyzed by SEM-EDS (Al Ka)

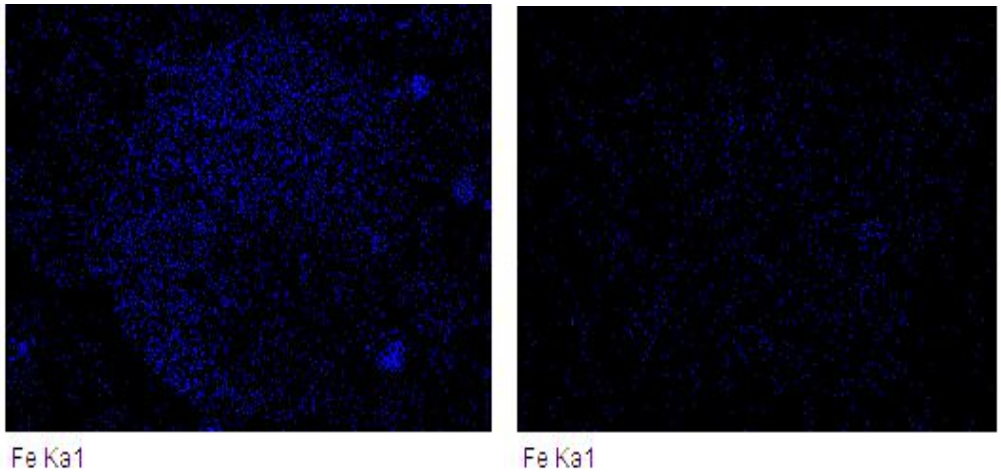

Figure 4.10 (c) Elemental mapping of coal fly ash and synthesized zeolite at 105°C for 12 hours analyzed by SEM-EDS (Fe Ka)

4.2 Sulfate Adsorption

To determine the sulfate quantity in the solution, Barium chloride ($BaCl_2$) is naturally soluble in water, barium (Ba^{2+}) ions binds sulfate SO_4^{2-} ions precipitating into white colloids in solution, hence sulfate ions is measured using spectrophotometer at

400 cm^{-1} of wavelength. Beyond detection limit of spectrophotometry on precipitated barium sulfate is 40 ppm, otherwise determination is less stable.

The interaction between SiO_2, Al_2O_3, Fe_2O_3, and CaO to sulfate uptake is more complicated to investigate than the pure phase component. Synthesized zeolites possess both high calcium content, and high specific surface area which has advantages over sulfate adsorption. Therefore, the removal efficiency will be compared between the coal fly ash with less specific surface area but high calcium content and selected adsorbents as shown in Table 4.3.

Table 4.3 Selected adsorbent for sulfate adsorption determination

Adsorbent	Synthesis Condition	S_{BET} (m^2/g)	Ca (% weight)
Coal Fly Ash	-	0.16	11.86
Synthesized Zeolite I (SZ I)	12 hrs, 180 ℃	25.22	1.3
Synthesized Zeolite II (SZ II)	6 hrs, 130 ℃	52.95	3.2
Synthesized Zeolite III (SZ III)	12 hrs, 105 ℃	65.38	2.43

4.2.1 Effects of pH on sulfate adsorption

The pH factor has been studied between 2 and 9 value. The highest percent removal obtained in the acidic region at pH 2 up to 52% and continuously reduce the uptake as the pH increase. At pH 4-6, the removals remain constant about 40% as shown in Figure 9. The higher initial concentration, the synthesized zeolite can increase the uptake until the equilibrium. The mild acidic at pH between 4 and 6 is as the

wastewater from coal fired power plant, hence, the non-adjust pH synthetic water which is about 5.5-6 is selected for further adsorption section.

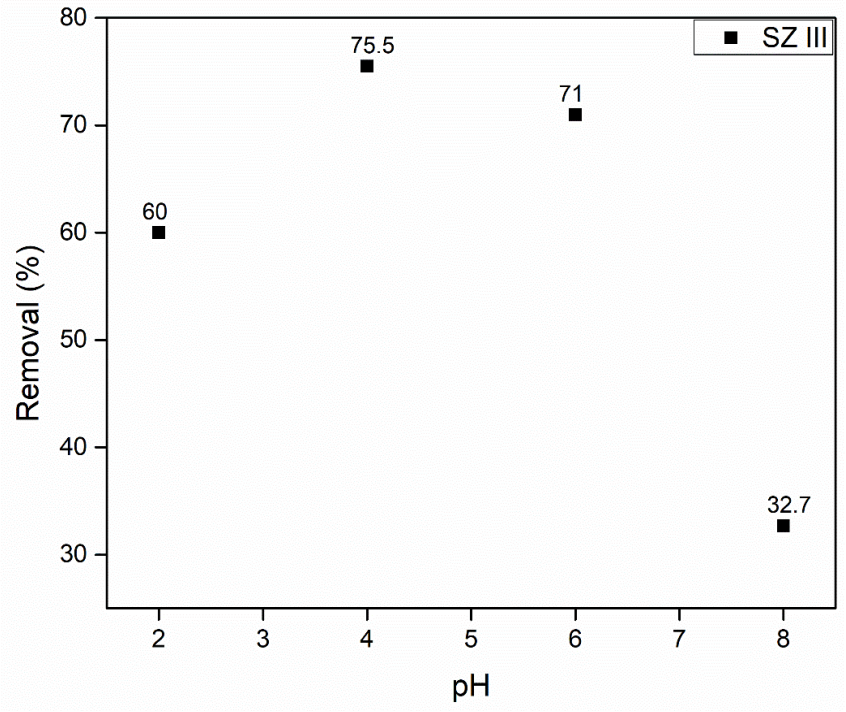

Figure 4.11 Effects of pH on sulfate removal of SZ III at 27°C, aging for 4 hours

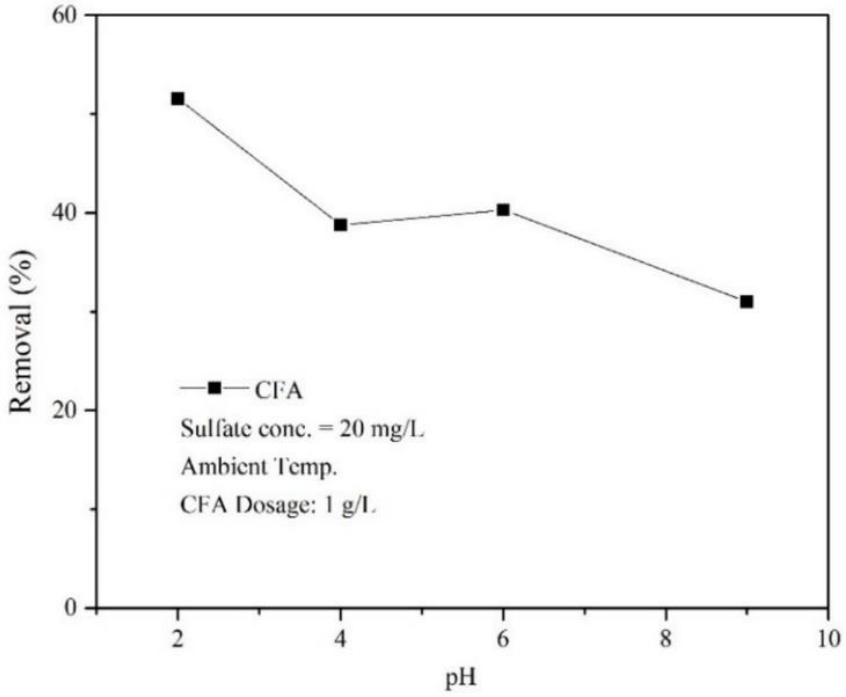

Figure 4.12 Removal (%) versus pH solution (CFA, 27 °C, 4 hours, 20 mg/L)

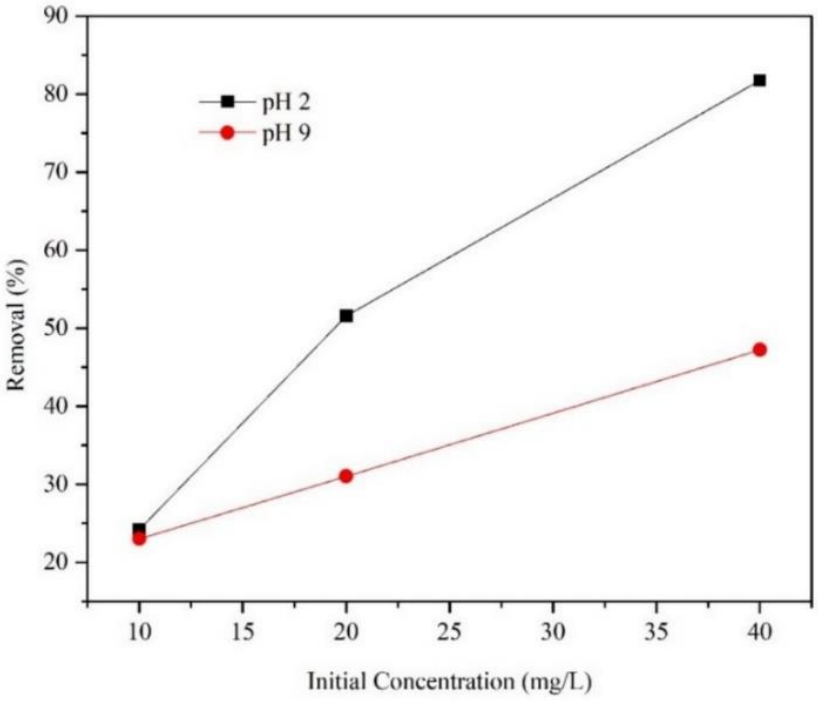

Figure 4.13 Removal (%) versus initial concentration (mg/L) with different pH

According to the results in Figure 4.11-4.13, sulfate continuously removed as the concentration increased 10- 40 ppm, average uptake was 81.7 % and 42.22% at pH 2 and 8, respectively. Sulfate removal is mainly enhanced by pH solution. Higher protons or acidic region the percent uptake is enlarged. The sulfate is satisfactory to be eliminated by the adsorbents in weak acidic region corresponding the previous studies reported that higher pH solution or the present of hydroxide ion does not influence the removal of sulfate [11, 56]

4.2.2 Effects of Contact time

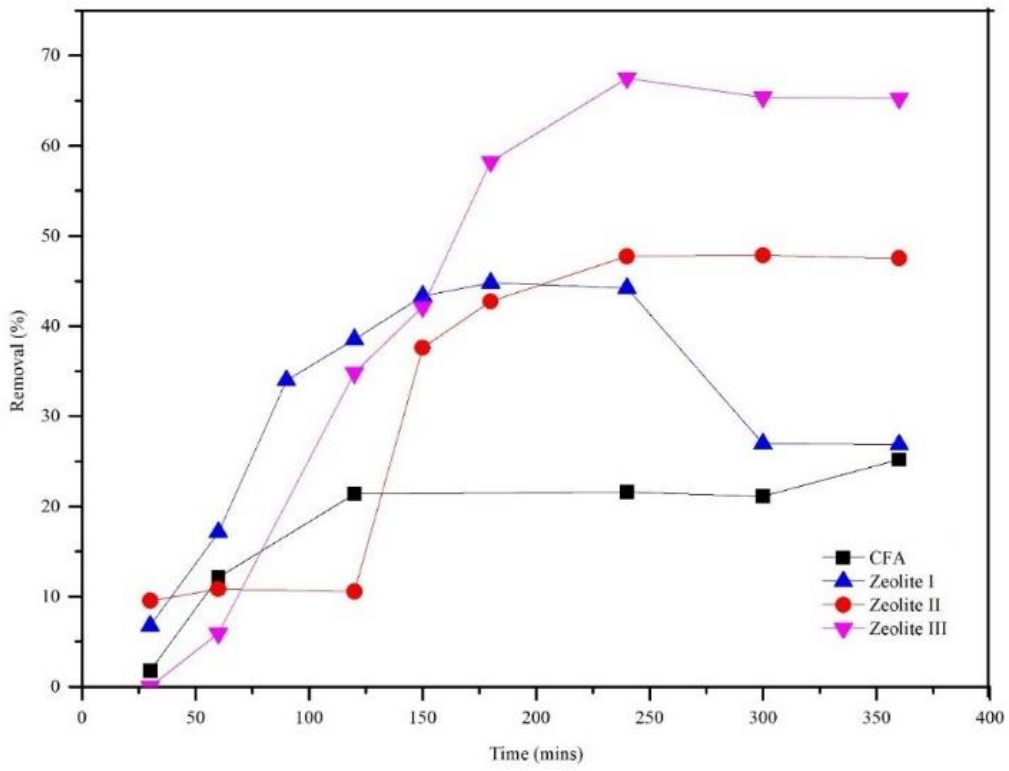

Figure 4.14 Adsorption equilibrium of CFA, Zeolite I, Zeolite II, and Zeolite III

At ambient adsorption in batch system, synthesis condition of zeolite III at 105℃ for 12 hours achieved highest percent removal, equilibrium at 240 minutes adsorption, correspondent to S_{BET} of each material. Higher S_{BET} is capable more removal efficiency. This is because of large specific surface area that highly influences removal onto their active sites. However, not on surface area has impacts to the sulfate removal, calcium can create strong bonding to sulfate ion as well. Therefore, another factor to concern is the effects of calcium content and specific surface area of material that enhance the higher removal of sulfate.

Adsorption equilibrium experiment was carried out at ambient. CFA and zeolite-I rapidly adsorb sulfate and gradually decreased approached the equilibrium after 240 minutes. However, I have found that after sulfate continuously increased after 360 minutes, as illustrated in Figure 4.14. This was implied that there is desorption of sulfate occurred. Hence, adsorption time was selected based on once the adsorption reaches an equilibrium point which is 4 hours.

4.2.3 Adsorption Isotherms

The experiment was carried out by varying sulfate concentration within 0-30 mg/L at constant temperature. The initial pH solution is controlled at 5.6. Three synthesized zeolites were evaluated by sorption capacity results, additional to comparison of adsorption by raw material (CFA) at same condition. Two adsorption isotherm models were applied which are Langmuir and Freundlich models. The experimental results were plotted with isotherms model to observe the data fitness.

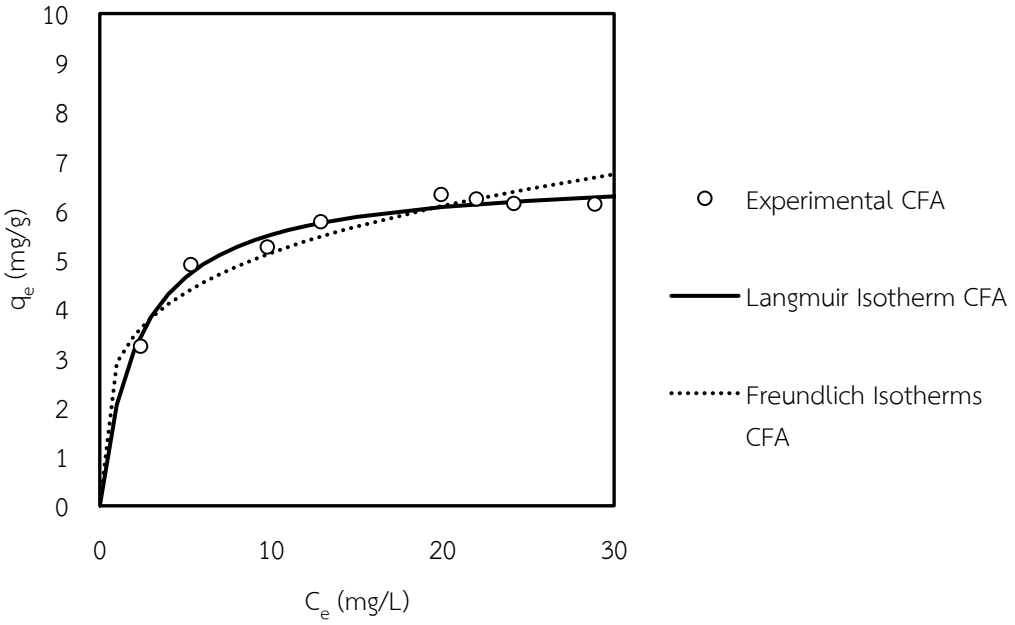

Figure 4.15 (a): Adsorption Isotherms of CFA

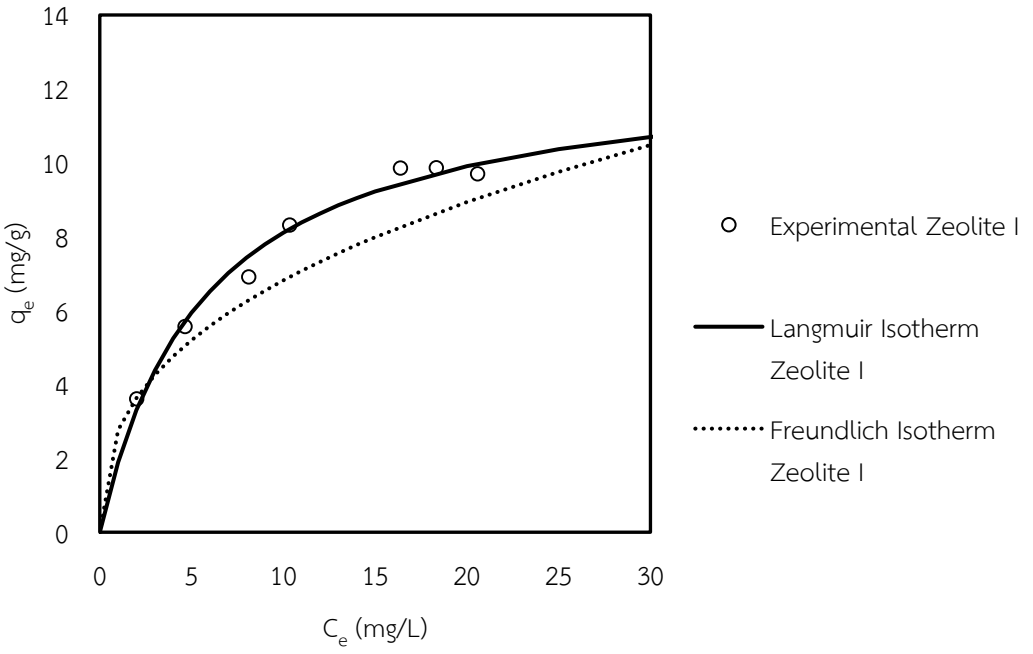

Figure 4.15 (b): Adsorption Isotherms of Zeolite I

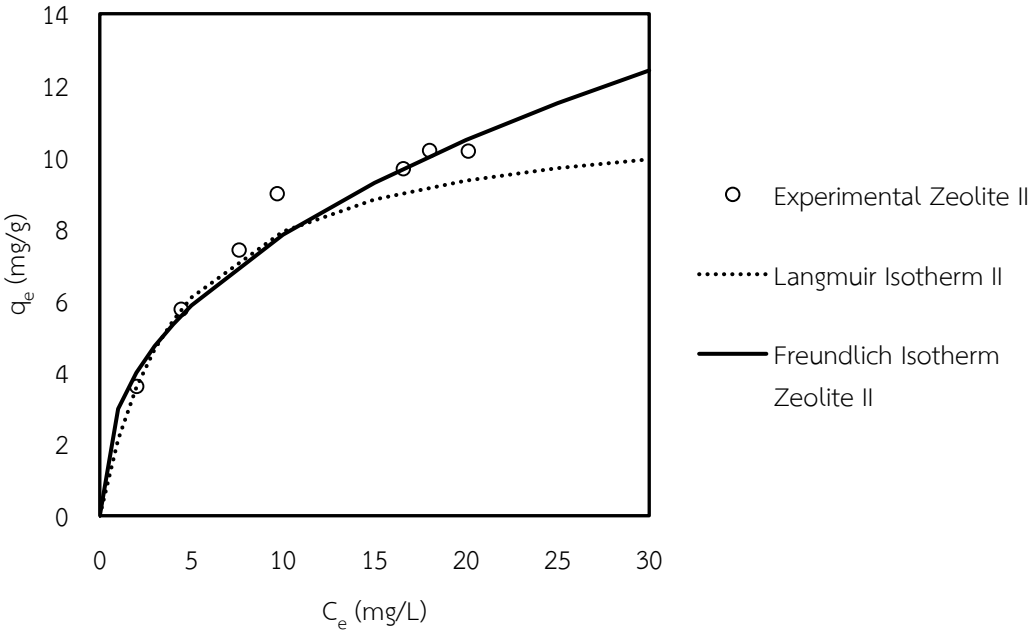

Figure 4.15 (c): Adsorption Isotherms of Synthesized Zeolite II

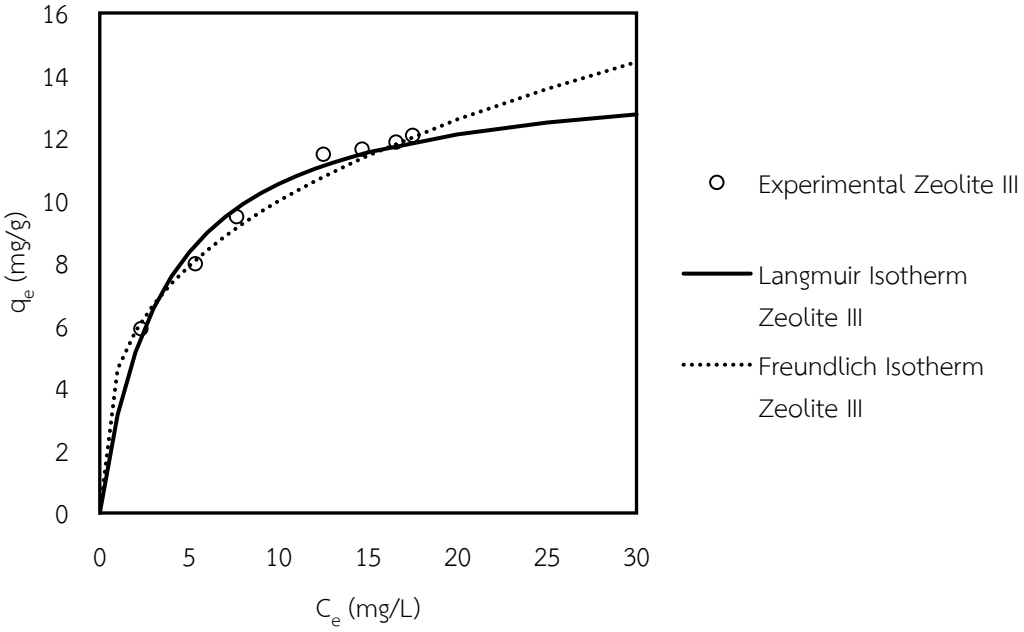

Figure 4.15 (d): Adsorption Isotherms of Synthesized zeolite III

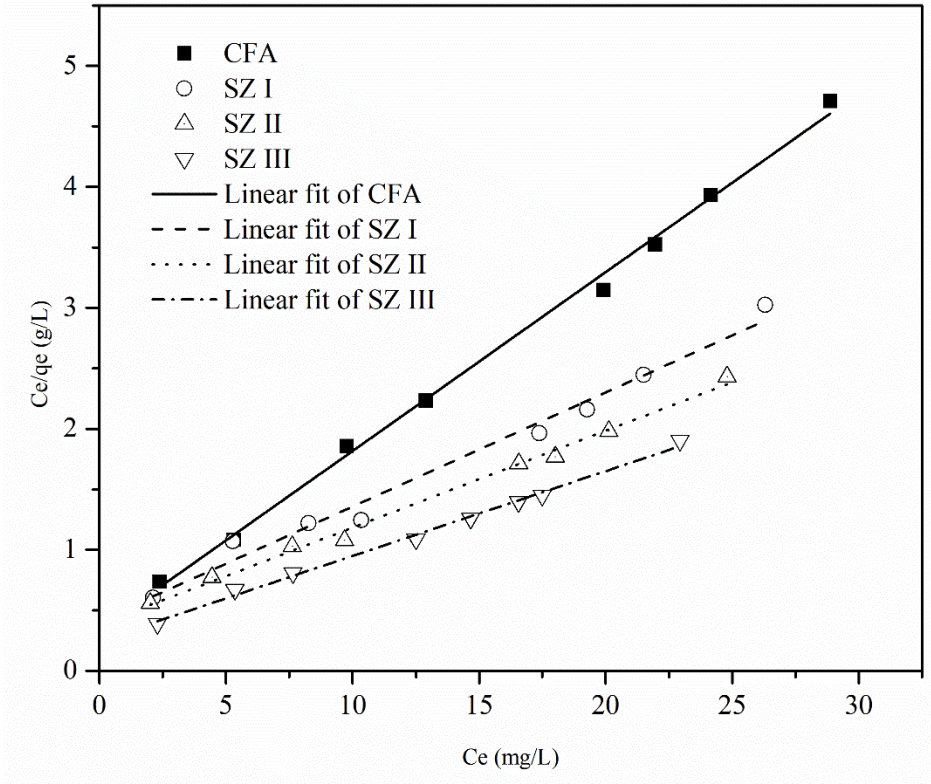

Figure 4.16 Lineaized Langmuir isotherm model of CFA, Zeolite I, II, and III (pH 5.6, contact time 240 mins, temperature 27°C)

For liquid adsorption, graphs are plotted between adsorbed capacity versus concentration at equilibrium to determine the maximum sorption capacity (q_{max}) and energy (K_L) (Fig 4.13). The uptake capacity at equilibrium was evaluated in the adsorption models; Langmuir and Freundlich isotherm. Generally, once the adsorption approaches the maximum capacity of adsorbent, the adsorbed molecules is a monolayer localized onto the surface (R^2>0.98). They only attracted to the active site surface. These results correlate to available specific surface area measure by BET method. This implies the strong adsorptivity between the active site. However, CFA has no specific area for sulfate uptake but contains high calcium content up to 11% weight which higher than zeolite II 80%. Langmuir isotherm model indicates the CFA has 6.93 mg/g adsorption capacity which lower than Zeolite II 54 % as illustrated in Figure 4.13-4.16. This implies that effect of S_{BET} is superior than calcium content from coal fly. Table 4.3 reveals that the adsorption is less favored on Fruendlich isotherm model since R^2<0.98 and lower than Langmuir regression value.

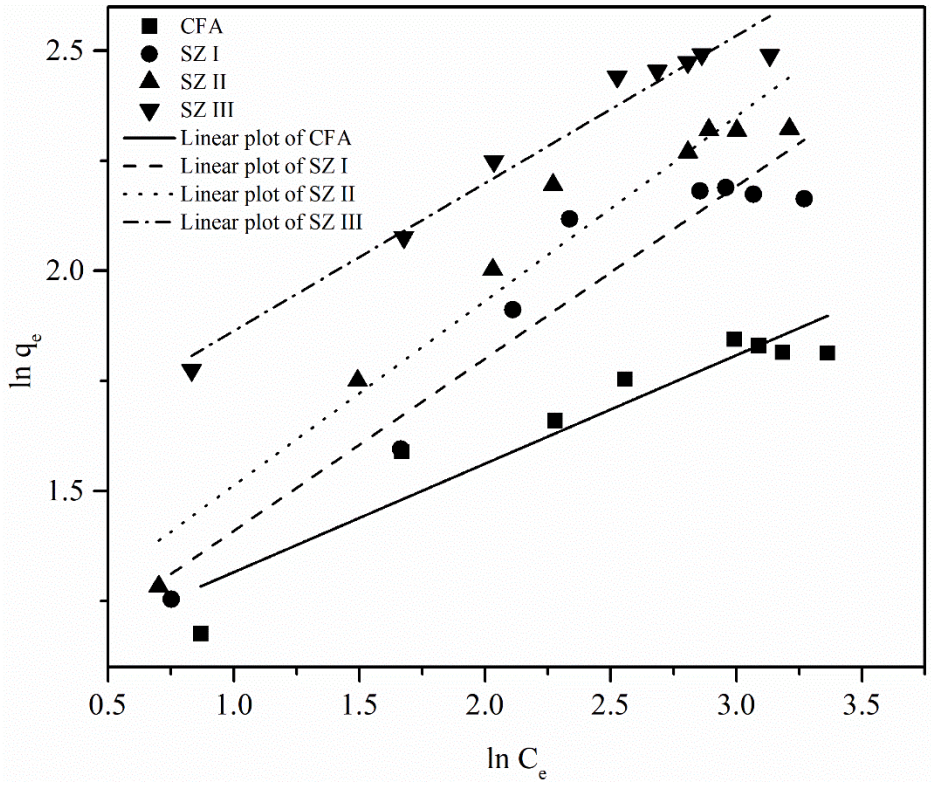

Figure 4.17 Linearized Freundlich isotherm model of CFA, Zeolite I, II, and III (pH 5.6, contact time 240 mins, temperature 27°C)

The freundlich model were obtained from the plot between ln q_e and ln C_e (Fig. 4.17). The 1/n and K_F results from its slope and intercept (log K_f). Langmuir adsorption model is a theoretical prediction of sorbate coverage on adsorbent surface. As an evident, sulfate is predicted to be favorable on nature adsorption since R_L is between 0-1. Therefore, sulfate adsorption employing Zeolite I, and Zeolite II is localized onto active surface as monolayer sorption between sulfate anions and specific surface area. Calcium content and S_{BET} has no significant difference on sulfate adsorption enhancement. CFA, Zeolite I, II, and III can practically and efficiently uptake sulfate in low acidic region.

Table 4.4 Lagmuir and Freudlich adsorption isotherm parameters

Adsorbent	Langmuir			Fruendlich		
	q_{max}	K_L	R^2	1/n	K_F	R^2
CFA	6.76	0.44	0.9964	0.26	2.9	0.8772
SZ I	10.6	0.23	0.9804	0.39	2.7	0.9032
SZ II	12.49	0.21	0.9936	0.42	2.97	0.9364
SZ III	14.26	0.29	0.99454	0.33	4.61	0.9616

Figure 4.4 shows adsorption isotherms parameters for Langmuir model and Freundlich model. All adsorbents were fitted well to Langmuir adsorption model observed from $R^2 > 0.98$. However, synthesized zeolite can be fitted to both Langmuir and Freundlich indicated that SZ III materials has both homogeneous and heterogeneous surface, the particles are accumulated into both monolayer as chemisorption and multilayer as physisorption. Predicting the adsorption factors on particles, not only pH, calcium and aluminum contents have also been reported adsorption enhanced parameters which has a great impact on sulfate precipitation. In previous research, sulfate removal was compared between utilizing aluminum and calcium contents which are 67% and 100%, respectively [56]. Besides, the aluminum enhances sorption capacity of the materials, 15.02 and 14.02 %weight in SZ III and CFA, respectively. Aluminum is implied to influence the performance of sulfate adsorption in synthetic solution for this study.

4.2.4 Kinetics Analysis

To determine the individual adsorption rate, the data between log (q_e-q_t) versus time (t, mins) are plotted (Figure 4.18 (a-d)). Different adsorbent with S_{BET} range of 0.16-65.38 cm^3/g selected. At 27 ℃, the highest rate constant; 0.016 and 0.014 min^{-1} obtained from both the CFA and SZ III with linear regression R^2>0.9. The reaction rates of SZ I and II are lower than CFA, because specific surface area is not high to be competed. The increasing specific surface area enhances the reaction rate, however, not only specific surface area provides highly impact but calcium content can also influence the removal rate.

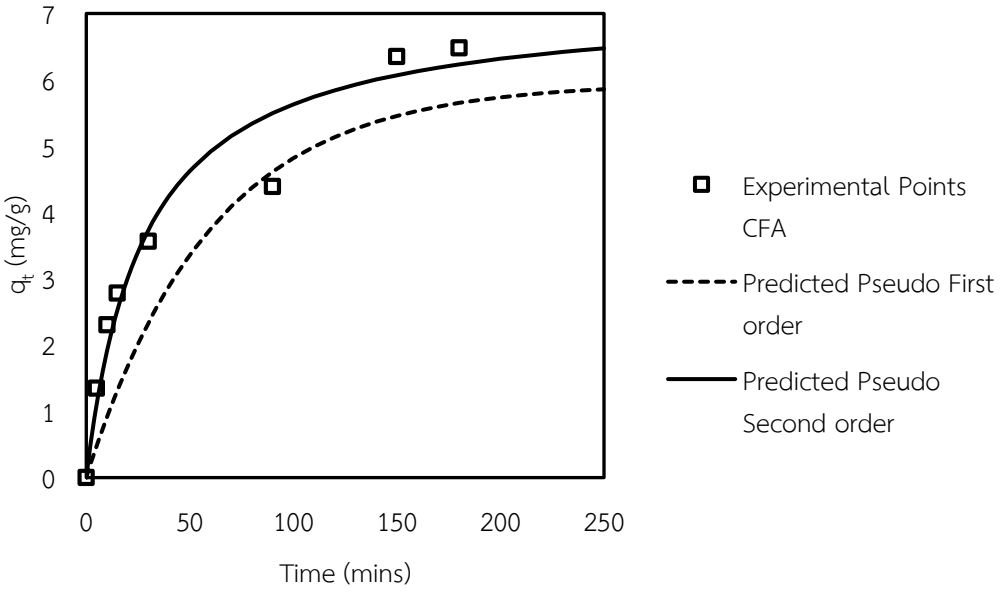

Figure 4.18 (a) Adsorption kinetics of CFA

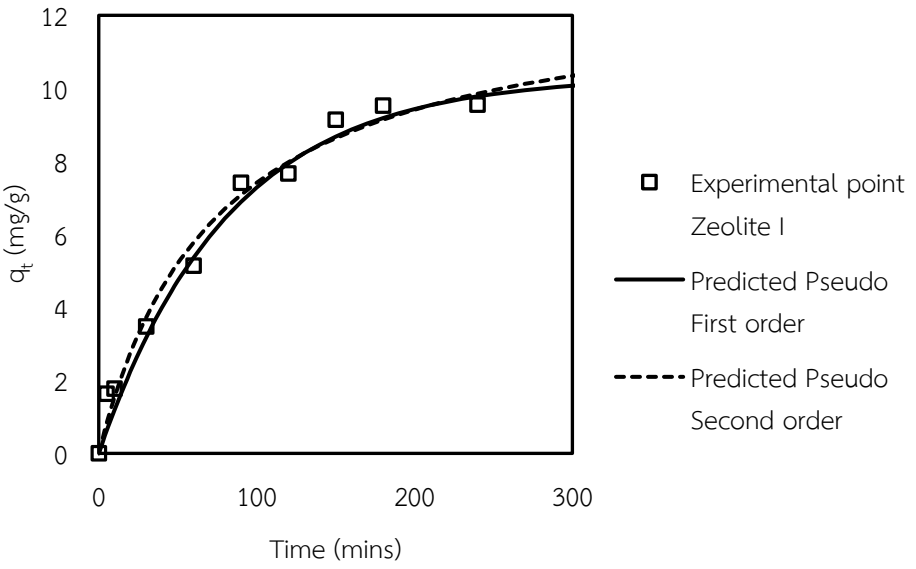

Figure 4.18 (b) Adsorption kinetics of synthesized zeolite I

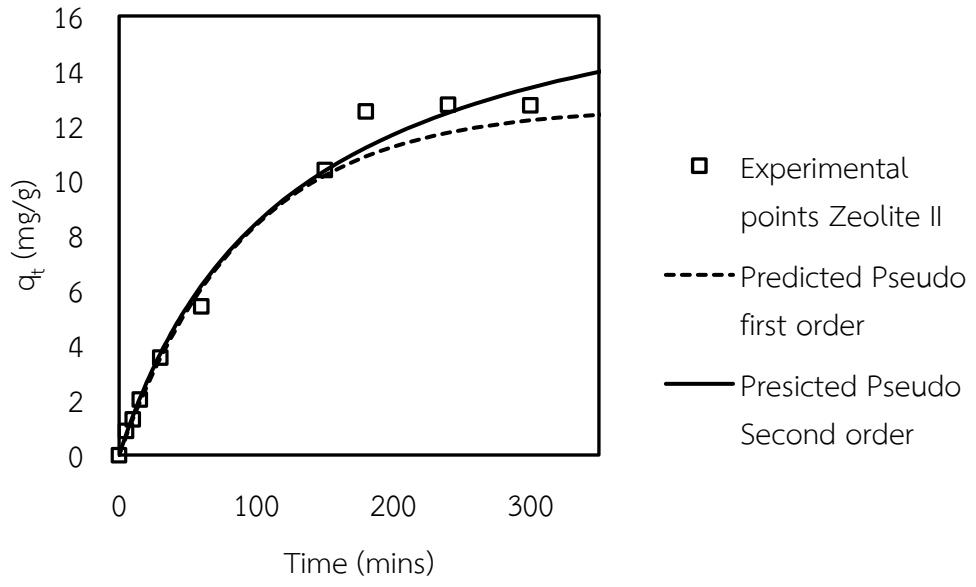

Figure 4.18 (c) Adsorption kinetics of synthesized zeolite II

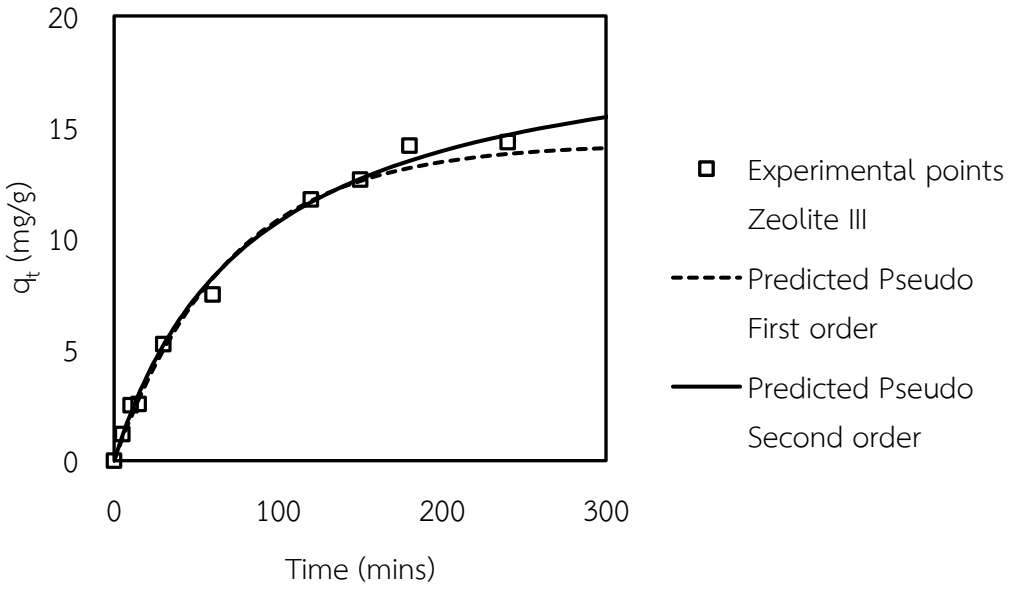

Figure 4.18 (d) Adsorption kinetics of synthesized zeolite III

The reaction takes place at 27°C with initial sulfate concentration of 30 mg/L. According to Figure 4.18(a-d), most of adsorption data were fitted into pseudo second order kinetics model determining their rate limiting step occurred as chemisorption with strong chemical bond. In general, the suitable adsorbent material should create chemisorption type to efficiently remove ion compounds from solution. The results are obviously indicated in Table 4.5. Parameters is predicted to be constant Pseudo second order kinetics model typically determines dimensional sorption behavior of adsorbed molecules onto sorbent surface.

Table 4.5 Adsorption Kinetics parameters

Adsorbent	Pseudo First Order			Pseudo Second Order		
	q_e	K_1	R^2	q_e	K_2	R^2
CFA	5.951	0.016	0.957	7.194	0.005	0.9659
SZ I	10.332	0.012	0.984	12.8866	0.001	0.9825
SZ II	12.688	0.011	0.997	18.903	0.0004	0.9717
SZ III	14.253	0.014	0.9737	19.802	0.0005	0.9835

4.2.5 Statistical Analysis

To determine the significance between two factors; pH and initial concentration of these coal fly ash as an adsorbent. The correlation between two parameters which impacts on sulfate elimination was analyzed based on two ways ANOVA factorial design. The F value and P value of pH factor reported are calculated (as shown in Figure 4.6) to be 16.65 and 0.006, respectively using Origin 9.0 software (Germany).

Table 4.6 Sulfate removal (%) at pH 2 and 9, intial concentration of 10, 20, 40 ppm

	Sum of Squares	Mean square	F Value	P value
pH	1036.28	1036.28	16.65	0.006
Initial Concentration	3362.97	1681.49	27.02	0.001
Interaction	557.21	278.61	4.48	0.06
Model	4956.47	991.29	15.93	0.002
Error	373.29	62.21	-	-
Total	5329.75	-	-	-

The significant difference of two factors; pH and initial concentration. The correlation between two parameters which was analyzed based on two ways ANOVA factorial design. P value obtained below 0.05 both pH and initial concentration factors which indicates the strong evidence against the null hypothesis. Thus, we reject the hypothesis that the mean of two factor is equal, Hence, the interaction between two factors was above 0.05. The results reveal pH and initial concentration has significance difference for adsorption performance, the interaction between two factors was insignificant.

Table 4.7 The comparison of sulfate uptake capacity by various adsorbents.

Adsorbent	Time (hours)	SBET (m^2/g)	q_{max} (mg/g)	Reference
Ba-modified acid washed analcime	2	238.42	13.7	[16]
Alpha alumina	24	-	7.7	[17]
Rice straw	2	-	11.68	[14]
Limestone	9	-	23.7	[4]
Synthesized zeolite	4	65.32	14.26	This study
Raw Mae Moh CFA	4	0.16	6.76	This study

The synthesized zeolite and CFA as its raw material were evaluated on sulfate removal and compared, their maximum adsorption capacity was 14.26 and 6.76 mg/g, respectively, as indicated in Figure 4.7. The amount uptake of synthesized zeolite is

higher than alpha alumina and rice straw as they are composed of Si and Al contents, however it might be different at their functional groups

4.3 Selenium Adsorption

Selenium adsorption was investigated employing zeolites III which has 65.38 m^2/g of specific surface area. According to the previous studies [33, 57-60], selenium adsorption was mainly influenced by S_{BET} of materials, pH solution and ionic strength. However, some studies have reported that functional group is an impacted factor that can enhance the sorption efficiency [57]. $HSeO_3^-$ represents as Se(IV) in the pH range of 2.7-8.5. In this study, Na_2SeO_3 was applied as the source of $Se_2O_3^{2-}$. Table 4.8 shows the Se (IV) uptake capacity employing different adsorbent. This study is incomplete, however there is sorption capacity value for selenium uptake.

Table 4.8 Comparison of Se (IV) Sorption capacities

Order	Adsorbent	pH	surface area (m^2/g)	q_{max} (mg/g)	Reference
1	Polyamine based magnetic graphene oxide nanocomposite	5.8	-	120.1	[57]
2	Conjugate adsorbent (Direct benzoic acid onto silica)	2.5	-	103.73	[58]
3	MgO nanosheet	10.5	166.44	103.52	[59]
4	Rice husk	2-6		41.02	[33]
5	FeOOH	5	361.4	26.46	[60]
6	Synthesized zeolite	6	65.32	0.86	This study

Batch adsorption was carried out at 27°C, synthesized zeolites of 50 mg was applied into 50 mL of 9.13 µg Se/L of Na_2SeO_3 solution at difference pH. Se (IV) was efficiently remove 36.47%, pH 6. Specific surface area after hydrothermal treatment with 2.8 M of NaOH solution. In aquatic system, Se (IV) can be oxidized into selenite (SeO_3^{2-}), biselenite ($HSeO^{3-}$) and selenious acid (H_2SeO_3) forms. Selenite specie was dominated at pH above 9.0, in contrast selenious acid was dominated at pH below 3.5 [61]. The pK_a value of selenic acid was 1.92 which pH was in the range between 2-6, biselenite and selenate are dominant species. In alkaline medium, selenite (SeO_3^{2-}) and selenate (SeO_4^{2-}) are the predominant species [62].

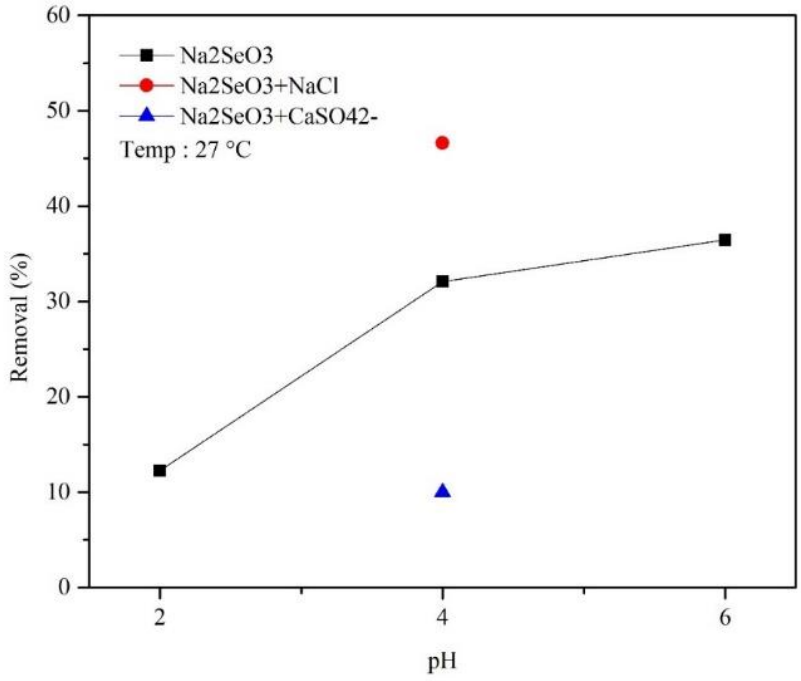

Figure 4.19 Percent removal as a function of pH solution

The adsorption approaches equilibrium points within 30 minutes with adsorbed capacity 0.8 mg Se/g sorbent which is much lower than other studies as illustrated in Table 4. 6. The adsorptivity of anion can correspond to the zeta potential of synthesized zeolites; +17, +13, and +16 mV on surface at pH 2, 4, and 6, respectively. Positive charge carrier attracts the selenite anions in the solution. Cations or alkaline region generates repulsion force of attraction, hence pH 2- 6 has been selected. Moreover, the effect of ionic strength by additional NaCl composition enhances Se(IV) uptake 82.7%.

Selenium adsorption study has been postponed due to the effects of high calcium content of coal fly ash inhibiting the crystallites growth. Basically, the crystallinity of adsorbent is highly introduced the Se (IV) or other anionic elements onto sorbent surface. Once, the surface has less crystallites, the sorption efficiency will not be high. However, the obtained uptake capacity of 0.8 mg Se(IV)/g sorbent is capable to be utilized in wastewater, groundwater around coal mining due to the contamination from coal activity is 500-1000 µg/L.

CHAPTER 5

CONCLUSIONS

5.1 Conclusions

The hydrothermal method plays a key role for coal fly ash surface and structural modification. The zeolite preparation requires the dissolution process to dissolve. The integrated zeolites were synthesized from lignite coal fly ash without additives containing sodalite (110, 211) planar, specific surface area 65.38 m^2/g and 15.02 cm^3/g. Higher temperature results higher amorphous and Na-P1 but decreasing the sodalite.

Sulfate adsorption was successfully performed utilizing synthesized integrated zeolites and coal fly ash as the adsorbents with maximum capacity of 14.26 and 6.76, respectively which calculated as 52.6%. The adsorptivity of the materials favor the acidic region for sulfate uptake, however, mild acidic condition is more practical for industrial applicability.

Two highest reaction rates were obtained from CFA, and the synthesized zeolites possessing highest surface area; 0.006 min^{-1}. The mathematical model supported that pH and sulfate initial concentration has significant difference, individually, and no significance of interaction.

The adsorption of selenium has been established according to the coming regulations for water contamination control, the high crystallinity is necessary for this metalloid. However, the synthesized material as sodalite phase can efficiently remove

sulfate up to 0.86 mg/g. Corresponding the required remaining amount in drinking water.

5.2 Recommendations

Since Mae Moh CFA composed of high calcium content, it inhibits the crystallinity growth. The adsorption is suggested to be further carried out in continuous system and perform with the competitive ions.

REFERENCES

1. Munawer, M.E., *Human health and environmental impacts of coal combustion and post-combustion wastes.* Journal of Sustainable Mining, 2017.
2. Suzuki, I., *Oxidation of inorganic sulfur compounds: Chemical and enzymatic reactions.* Canadian Journal of Microbiology, 1999. **45**(2): p. 97-105.
3. INAP, *Treatment of sulphate in mine effluentes,.* International network for acid prevention, 2003.
4. Silva, A.M., R.M.F. Lima, and V.A. Leão, *Mine water treatment with limestone for sulfate removal.* Journal of Hazardous Materials, 2012. **221-222**: p. 45-55.
5. Tait, S., et al., *Removal of sulfate from high-strength wastewater by crystallisation.* Water Research, 2009. **43**(3): p. 762-772.
6. Gnana kumar, G., *Zeolites and Composites*, in *Nanomaterials and Nanocomposites*, V.P.M.M.J.M. Morlanes, Editor. 2016, Wiley VCH Verlag GmbH & Co. KGaA.
7. Cardoso, A.M., et al., *Synthesis of zeolite Na-P1 under mild conditions using Brazilian coal fly ash and its application in wastewater treatment.* Fuel, 2015. **139**: p. 59-67.
8. C Barnes, M., J. Addai-Mensah, and A. R Gerson, *The mechanism of the sodalite-to-cancrinite phase transformation in synthetic spent Bayer liquor*. Vol. 31. 1999. 287-302.
9. Coulson, C.A., *d Electrons and Molecular Bonding.* Nature, 1969. **221**: p. 1106.
10. Jeong, S., et al., *Mechanisms of direct and in-direct sulfation of limestone.* Fuel, 2015. **161**: p. 1-11.

11. Benatti, C. T. , C. R. G. Tavares, and E. Lenzi, *Sulfate removal from waste chemicals by precipitation.* Journal of Environmental Management, 2009. **90**(1): p. 504-511.

12. Burgess, B.A., K.L. Lohmann, and B.R. Blakley, *Excessive sulfate and poor water quality as a cause of sudden deaths and an outbreak of diarrhea in horses.* The Canadian Veterinary Journal, 2010. **51**(3): p. 277-282.

13. Hydrometrics, *A New Process For Sulfate Removal From Industrial Waters*. VertMarkets, Inc.: MY, USA.

14. Cao, W., et al., *Removal of sulphate from aqueous solution using modified rice straw: Preparation, characterization and adsorption performance.* Carbohydrate Polymers, 2011. **85**(3): p. 571-577.

15. De Luna, M. D. G. , et al. , *Removal of sulfate by fluidized bed crystallization process.* Journal of Environmental Chemical Engineering, 2017. **5**(3): p. 2431-2439.

16. Runtti, H., et al., *Utilisation of barium-modified analcime in sulphate removal: Isotherms, kinetics and thermodynamics studies.* Journal of Water Process Engineering, 2017. **16**: p. 319-328.

17. Wu, C. - H. , et al. , *Modeling competitive adsorption of molybdate, sulfate, selenate, and selenite using a Freundlich- type multi- component isotherm.* Chemosphere, 2002. **47**(3): p. 283-292.

18. Castillo, X. , et al. , *A cheap mesoporous silica from fly ash as an outstanding adsorbent for sulfate in water.* Microporous Mesoporous Mat.

19. Halajnia, A., et al., *Adsorption–desorption characteristics of nitrate, phosphate and sulfate on Mg–Al layered double hydroxide.* Applied Clay Science, 2013. **80-81**: p. 305-312.

20. Hannachi, C. , et al. , *Adsorption of F<sup>- </ sup>, NO<sub>3</ sub><sup>- </ sup> and SO₄²⁻ on AFN Anionic Membrane: Kinetics and Thermodynamics Studies.* American Journal of Analytical Chemistry, 2013. **Vol.04No.09**: p. 9.

21. Welling Sum, et al., *Sorption of Se (IV) and Se (VI) to coal fly ash/cement composite: effect of Ca^{2+} and high ionic strength.* Chemical Geology, 2016. **464**: p. 76-83.

22. Santos, S., et al., *Selenium contaminated waters: An overview of analytical methods, treatment options and recent advances in sorption methods.* Science of The Total Environment, 2015. **521–522**: p. 246-260.

23. Dubrovsky, M., *Selenium removal method*. 2005, Google Patents.

24. Ruhl, L., et al., *The impact of coal combustion residue effluent on water resources: a North Carolina example.* Environ. Sci. Technol., 2012. **46**: p. 12226-12233.

25. Roberson, M.J., *Removal of Selenate from Irrigation Drainage Water Using Zero-Valent Iron*. 1999, University of California, : Riverside, CA.

26. Shashi B. Lalvani, P.E., *Selenium removal from agricultural drainage water: lab scale studies*. 2004, Miami University: Sacramento, California.

27. Bakather, O.Y., et al., *Enhanced Adsorption of Selenium Ions from Aqueous Solution Using Iron Oxide Impregnated Carbon Nanotubes.* Bioinorganic Chemistry and Applications, 2017. **2017**: p. 12.

28. Zelmanov, G. and R. Semiat, *Selenium removal from water and its recovery using iron (Fe3+) oxide/hydroxide-based nanoparticles sol (NanoFe) as an adsorbent.* Separation and Purification Technology, 2013. **103**: p. 167-172.

29. Bleiman, N. and Y.G. Mishael, *Selenium removal from drinking water by adsorption to chitosan-clay composites and oxides: Batch and columns tests.* Journal of Hazardous Materials, 2010. **183**(1-3): p. 590-595.

30. Zhang, N., L.S. Lin, and D. Gang, *Adsorptive selenite removal from water using iron-coated GAC adsorbents.* Water Research, 2008. **42**(14): p. 3809-3816.

31. Kongsri, S., et al., *Nanocrystalline hydroxyapatite from fish scale waste: Preparation, characterization and application for selenium adsorption in aqueous solution.* Chemical Engineering Journal, 2013. **215-216**: p. 522-532.

32. Kuan, W.H., et al., *Removal of Se(IV) and Se(VI) from water by aluminum-oxide-coated sand.* Water Research, 1998. **32**(3): p. 915-923.

33. El-Shafey, E.I., *Sorption of Cd(II) and Se(IV) from aqueous solution using modified rice husk.* Journal of Hazardous Materials, 2007. **147**(1-2): p. 546-555.

34. Simone Pollastri, A.F.G., Magdalena Lassinantti Gualtieri, Miriam Hanuskova, Alessandro Cavallo, Giovanni Gaudino, *The zeta potential of mineral fibers.* Journal of Hazardous Materials, 2014. **276**: p. 469-479.

35. B., J. and S. D.N., *A review on synthesis, characterization and industrial application of fly ash zeolites.* J. Mater Edu., 2011. **33**(1-2): p. 65-132.

36. Manique, M.C., et al., *Biodiesel production using coal fly ash-derived sodalite as a heterogeneous catalyst.* Fuel, 2017. **190**: p. 268-273.

37. Mon, J., et al., *Cesium incorporation and diffusion in cancrinite, sodalite, zeolite, and allophane.* Microporous Mesoporous Mat., 2005. **86**(1): p. 277-286.

38. Cundy, C.S. and P.A. Cox, *The hydrothermal synthesis of zeolites: Precursors, intermediates and reaction mechanism.* Microporous Mesoporous Mat., 2005. **82**(1): p. 1-78.

39. E., H., *Synthesis of Phase-Pure Zeolite Sodalite from Clear Solution Extracted from Coal Fly Ash.* J Thermodyn Catal 2017. **8**(187).

40. Musyoka, N.M., et al., *Synthesis of hydroxy sodalite from coal fly ash using waste industrial brine solution.* Journal of environmental science and health. Part A, Toxic/hazardous substances & environmental engineering, 2011. **46**(14): p. 1699-1707.

41. Králik, M., *Adsorption, chemisorption, and catalysis*. Vol. 68. 2014.

42. Haciyakupoglu, S. and E. Orucoglu, *75Se radioisotope adsorption using Turkey's Reşadiye modified bentonites.* Applied Clay Science, 2013. **86**: p. 190-198.

43. Karnitz, J.R.O., et al., *Adsorption of heavy metal ion from aqueous single metal solution by chemically modified sugarcane bagasse.* Bioresour. Technol., 2007. **98**: p. 1291-1297.

44. Kumar, U. and M. Bandyopadhyay, *Sorption of cadmium from aqueous solution using pretreated rice husk.* Bioresour. Technol., 2006. **97**: p. 104-109.

45. Hui QIU, et al., *Critical review in adsorption kinetic models.* Journal of Zhejiang University SCIENCE A, 2009. **10**(5): p. 716-724.

46. Liu, Y., *New insights into pseudo-second-order kinetic equation for adsorption.* Colloids and Surfaces A: Physicochemical and Engineering Aspects, 2008. **320**(1): p. 275-278.

47. Chansiriwat, W., D. Tanangteerapong, and K. Wantala, *Synthesis of Zeolite from Coal Fly Ash by Hydrothermal Method Without Adding Alumina and Silica Sources: Effect of Aging Temperature and Time.* Sains Malaysiana, 2016. **45**(11): p. 1723-1731.

48. Tanaka, H. and A. Fujii, *Effect of stirring on the dissolution of coal fly ash and synthesis of pure-form Na-A and -X zeolites by two-step process.* Advanced Powder Technology, 2009. **20**(5): p. 473-479.

49. McMurdie, H.F., et al., *Standard X-ray diffraction powder patterns from the JCPDS research associateship.* Powder Diffraction, 1986. **1**(267).

50. Sanchez Hernandez, R., et al., *One-step synthesis of NaP1, SOD and ANA from a hazardous aluminum solid waste*. Vol. 226. 2016.

51. Subotić, B., et al., *Transformation of zeolite A into hydroxysodalite: I. An approach to the mechanism of transformation and its experimental evaluation.* Journal of Crystal Growth, 1980. **50**(2): p. 498-508.

52. Flaningen, E.M., H.A. Khatami, and H.A. Szymanski, Mol. Sieve Zeolites, 1971. **16**: p. 201.

53. Sharma, P., et al., *GIS-NaP1 zeolite microspheres as potential water adsorption material: Influence of initial silica concentration on adsorptive and physical/topological properties.* Scientific Reports, 2016. **6**: p. 22734.

54. Flaningen, E.M., H. Khatami, and H.A. Szymanski, 1971: p. 201-215.

55. Wang, D.J., et al., *Hollow cancrinite zeolite spheres in situ transformed fly ash cenosphere.* Chin. Chem. Lett., 2003. **14**(12): p. 1299-1302.

56. Almasri, D., K.A. Mahmoud, and A. Abdel-Wahab, *Two-stage sulfate removal from reject brine in inland desalination with zero-liquid discharge.* Desalination, 2015. **362**: p. 52-58.

57. Lu, Z., et al., *Polyamine-modified magnetic graphene oxide nanocomposite for enhanced selenium removal.* Separation and Purification Technology, 2017. **183**: p. 249-257.

58. Awual, M.R., et al., *Mesoporous silica based novel conjugate adsorbent for efficient selenium(IV) detection and removal from water.* Microporous Mesoporous Mat., 2014. **197**: p. 331-338.

59. Cui, W., et al., *Adsorption study of selenium ions from aqueous solutions using MgO nanosheets synthesized by ultrasonic method.* Journal of Hazardous Materials, 2018. **341**: p. 268-276.

60. Sharrad, M.O.M., H.J. Liu, and M.H. Fan, *Evaluation of FeOOH performance on selenium reduction.* Separation and Purification Technology, 2012. **84**: p. 29-34.

61. S.D. Faust and O.M. Aly, *Chemistry of Natural Waters* Ann Arbor Science, Ann Arbor, MI, 1981: p. 359–371.

62. Zhang, L., et al., *Sorption behavior of nano-TiO2 for the removal of selenium ions from aqueous solution.* Journal of Hazardous Materials, 2009. **170**(2): p. 1197-1203.

APPENDIX

APPENDIX A

Calibration Curve of Sulfate

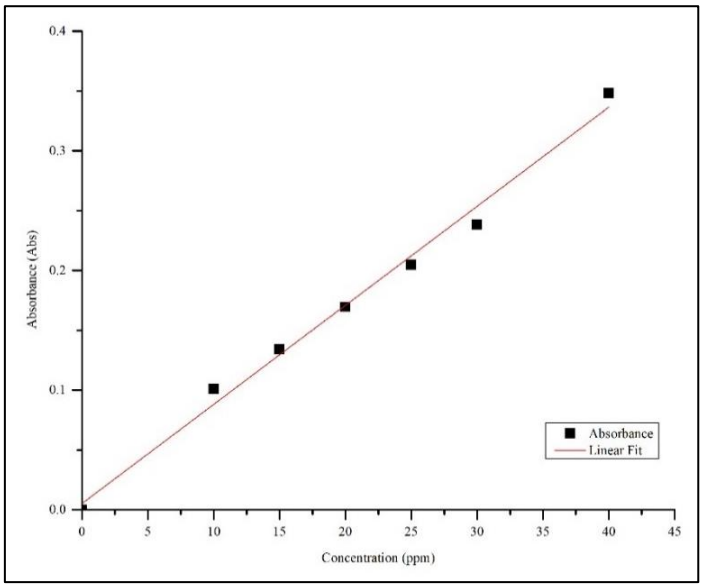

Table A-1: Statistics

Absorbance	
Number of Points	7
Degrees of Freedom	5
Residual Sum of Squares	6.35546E-4
Pearson's r	0.99562
Adj. R-Square	0.9895

Table A-2 Statistics of Calibration curve

	Intercept		Slope		Statistics
	Value	Standard Error	Value	Standard Error	Adj. R-Square
Absorbance	0.00521	0.00816	0.00828	3.47932E-4	0.9895

Table A-3 Summary Sulfate leaching from coal fly ash in synthetic sulfate solution as a function of pH

pH	Concentration (mg/L)
2.3 ± 0.2	32.2714
5.7 ± 0.1	38.7562 ± 0.334
9.3 ± 0.15	12.96421245 ± 0.6153

(1) pH 5.7 ± 0.1

Absorbance	Conc. (mg/L)
0.363837	39.10296703
0.360425	38.72802198
0.357782	38.43758242
Average	38.75619048
S.D.	0.333585476

(2) pH 9.3 ± 0.15

Absorbance	Conc. (mg/L)
0.128293	12.64758242
0.127602	12.57164835
0.137628	13.67340659
Average	12.96421245
S.D.	0.615352534

APPENDIX B

Table B-1: Sulfate removal of coal fly ash independent of initial Sulfate concentration

	pH	C_0 (mg/L)	C_1(mg/L)	q_e (mg/g)	Removal (%)
Average	9	11.08	8.53	2.55	23.00
S.D.			0.40	0.40	3.68
Average	9	22.30	15.38	6.92	31.03
S.D.			1.02	1.02	4.59
Average	9		21.18	18.95	47.22
S.D.			0.95	0.95	2.38

Table B-2: Sulfate removal of coal fly ash independent of initial Sulfate concentration (pH 2.38 ± 0.0379)

	pH	C_0 (mg/L)	C_1(mg/L)	q_e (mg/g)	Removal (%)
Average	2.41	10	8.40	2.68	21.65
S.D.	0.0566		0.40	0.40	3.62
Average	2.36	20	10.80	11.50	51.57
S.D.	0.1772		0.183	0.18	0.82
Average	2.38	40	7.34	32.80	81.71
S.D.	0.0424		7.17	7.17	17.88

Table B-3: Sulfate removal designed for DOE analysis

Adsorbent	pH	C_e (mg/L)	C_0 (mg/L)	Q_e (mg/g)	Removal (%)	C/C0	1/C	1/qe
Zeolite	4	23.64	30.30	6.66	21.98	0.78	0.04	0.15
	6	25.95	30.30	2.173	14.34	0.85	0.038	0.46
CFA	4	25.78	30.30	4.52	14.92	0.85	0.038	0.22
	6	9.21	30.30	21.08	69.58	0.30	0.10	0.047
Zeolite	4	19.60	19.95	0.347	1.74	0.98	0.05	2.87
	6	16.04	19.95	1.95	19.60	0.80	0.06	0.51
CFA	4	12.21	19.95	7.74	38.78	0.61	0.08	0.13
	6	11.91	19.95	4.02	40.30	0.59	0.084	0.25

Table B-4 Effects of initial concentration (1hour)

C_0 Se (mg/L)	µmol/L	C_t	q_t (mg se/g)	% removal
0.228	2.887	0.23	-	-
0.913	11.56	0.62	0.293	32.09
2.28	28.87	1.42	0.86	37.7
3.65	46.23	7.25	-	-

Table B-5 Effects of pH solution (1 hour)

pH	C_0 Se (mg/L)	C_t	q_t (mg se/g)	% removal
2	0.913	0.8	0.113	12.27
4	0.913	0.84	0.073	7.99
6	0.913	0.58	0.333	36.47

Table B-6 Chemical composition of coal fly ash analyzed by XRF, Samples were collected from each unit operation in Mae Moh coal fired power plant (Lampang, Thailand); (Accessed from http://maemoh.egat.com/ash/index.php).

Samp.Date	Unit	LOI(%)	SiO_2	Al_2O_3	TiO_2	Fe_2O_3	CaO	MgO	Na_2O	K_2O	P_2O_5	SO_3	MnO_2
2017-06-21	07	0.05	32.52	16.41	0.30	13.38	25.52	3.00	1.82	1.91	0.28	4.75	0.13
2017-06-21	08	0.01	31.90	16.41	0.30	14.31	26.14	3.30	2.15	2.08	0.27	3.03	0.13
2017-06-21	09	0.04	30.92	15.97	0.28	14.11	26.45	3.27	2.18	2.00	0.28	4.42	0.13
2017-06-21	10	0.04	32.63	16.94	0.31	13.77	24.81	3.18	2.13	2.08	0.27	3.76	0.13
2017-06-21	11	0.04	31.65	16.47	0.30	13.84	25.94	3.32	2.16	2.05	0.27	3.89	0.13
2017-06-21	12	0.02	32.90	17.03	0.32	13.84	24.96	3.28	2.00	2.04	0.27	3.25	0.13
2017-06-21	13	0.04	31.72	16.58	0.30	14.03	25.36	3.28	2.11	2.00	0.28	4.21	0.13
2017-06-28	04	0.06	32.14	16.51	0.33	12.78	26.02	2.80	2.07	1.90	0.26	5.08	0.12
2017-06-28	05	0.03	31.77	16.40	0.32	13.09	26.49	2.86	2.11	1.89	0.27	4.70	0.12
2017-06-28	06	0.05	29.13	15.18	0.27	13.22	28.37	2.87	2.16	1.75	0.28	6.66	0.11
2017-06-28	07	0.04	31.00	16.01	0.30	13.08	27.14	2.91	2.14	1.88	0.26	5.16	0.12
2017-06-28	08	0.06	31.14	16.17	0.28	13.63	27.54	3.24	2.25	1.95	0.27	3.40	0.15
2017-06-28	09	0.02	31.29	16.32	0.28	13.44	26.87	3.13	2.21	1.96	0.26	4.08	0.15
2017-06-28	10	0.01	35.64	18.44	0.32	13.44	22.07	2.73	1.87	2.22	0.23	2.92	0.14
2017-06-28	11	0.04	36.71	18.58	0.33	12.84	22.18	2.72	1.66	2.05	0.24	2.58	0.14
2017-06-28	12	0.03	31.49	16.03	0.29	13.45	27.50	3.19	2.21	1.96	0.27	3.48	0.14
2017-06-28	13	0.07	30.34	15.50	0.29	13.66	27.42	3.12	2.34	1.98	0.26	4.96	0.14
2017-07-05	04	0.06	36.61	18.60	0.37	13.60	20.67	2.92	1.67	2.14	0.22	3.09	0.12
2017-07-05	05	0.10	35.25	17.82	0.37	14.11	21.00	2.90	1.82	2.22	0.22	4.20	0.12
2017-07-05	06	0.08	32.88	16.85	0.33	14.93	22.89	3.17	1.82	2.06	0.23	4.74	0.12
2017-07-05	07	0.05	37.66	19.16	0.39	13.52	20.27	3.00	1.51	2.08	0.23	2.07	0.12
2017-07-05	08	0.05	35.61	19.17	0.33	14.64	19.85	2.73	1.83	2.25	0.22	3.28	0.12
2017-07-05	09	0.08	35.26	18.36	0.32	13.69	21.51	2.82	1.97	2.25	0.22	3.49	0.12
2017-07-05	10	0.06	35.89	17.74	0.33	13.24	22.40	2.96	1.95	2.11	0.24	3.03	0.13
2017-07-05	11	0.02	35.80	17.67	0.33	13.27	22.41	2.96	1.98	2.12	0.25	3.10	0.13
2017-07-05	13	0.01	34.79	17.14	0.31	13.46	23.27	2.92	1.98	2.07	0.26	3.67	0.14
2017-07-12	04	0.02	35.17	17.13	0.32	13.95	22.65	2.77	1.44	2.11	0.23	4.14	0.12
2017-07-12	05	0.02	33.82	16.63	0.31	14.25	23.73	2.70	1.41	2.13	0.23	4.69	0.12
2017-07-12	06	0.05	35.10	17.24	0.33	14.08	22.19	2.68	1.44	2.14	0.21	4.48	0.11
2017-07-12	07	0.05	34.83	17.52	0.32	14.31	21.89	2.81	1.46	2.15	0.22	4.39	0.11

Samp.Date	Unit	LOI(%)	SiO_2	Al_2O_3	TiO_2	Fe_2O_3	CaO	MgO	Na_2O	K_2O	P_2O_5	SO_3	MnO_2
2017-07-12	08	0.00	33.40	17.10	0.31	14.07	24.42	2.99	1.89	2.07	0.28	3.36	0.14
2017-07-12	09	0.01	32.75	16.71	0.30	13.97	24.84	2.92	1.95	2.10	0.28	4.07	0.14
2017-07-12	10	0.00	36.21	19.00	0.33	13.69	20.49	2.90	1.84	2.28	0.21	2.96	0.12
2017-07-12	11	0.04	35.33	18.47	0.34	14.49	21.25	2.83	1.79	2.22	0.23	2.95	0.13
2017-07-12	12	0.02	30.34	15.52	0.26	14.12	28.34	3.09	2.08	1.90	0.31	3.91	0.17
2017-07-12	13	0.05	30.75	15.89	0.26	13.97	27.75	3.04	2.13	1.97	0.30	3.78	0.16
2017-07-19	04	0.14	33.92	16.14	0.30	13.62	25.21	2.39	1.22	2.14	0.23	4.71	0.12
2017-07-19	05	0.12	33.45	16.10	0.29	13.91	25.07	2.45	1.24	2.14	0.23	5.00	0.12
2017-07-19	06	0.19	31.55	15.05	0.27	13.60	26.36	2.32	1.13	2.23	0.22	6.90	0.12
2017-07-19	08	0.11	34.00	16.65	0.31	13.68	24.51	3.24	2.22	2.08	0.29	2.91	0.13
2017-07-19	10	0.12	33.49	16.07	0.29	13.13	25.94	3.02	2.07	2.11	0.28	3.48	0.14
2017-07-19	11	0.15	33.14	15.71	0.27	13.05	26.48	2.99	1.97	2.02	0.29	3.96	0.14
2017-07-19	12	0.11	34.76	16.72	0.32	12.99	24.34	3.07	2.08	2.06	0.27	3.26	0.13
2017-07-19	13	0.15	33.20	15.78	0.30	13.07	25.82	3.08	2.19	2.02	0.28	4.17	0.14
2017-07-26	04	0.20	30.70	16.79	0.32	14.38	24.48	3.00	2.37	2.09	0.22	5.55	0.12
2017-07-26	05	0.17	30.05	16.36	0.30	14.17	25.99	2.99	2.27	1.97	0.24	5.56	0.12
2017-07-26	06	0.11	26.58	15.02	0.26	14.79	29.41	3.25	2.32	1.71	0.25	6.29	0.13
2017-07-26	08	0.08	33.69	17.78	0.34	14.49	22.36	3.20	2.40	2.22	0.24	3.17	0.11
2017-07-26	10	0.04	34.15	17.73	0.34	13.26	23.54	2.88	2.16	2.25	0.23	3.34	0.13
2017-07-26	11	0.12	33.98	17.16	0.32	13.36	24.45	2.79	2.05	2.15	0.24	3.39	0.13
2017-07-26	12	0.14	32.39	17.17	0.32	13.77	24.42	3.04	2.28	2.14	0.25	4.12	0.13
2017-07-26	13	0.15	32.66	17.48	0.32	13.70	24.14	3.06	2.24	2.15	0.25	3.90	0.12
2017-08-02	04	0.00	40.66	20.17	0.48	11.22	17.65	2.10	1.70	2.31	0.21	3.41	0.10
2017-08-02	05	0.00	40.85	20.37	0.48	11.32	17.76	2.17	1.65	2.30	0.21	2.81	0.10
2017-08-02	06	0.01	40.38	19.57	0.48	11.23	18.32	2.12	1.67	2.24	0.23	3.68	0.11
2017-08-02	08	0.00	32.97	16.25	0.28	14.17	25.40	3.39	2.30	1.99	0.29	2.84	0.14
2017-08-02	10	0.00	32.00	15.01	0.25	13.48	27.88	3.18	2.25	1.92	0.29	3.59	0.16
2017-08-02	11	0.00	32.57	15.56	0.27	13.40	26.83	3.17	2.12	1.90	0.28	3.75	0.15
2017-08-02	12	0.00	31.70	15.43	0.25	13.80	27.88	3.21	2.08	1.93	0.28	3.30	0.16
2017-08-02	13	0.00	31.02	15.22	0.24	14.05	27.85	3.28	2.16	1.93	0.27	3.84	0.16
2017-08-09	04	0.04	36.93	17.52	0.32	13.98	20.15	2.91	1.99	2.07	0.21	3.80	0.12
2017-08-09	05	0.04	36.10	17.78	0.33	14.06	20.96	2.85	1.96	2.05	0.22	3.59	0.13
2017-08-09	06	0.10	35.69	16.52	0.29	14.17	21.00	3.30	2.41	2.04	0.24	4.23	0.14

Samp.Date	Unit	LOI(%)	SiO_2	Al_2O_3	TiO_2	Fe_2O_3	CaO	MgO	Na_2O	K_2O	P_2O_5	SO_3	MnO_2
2017-08-09	10	0.09	36.17	18.58	0.37	12.89	21.05	2.61	1.98	2.24	0.24	3.15	0.12
2017-08-09	11	0.04	37.27	18.64	0.38	12.64	20.82	2.58	1.93	2.22	0.24	3.18	0.12
2017-08-09	12	0.02	36.00	18.33	0.36	13.29	21.34	2.79	2.04	2.18	0.23	3.34	0.12
2017-08-09	13	0.03	37.25	18.67	0.39	13.06	20.23	2.56	1.91	2.23	0.22	3.38	0.12
2017-08-16	04	0.11	39.27	19.11	0.39	12.17	18.70	2.57	1.61	2.25	0.21	3.64	0.09
2017-08-16	05	0.11	40.07	19.12	0.39	12.23	18.83	2.65	1.51	2.15	0.22	2.74	0.11
2017-08-16	06	0.14	39.54	19.22	0.40	12.09	19.20	2.69	1.59	2.15	0.22	2.83	0.10
2017-08-16	07	0.16	38.56	18.74	0.37	12.30	20.21	2.70	1.67	2.11	0.22	3.02	0.11
2017-08-16	08	0.12	35.39	17.89	0.35	12.91	22.93	2.87	2.11	2.14	0.23	3.08	0.10
2017-08-16	09	0.18	35.16	17.97	0.35	13.26	22.82	2.94	2.02	2.07	0.23	3.08	0.10
2017-08-16	10	0.11	33.56	17.73	0.31	13.99	23.19	3.15	2.30	2.13	0.22	3.32	0.12
2017-08-16	11	0.11	32.76	17.48	0.30	14.22	23.66	3.31	2.27	2.05	0.23	3.62	0.12
2017-08-16	12	0.14	33.36	17.21	0.31	13.69	23.79	3.02	2.16	2.02	0.24	4.08	0.12
2017-08-16	13	0.15	33.61	17.61	0.31	14.04	23.32	3.17	2.18	2.04	0.23	3.39	0.12
2017-08-23	04	0.01	40.25	18.86	0.38	11.91	18.71	2.35	1.59	2.21	0.20	3.44	0.11
2017-08-23	05	0.00	40.52	19.22	0.39	11.98	18.50	2.39	1.59	2.21	0.20	2.91	0.11
2017-08-23	06	0.03	39.85	19.03	0.38	12.01	18.92	2.38	1.63	2.24	0.20	3.24	0.11
2017-08-23	07	0.00	40.99	19.42	0.40	11.68	18.73	2.43	1.51	2.14	0.21	2.40	0.11
2017-08-23	08	0.00	35.28	17.95	0.35	13.57	22.44	2.89	2.15	2.16	0.24	2.86	0.12
2017-08-23	09	0.00	34.03	17.47	0.34	13.85	22.91	2.93	2.25	2.12	0.25	3.73	0.12
2017-08-23	10	0.00	33.25	16.72	0.31	14.28	24.10	3.01	2.29	2.05	0.26	3.62	0.13
2017-08-23	11	0.00	33.63	16.93	0.31	14.13	23.82	3.03	2.26	2.00	0.26	3.53	0.12
2017-08-23	12	0.00	35.44	17.65	0.33	13.40	22.96	2.85	1.96	2.10	0.23	2.98	0.13
2017-08-30	04	0.14	37.05	18.89	0.37	13.05	19.96	2.59	1.74	2.25	0.19	3.81	0.11
2017-08-30	05	0.12	37.34	19.13	0.39	13.53	19.26	2.66	1.73	2.22	0.19	3.45	0.11
2017-08-30	06	0.12	37.91	19.90	0.39	13.45	18.03	2.66	1.78	2.25	0.18	3.35	0.11
2017-08-30	07	0.15	37.14	19.43	0.37	13.44	19.14	2.65	1.73	2.17	0.19	3.64	0.11
2017-08-30	08	0.06	36.75	18.69	0.36	13.10	21.24	2.69	1.74	2.20	0.21	2.93	0.12
2017-08-30	09	0.06	36.25	18.48	0.36	13.38	21.60	2.72	1.77	2.19	0.20	2.95	0.12
2017-08-30	10	0.15	39.44	20.73	0.41	12.42	17.00	2.72	1.84	2.38	0.19	2.79	0.09
2017-08-30	11	0.16	39.50	20.54	0.40	12.60	17.24	2.70	1.78	2.35	0.20	2.61	0.09
2017-08-30	12	0.13	39.02	20.34	0.39	12.30	18.26	2.74	1.78	2.29	0.22	2.57	0.09

2018 CreTech
Rajamangala University of Technology Krungthep, Bangkok, Thailand.
6th International Conference on Creative Technology
2nd National Conference on Creative Technology
July 24–26, 2018

UTK RAJAMANGALA KRUNGTHEP

Synthesis of zeolite derived from coal fly ash via hydrothermal method for sulfate adsorption

Anis Usmani[1*], Lupong Kaewsichan[1]
[1]*Department of Chemical Engineering, Faculty of Engineering, Prince of Songkla University, Songkhla, Thailand*
**E-mail: anisusmani39@gmail.com*

ABSTRACT

Coal is generally composed of inorganic matters and minerals. The utilization in coal fired generating plant releases SO_x, NO_x, and other heavy metals which produces severe problems to the environment. In coal combustion process, fly ash was considered as a major solid waste enriched of SiO_2. There have been attempts on value adding these waste utilization, the applicability as an adsorbent has been interested. This study is aimed to develop a functional zeolite material from alkali activated coal fly ash through hydrothermal treatment without prior purification. As being a porous and small feature size material of synthesized zeolite, it is subjected for sulfate adsorption. Since sulfate behaves highly toxic when overdosing in living organism. The investigations were carried out at 105-180^{o}C for 6-72 hours. Different instrumental techniques were used to characterize viz. XRF, XRD, FTIR, BET, and zeta potential. It was found that solid surface improvement by NaOH can generate crystalline phases. The XRD reveals the mineralogical phase of Na-P1, sodalite, and cancrinite. FTIR spectra confirm the present of functional group of aluminosilicates connected into tetrahedral/hexagonal, with the hydrate groups. At higher temperature and longer hydrothermal time, sodalite phases generated along with cancrinite and other phases, however lowering in specific surface area and pore volumes. Since the larger specific surface area and pore volume are important parameters influencing reactivity of zeolite. The selection was based on the maximum surface area, pore volume, and percent product. Zeolite is successfully synthesized without prior purification. Lastly, this material is further applied for sulfate removal from synthetic water with the maximum uptake 14.26 mg among selected adsorbents.

***Keywords**: Hydrothermal, Zeolite, Coal Fly Ash*

INTRODUCTION

In coal electricity generating plant, the effluents contain several pollutants including sulfate. Coal typically contains large amounts of trace elements including elemental sulfur which can be leached to the environment with the disposal. Moreover, several forms of sulfur in the aqueous system appears predominantly depending on pH. There are six oxidation states of sulfur seems in various sulfur compounds; sulfate ion is an oxidized form with +6 of sulfur. Sulfur oxidation can be stimulated by both chemical and enzymatic reaction [1] forming into sulfate. The sulfate contamination in disposed water pond has been experienced in the range of 500-2000 ppm concentration. Sulfate is a mild hazardous. Hence there is no strict regulation in many countries. The excessive contamination causes taste change and the laxative effects for a human at above 600 ppm. The health agencies have set the maximum amount of sulfate in drinking water vary between 250-500 ppm for mine drainage and industrial effluents [2, 3].

Coal as an energy enriched material has become a major source for electricity generation owning to the lowest operating cost compared to other alternative sources. Natural gas operating cost is about 3.96 B while using coal is only 2.7 B. However, utilizing coal has gained lots of attention in public, since coal generally contains sulfur and heavy metals. Processing water, and by-products discharged during combustion certainly leaches pollutants more unfriendly like SO_2 and particulates. Severe environmental problems have been experienced from the existing plant particular to highly toxic wastewater, prior remediation process is recommended before the discharge.

Combustion of lignite coal releases ashes as by-products called fly ash, and bottom ash. Interestingly, Coal ashes utilization has diversely

advantages. Coal fly ash (CFA) has been emerged as a promising material playing a crucial role in geopolymer, cement, wastewater remediation and stabilization, and catalyst [4]. Aluminosilicate amorphous and crystalline phases, generally quartz (SiO_2), mullite ($3Al_2O_3 \cdot 2SiO_2$), hematite (α-Fe_2O_3), and magnetite (Fe_3O_4), these compounds allowed the conversion of CFA into zeolites via hydrothermal method.

Various sulfate treatment methods have been introduced both chemical and biological route. The common chemical treatment method, lime or limestone containing calcium tends to bind sulfates ions precipitating as gypsums. Another method, barium sedimentation in acidic region with low residual sulfate, however, this method is toxicant, expensive and capable to remove the ions approaching the regulatory limits. Ettringite formation, it requires alkalinity for active sulfate uptake [3]. Metal cations or iron can also precipitate with sulfate and react in the gas stream for sulfide removal in scrubber, which responses in a Fe or Zn packed bed [5]. Amongst various treatment techniques, adsorption is a cost-effective and straightforward for the reaction with an adsorbent. The adsorbent is mainly synthesized providing high surface area with structural and surface modification and surface potential which enhance the removal efficiency.

In this study, zeolites as a molecular sieve were synthesized via hydrothermal method employing Mae Moh coal fly ash with high, Ca and Fe. Both of raw material and synthesized zeolites were utilized as the adsorbent in synthetic sulfate water. XRD, EDS, BET techniques characterized the synthesized materials. Batch sulfate adsorption performance was carried out and evaluated by Langmuir and Freundlich adsorption isotherm, the effects of pH solution, initial concentration, and contact time was investigated.

MATERIALS AND METHODS

Mae Moh coal fly ash (Lampang, Thailand) as a raw material undergoes hydrothermal treatment for zeolites. Zeolite synthesis was conducted in a 400ml stainless steel autoclave equipped with heating jacket and thermocouple which pressurized due to the heat generation inside the closed system as shown in Figure 1. Synthesis methodology was modified [6] 30.25 g of deionized water, 10 g of NaOH, and 16.86 of CFA was vigorously mixed. 10 g of the filtrates was transferred into NaOH solution of 61.2 g DI water and 5.61 g of NaOH anhydrous, namely seed gel. The mixture was thoroughly. Mother gel was prepared. Two gels were thoroughly mixed for 3 hours at 100°C. The mixture was transfer into the autoclave. The operating temperature was set by various condition (105, 130, 155, and 180 °C) aging for 6-72 hours.

1.1 Characterization

Synthesized zeolite powder was characterized via instrumental techniques; x-ray diffraction (XRD, D8 advance Bruker, Germany) with Cu-Kα radiation, wavelength of 1.5406 Å, data collected at 0.02 steps within 10-50° of 2theta. Particles surface was analyzed by SEM (SEM-EDS, JEOL 6110LV, USA). Small portion of samples take place onto tape coated on aluminum holder. EDS analysis, aluminum holder painted by silver to electrically enhance image resolution. Bruneaur-Emmett-Teller (BET) was used to determined specific surface area. In this work nitrogen sorption was performed at 573 K for 3 hours.

1.2 Sulfate Adsorption

Batch adsorption experiments were carried out at ambient. Synthetic sulfate solution was prepared by weighing Na_2SO_4 1.4878 g, then added up deionized water to 1000 ml, calculated concentration was 1000 mg sulfate/L, dilution factor 10-100x. The standard solution was plotted into calibration curve within 0 - 40 mg/L. Synthesize zeolite 50 g was added to 50 ml the synthetic solution under constant agitation by a magnetic stirrer. Then, the suspension was filtered through Nylon filter 0.45 µm. Sulfate measurement using spectrophotometer (Jasco 730V, Japan) at 400 nm wavelength, the method is involved sulfur determination in solution, barium chloride ($BaCl_2$) binds sulfur in acidic solution resulting as white precipitates of barium sulfate ($BaSO_4$). The remaining sulfate in adsorbed solution was determined by calibration curve preparation with the range of 0-40 ppm sulfate. Above 40 ppm is beyond detection limit, hence the reading value will be less accurate.

1.3 Adsorption Isotherms

To predict the adsorption behavior between adsorbent and adsorbate, adsorption Isotherm models have been proposed. Firstly, Langmuir isotherm model is the simplest model describing coverage behavior between adsorbed molecules to active sites, can be obtained from equation 1. Linearized formula is illustrated in equation 1. [7].

$$q = q_{max}\frac{K_L C}{1+K_L C} \quad (1)$$

$$\frac{C_e}{q_e} = \frac{1}{q_m K_L} + \frac{C_e}{q_m} \quad (2)$$

Where; Ce represents concentration at equilibrium (mg/L), q_e is adsorbed capacity at equilibrium (mg/g), q_m is maximum capacity (mg/g), and K_L is adsorption constant or energy of adsorption (L/mg). Another simple adsorption model frequently used is Freundlich isotherm. It is an empirical model which implies the suited data to be multilayer sorption onto a heterogeneous surface. The model is described following equation 3. The adsorption parameters can be obtained from equation 4.

$$q = K_f C_e^{\frac{1}{n}} \quad (3)$$

$$\ln q_e = \ln K_f + \frac{1}{n}\ln C_e \quad (4)$$

Where; K_f indicates sorption capacity per unit mass sorbent (mg/g), 1/n represents sorption intensity. The 1/n value allows predicting sorption phenomena. The slope between 0-1 correlates to a chemisorption process; it is more heterogeneous as the value get closer to 0. The obtained slope is above 1, that it is consistent with multi-adsorption [8, 9].

RESULTS AND DISCUSSION

3.1 Characterization

Prior to the synthesize the zeolite using CFA, the CFA was characterized for its chemical species. Si and Al generally play a crucial role in zeolite synthesis, CFA as a raw material composed of O, Si, Al, Ca, and Fe as the main component with 17.7, 12.4, 11.86, and 12.70 % weight, respectively. Zeolite often gains cations during synthesis like Na^+ and K^+. This synthesized material was categorized into low silica zeolite grade due to Si/Al obtained as 1.27 which is below 2. The common mineralogical phase of low silica zeolite that can be converted into cancrinite (CAN), sodalite (SOD), Na-X, analcime, natrolite, and philipsite phases [10] which is corresponded to XRD results in this study. Sodalite is strongly presented and consistently decreased as other phase formed. Figure 1 illustrates the mineralogical composition in CFA, the sharpest peak of quartz presents at 25.5° as the main phase, with minor peaks of anhydrite, calcite, magnetite, and hematite.

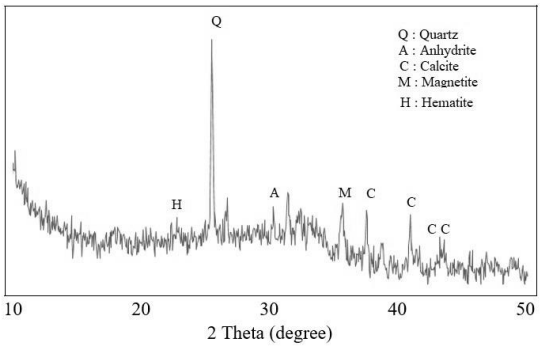

Figure 1: XRD patterns of coal fly ash

The raw materials were then studied on the effects of temperature on the range of 105-180°C. Figure 1 reveals that sodalite, cancrinite, and Na-P1 [11] phases are mainly presented at 13.9 (6.3977 Å), 24.3, 28.92, 29.97, 33.08, 34.48, 39.61, 40.11, and 45.84 degree of 2theta, respectively. Sodalite generally has 0.3 meq/g of CEC, and channel diameter of 2.3 Å [10]. The condition at 105°C was selected based on high intensity and integrity of sodalite. It was observed that at 180°C can generate more uniform phase of sodalite, higher crystallization temperature creates other zeolites and amorphous phases.

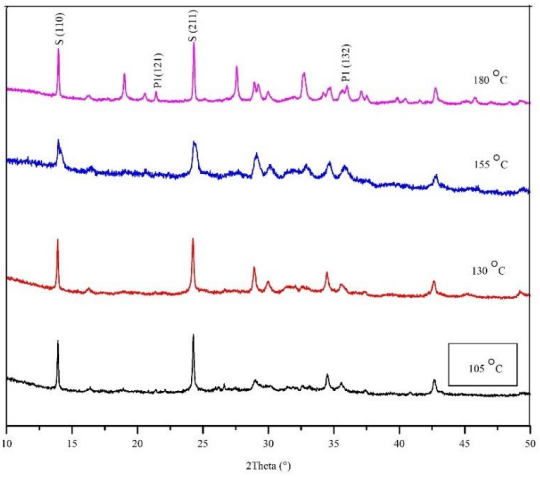

Figure 2: XRD patterns of zeolite synthesis as a function of hydrothermal temperature

However, surface area was used to select the materials which was characterized by BET method as shown in Table 1. It plays an important role for adsorption. The synthesis condition was then selected at 130°C for synthesis time investigation.

Table 1: Specific surface area and pore volumes of synthesized zeolies

Adsorbent/Condition	S_{BET} (m^2/g)	Pore volume (cm^3/g)
CFA	0.16	N.A.
105 °C, 12 hrs	65.38	15.02
130 °C, 12 hrs	45.24	12.165
155 °C, 12 hrs	40.70	9.35
180 °C, 12 hrs	25.22	5.80
130 °C, 6 hrs	52.95	12.165
130 °C, 24 hrs	42.95	9.65
130 °C, 48 hrs	39.94	9.175
130 °C, 72 hrs	36.47	8.38

Figure 3 illustrated the surface and morphology of CFA and selected synthesized adsorbents (105°C for 12 hours, 130°C for 6 hours, and 130°C for 72 hours). The synthesized materials morphology and their surface were also investigated at 10,000 magnificent image resolutions. CFA was spherical shape, and less porous surface, as shown in Figure 3(a), Figure 3(b) shows sodalite phase with porous surface, larger size with aggregation, and cubic wall with channels connecting on the surface.

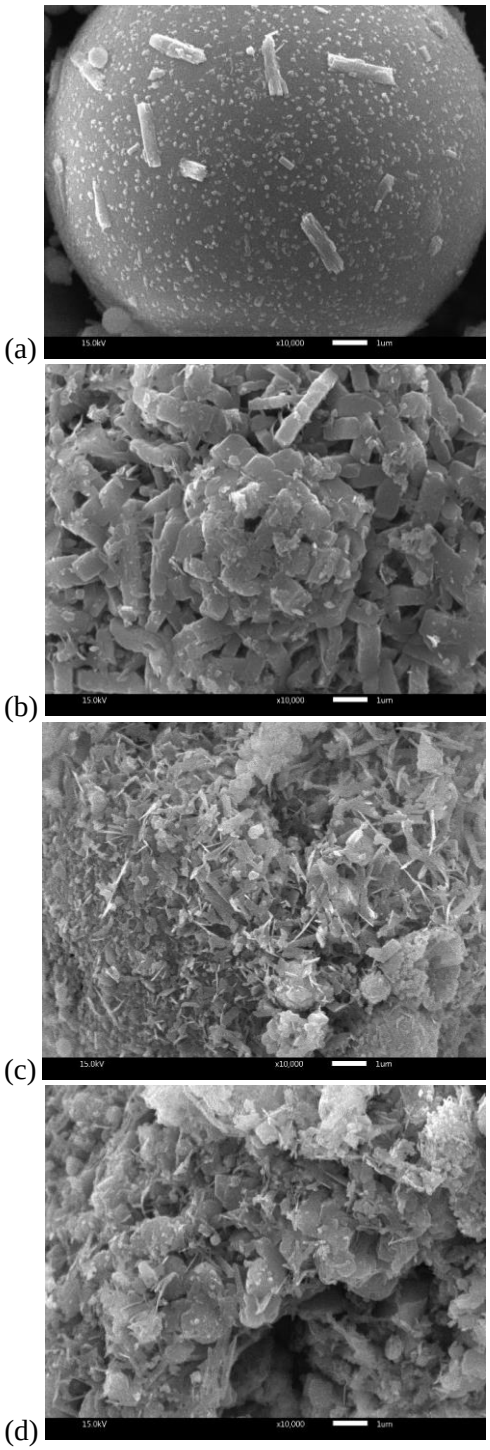

Figure 3: Morphology of CFA (a), zeolite synthesized at 105 °C, 12 hours (b); 130 °C, 6 hours (c); and 130 °C, 72 hours (d).

Figure 3(c) exhibits the particle surface like sodalite grown along with cancrinite, this confirmed by the previous studies [10, 13]. The particles possess high porosity as seen in Figure 3(b), at synthesis condition at 105°C for 12 hours, the larger pores influence the higher specific surface area of material which providing the impacts to their application. Generally, sodalite and cancrinite has hexagonal shape sizing of 20-30 µm, while Na-P1 with fibrous morphology [10]. The fly ash particles might be affected by several factors; chemical composition, high alkalinity, temperature, pressure, and stirring speed. consequently, structural and surface were modified as described previously.

In addition, the utilization of the synthesized zeolites as the adsorbents, point of zero charge is necessary to determine the appropriate pH according to the application. Surface charge of the material was observed in the pH range of 2-12, the isoelectric point (IEP) or zero-point charge where surface charge is neutral was about 6.5-7. The pH below IEP appears as positive value meanwhile the above presents the negative surface as exhibit in Figure 4(a) and 4(b).

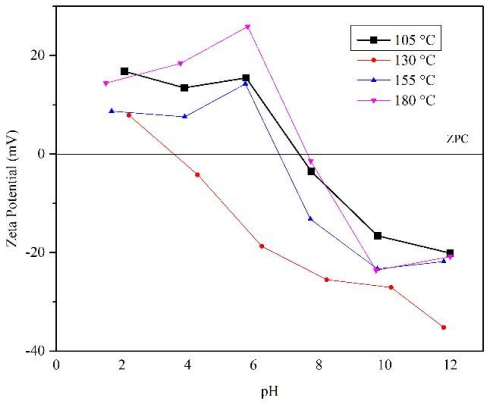

Figure 4 (a): Zeta potential of the synthesized zeolite with different hydrothermal temperature

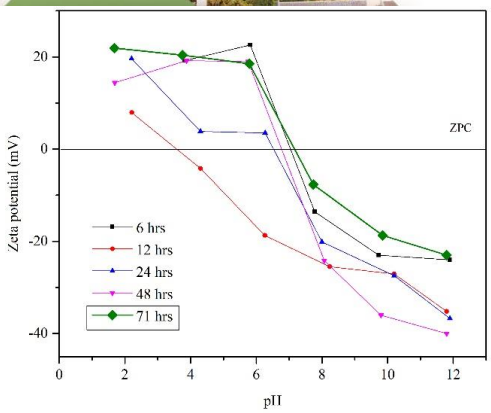

Figure 4 (b): Zeta potential of the synthesized zeolite with different hydrothermal time

The potential is resulted from interaction of NaOH medium during hydrothermal synthesis, cation of Na^+ develops on pores surface of zeolites. The displace of Si by Al attributed into the tetrahedral $[Al_4O_4]^{5-}$ interconnected to $[SiO_4]^{4-}$ by oxygen. The previous findings suggested that a general ion exchange process of wastewater treatment at room temperature, by allowing the anions exchange on the cations generated-specific surface.

3.2 Sulfate adsorption

To determine the sulfate quantity in the solution, Barium chloride ($BaCl_2$) is naturally soluble in water, barium (Ba^{2+}) ions binds sulfate SO_4^{2-} ions precipitating into white colloids in solution, hence sulfate ions is measured using spectrophotometer at 400 cm^{-1} of wavelength. Beyond detection limit of spectrophotometry on precipitated barium sulfate is 40 ppm, otherwise determination is less stable. The interaction between SiO_2, Al_2O_3, Fe_2O_3, and CaO to sulfate uptake is more complicated to investigate than the pure phase component. Synthesized zeolites possess both high calcium content, and high specific surface area which has advantages over sulfate adsorption. Therefore, the removal efficiency will be compared between the coal fly ash with less specific

Table 2: Langmuir and Freundlich adsorption parameters

Adsorbent	Langmuir			Fruendlich		
	q_{max}	K_L	R^2	1/n	K_F	R^2
CFA	6.76	0.44	0.9964	0.26	2.9	0.8772
Zeolite I	10.6	0.23	0.9804	0.39	2.7	0.9032
Zeolite II	12.49	0.21	0.9936	0.42	2.97	0.9364
Zeolites III	14.26	0.29	0.9945	0.33	4.61	0.9616

surface area but high calcium content and selected adsorbents which shown in Table 3.

Table 3: Selected adsorbent for sulfate adsorption

Adsorbent	Synthesis Condition	S_{BET} (m^2/g)
Coal Fly Ash	-	0.16
Zeolite I	12 hrs, 180 ℃	25.22
Zeolite II	6 hrs, 130 ℃	52.95
Zeolite III	12 hrs, 105 ℃	65.38

For liquid adsorption, the graphs are plotted between adsorbed capacity versus concentration at equilibrium to determine the maximum sorption capacity (q_{max}) and energy (K_L), the results are shown in Table 2. The sulfate uptake capacity at equilibrium was evaluated in the adsorption models; Langmuir and Freundlich isotherm. Generally, once the adsorption approaches the maximum capacity of adsorbent, the adsorbed molecules is a monolayer localized onto the surface (R^2>0.98).

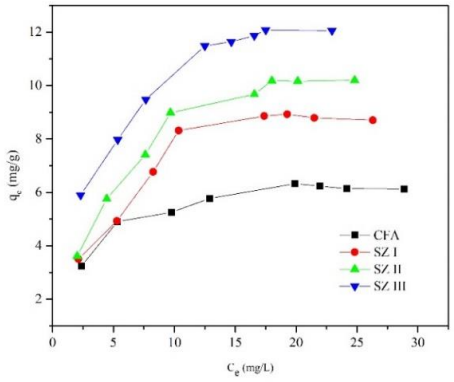

Figure 5(a): Experimental plot of isotherm

They only attracted to the active site surface. These results correlate to available specific surface area measure by BET method. This implies the strong adsorptivity between the active site. However, CFA has no specific area for sulfate uptake but contains high calcium content up to 11%weight which higher than zeolite II 80%. Langmuir isotherm model indicates the CFA has 6.93 mg/g adsorption capacity which lower than Zeolite II 54 %. This implies that effect of S_{BET} is superior than calcium content from coal fly. Figure 5(b-c) shows that adsorption is more favored on Langmuir isotherm model.

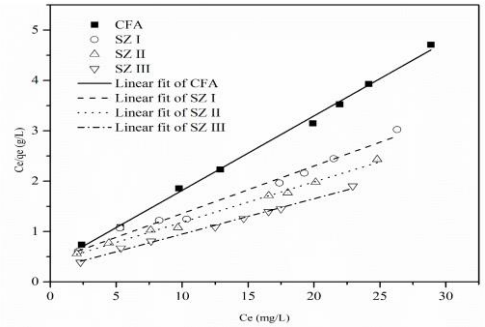

Figure 5 (b): Linear plot of Langmuir isotherm model

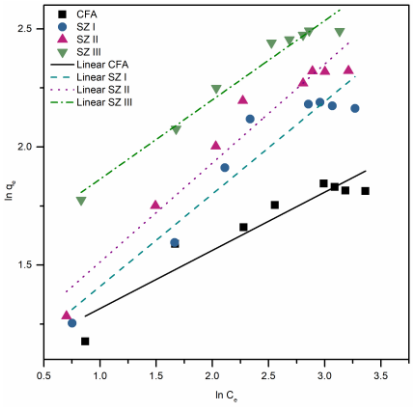

Figure 5 (c): Linear plot of Freundlich isotherm model

Langmuir adsorption model is a theoretical prediction of sorbate coverage on adsorbent surface. Sulfate is predicted to be favorable on nature adsorption. Therefore, sulfate adsorption employing Zeolite I, and Zeolite II is localized onto active surface as monolayer sorption between sulfate anions and specific surface area. Zeolite I, and Zeolite II can practically and efficiently uptake sulfate in low acidic region. The maximum sorption capacity of synthesized zeolite containing 2.43 % calcium, 65.38 m^2/g specific surface area and 15.02 cm3/g pore volumes, is higher than the CFA with 11% calcium 0.16 m^2/g specific surface area without porosity were 52.6%. Higher surface area results higher sorption capacity.

CONCLUSION

The integrated zeolites were synthesized from lignite coal fly ash without additives containing sodalite phase, specific surface area 65.38 m^2/g and 15.02 cm^3/g. Higher temperature results higher amorphous and Na-P1 but decreasing the sodalite. Sulfate adsorption was successfully performed utilizing synthesized integrated zeolites and coal fly ash as the adsorbents with maximum capacity of 14.26 and 6.76, respectively which calculated as 52.6%.

ACKNOWLEDGEMENT

The authors would like to acknowledge Graduate Scholarship of Prince of Songkla University for financial support (PSU.GS. Financial Support for Thesis).

REFERENCES

1. Suzuki, I., *Oxidation of inorganic sulfur compounds: Chemical and enzymatic reactions.* Canadian Journal of Microbiology, 1999. **45**(2): p. 97-105.
2. INAP, *Treatment of sulphate in mine effluentes,*. International network for acid prevention, 2003.
3. Silva, A.M., R.M.F. Lima, and V.A. Leão, *Mine water treatment with limestone for sulfate removal.* Journal of Hazardous Materials, 2012. **221-222**: p. 45-55.
4. Gnana kumar, G., *Zeolites and Composites*, in *Nanomaterials and Nanocomposites*, V.P.M.M.J.M. Morlanes, Editor. 2016, Wiley-VCH Verlag GmbH & Co. KGaA.
5. Tait, S., et al., *Removal of sulfate from high-strength wastewater by crystallisation.* Water Research, 2009. **43**(3): p. 762-772.
6. Chansiriwat, W., D. Tanangteerapong, and K. Wantala, *Synthesis of Zeolite from Coal Fly Ash by Hydrothermal Method Without Adding Alumina and Silica Sources: Effect of Aging Temperature and Time.* Sains Malaysiana, 2016. **45**(11): p. 1723-1731.
7. Haciyakupoglu, S. and E. Orucoglu, *75Se radioisotope adsorption using Turkey's Reşadiye modified bentonites.* Applied Clay Science, 2013. **86**: p. 190-198.
8. Karnitz, J.R.O., et al., *Adsorption of heavy metal ion from aqueous single metal solution by chemically modified sugarcane bagasse.* Bioresour. Technol., 2007. **98**: p. 1291-1297.
9. Kumar, U. and M. Bandyopadhyay, *Sorption of cadmium from aqueous solution using pretreated rice husk.* Bioresour. Technol., 2006. **97**: p. 104-109.
10. B., J. and S. D.N., *A review on synthesis, characterization and industrial application of fly ash zeolites.* J. Mater Edu., 2011. **33**(1-2): p. 65-132.
11. McMurdie, H.F., et al., *Standard X-ray diffraction*

powder patterns from the JCPDS research associateship. Powder Diffraction, 1986. **1**(267).
12. Ishikawa, K., et al., *Solubility of hematite in LiOH, NaOH and KOH solutions.* Hydrometallurgy, 1997. **45**(1): p. 129-135.
13. Wang, D.J., et al., *Hollow cancrinite zeolite spheres in situ transformed fly ash cenosphere.* Chin. Chem. Lett., 2003. **14**(12): p. 1299-1302.

VITAE

Name Anis Usmani

Student ID 5910120066

Educational Attainment

Degree	Name of Institution	Year of Graduation
Bachelor of Engineering (Bioprocess)	University of Malaysia Perlis	2016

Scholarship Awards during Enrolment

GS. Scholarship for Teaching Assistant

GS. Scholarship for Graduate Student Research

List of Publication and Proceedings

A. Usmani, and L. Kaewsichan, Synthesis of zeolite derived from coal fly ash via hydrothermal method for sulfate adsorption, 6th International Conference on Creative Technology, Pattaya, Thailand, July 24-26, 2018.